

EXPERIMENTAL TESTING OF MICROCONTROLLER  
BASED PROTECTION FOR THREE PHASE POWER  
DISTRIBUTION TRANSFORMER

IMRAN RIAZ DAR







**Experimental Testing of Microcontroller Based Protection for  
Three Phase Power Distribution Transformer**

By

**Imran Riaz Dar**

A thesis submitted to the School of Graduate Studies in partial fulfillment of

**Master of Engineering**

Faculty of Engineering and Applied Science

Memorial University of Newfoundland

November, 2011

St John's, Newfoundland, Canada

## **Abstract**

The differential protection technique is very popular for protecting power transformers of various ratings and configurations and is based on the differences between the primary side and secondary side currents. The difference currents contain information when adequately processed and provide a clear picture about the transformer operating conditions. Among several approaches developed to process differential currents, harmonic analysis is widely employed for several utilities, industrial, commercial and residential applications.

The extraction of certain harmonic components present in the differential currents can be critical in distinguishing between the magnetizing inrush current and any internal fault current. The discrete Fourier transform can be the preferred choice in the analysis that leads to an improvement in the protection of power transformers. The implementation of a digital filtering approach is usually accomplished using microprocessor platforms, which offer accuracy, speed, reliability and simplicity for protection of distribution transformers.

This thesis implements, for the first time, harmonic analysis of differential currents for protection of power transformers in a microcontroller. The analysis is based on a discrete Fourier transform and is realized using a c-code for testing the 3-phase laboratory transformer. Performances of the microprocessor digital relay show simple implementation, reliability, speed and accuracy for distribution type transformers.

## **Acknowledgement**

I am thankful to my supervisor Professor Dr. M.A. Rahman for his continuous advice and assistance during the course of graduate studies, research work and the writing of this thesis.

I would like to pay special regards to Dr. Saleh for his help with my experimental research work.

Special thanks to my colleagues and lab technicians for their support.

Financial Assistance, in the form of a Teaching Assistantship by the Faculty of Engineering and Applied Science, is worth mentioning here.

Finally, I must mention the patience of my wife who stood by me for the last three years, as I was doing, my studies, and the same feelings go for my children.

# Contents

Abstract	ii
Acknowledgement	iii
List of Figures	viii
1. Introduction	1
1.1 General	1
1.2 Summary of Short Literature Review	2
1.3 Pertinent and Brief Literature Review on Digital Protection	4
1.3.1 Digital Algorithms for Power Transformer Protection	7
1.3.2 Discrete Fourier Transform (DFT)	7
1.3.3 Application of Discrete Fourier Transform (DFT) in Power Distribution Transformer Protection	9
1.4 Purpose of This Thesis	10
1.5 Outline of The Thesis	11
2. Transformer Protection Concepts	12
2.1 Differential Protection Technique	12
2.2 Tripping Characteristics of Differential Relay	13

2.3 Magnetizing Inrush Current	14
2.4 Over –excitation	20
2.5 Current Transformer Saturation	21
2.6 Three phase Transformer Protection	21
2.6.1 Current Transformers	21
2.6.2 Harmonic Restraints for Differential Protection	23
3. Hardware Design of Microcontroller–based Protection of Three Phase Power Transformer	25
3.1 Introduction	25
3.2 Power Transformer	29
3.3 Current Transformers	29
3.4 Relay Control Circuit	30
3.5 Solid State Relay	32
3.6 Scaling Circuit	33
3.7 Filtering Circuit	38
3.8 Microcontroller	45
4. Software Design of Microcontroller based Three Phase Power Transformer Protection	47

4.1 Introduction	47
4.2 Software Design	47
4.2.1 DFT Method for Harmonics Calculations	49
4.2.2 Criteria for Harmonic Calculations	51
4.3 Protection Scheme	52
5. Experimental Testing For Digital Protection of Power Transformer	53
5.1 Introduction	53
5.2 Magnetizing Inrush Current Tests	55
5.3 Internal Fault Tests	59
5.3.1 Phase to Ground Fault (Primary side-secondary unloaded)	59
5.3.2 Phase to Ground Fault (Primary side-secondary at equal resistive load)	62
5.3.3 Phase to Ground Fault (Primary side-secondary at different resistive load)	64
5.3.4 Phase to Phase Fault (Primary side-secondary at no load)	66
5.3.5 Phase to Neutral Fault (Secondary side-secondary at equal resistive load)	69
5.3.6 Phase to Neutral Fault (Secondary side-secondary at different resistive load)	71

5.3.7 Phase to Phase Fault (Secondary side-secondary-open)	73
5.3.8 Phase to Phase Fault (Secondary side-secondary at equal resistive load)	76
5.3.9 Phase to Phase Fault (Secondary side-secondary at different resistive load)	78
5.4 Summary of Experimental Results	80
6. Conclusions and Future Works	82
6.1 Conclusion	82
6.2 Future Works	83
<b>References</b>	84
<b>Appendices</b>	94
A Design of Chebyshev Filter for Antialiasing	95
B MATLAB Programme for Inrush analysis	114
C Discrete Fourier Transform (DFTs) Algorithm	124
D Real Time Testing	128
E Programme for Microcontroller	196

## List of Figures

Figure 2.1: Biased Transformer Differential Protection	13
Figure 2.2: Differential Relay Tripping Characteristics	14
Figure 2.3: Input Voltage and Inrush Current when Switching Angle = $0^\circ$	15
Figure 2.4: Voltage, flux and current during the magnetizing inrush current.	16
Figure 2.5: Derivation of magnetizing inrush current from the excitation characteristic	17
Figure 2.6: Effect of residual flux on inrush current, at saturation density	18
Figure 2.7: Effect of residual flux on inrush current, at 90% saturation density	19
Figure 2.8: Magnetizing Curve for Steel Core Transformers	20
Figure 2.9: Differential protection Scheme for Three Phase Power Transformer	22
Figure 2.10: Basic circuit for harmonic restraint relay	23
Figure 3.1: Experimental Set Up	26
Figure 3.2: System Block Diagram	27
Figure 3.3: Experimental Set Up for Internal Faults Tests	28

Figure 3.4: Relay Control Circuit	31
Figure 3.5: Equivalent circuit of Solid State Relay	33
Figure 3.6: Quad Operational Amplifier	34
Figure 3.7: Scaling circuit	35
Figure 3.8: Scaling circuit when Low gain, $R_A = 0$	36
Figure 3.9: Scaling circuit when medium gain, $R_A = 2.5K\Omega$	37
Figure 3.10: Scaling circuit when high gain, $R_A = 5K\Omega$	38
Figure 3.11: Chebyshev low pass filter specifications	40
Figure 3.12: Circuit diagram for 6 <sup>th</sup> order Chebyshev filter (Anti-aliasing filter)	44
Figure 3.13: Output of Chebyshev filter	45
Figure 4.1: Flow Chart for Differential Relay Protection	48
Figure 4.2: Flow Chart for Harmonics Calculations	50
Figure 5.1: Photograph of Experimental set up	54
Figure 5.2: Experimental inrush current response for phase A	56
Figure 5.3: Experimental current harmonics in phase A	57
Figure 5.4: Experimental magnetizing inrush current and response of electronic switch	58

Figure 5.5: Experimental phase to ground fault and response of the electronic switch	60
Figure 5.6: Phase A to ground fault at no load power transformer, harmonics and response of electronic switch.	61
Figure 5.7: Phase A to ground fault at equal resistive load ( $600\Omega$ ), power transformer and response of electronic switch	62
Figure 5.8: Phase A to ground fault at equal resistive load ( $600\Omega$ )-power transformer, harmonics and response of electronic switch	63
Figure 5.9: Phase A to ground fault at unequal resistive load ( $600/1200/2400\ \Omega$ ), power transformer and response of electronic switch	64
Figure 5.10: Phase A to ground fault at unequal resistive load ( $600/1200/2400\ \Omega$ ), power transformer, harmonics and response of electronic switch.	65
Figure 5.11: Phase A to Phase B fault primary side and secondary open and response of electronic switch	67
Figure 5.12: Phase A to Phase B fault primary side and secondary open, harmonics and response of electronic switch	68
Figure 5.13: Phase to neutral fault current (secondary side) in Phase A when secondary side of power transformer at equal resistive load ( $600\ \Omega$ ) and response of electronic switch.	69

Figure 5.14: Phase to neutral fault current (secondary side) in Phase A when secondary side of power transformer at equal resistive load ( $600 \Omega$ ), harmonics and response of electronic switch 70

Figure 5.15: Phase to neutral fault current (secondary side) in Phase A when secondary side of power transformer at unequal resistive load ( $600/1200/2400 \Omega$ ) and response of electronic switch. 71

Figure 5.16: Phase to neutral fault current (secondary side) in Phase C when secondary side of power transformer at unequal resistive load ( $600/1200/2400 \Omega$ ) and response of electronic switch. 72

Figure 5.17: Phase to Phase fault current (secondary side) in Phase A when secondary side of power transformer open and response of electronic switch. 74

Figure 5.18: Phase to Phase fault current (secondary side) in Phase A when secondary side of power transformer open and response of electronic switch. 75

Figure 5.19: Phase to Phase fault current (secondary side) in Phase C when secondary side of power transformer at equal resistive load ( $600 \Omega$ ) and response of electronic switch. 76

Figure 5.20: Phase to Phase fault current (secondary side) in Phase C when secondary side of power transformer at equal resistive load (600  $\Omega$ ) and response of electronic switch.

77

Figure 5.21: Phase to Phase fault current (secondary side) in Phase C when secondary side of power transformer at different resistive load (600/1200/2400  $\Omega$ ) and response of electronic switch.

78

Figure 5.22: Phase to Phase fault current (secondary side) in Phase C when secondary side of power transformer at different resistive load (600/1200/2400  $\Omega$ ) and response of electronic switch.

79

Figure A.1: Poles location for the 6<sup>th</sup> order Chebyshev filter

101

Figure A.2: Magnitude and phase response of three transfer functions separately for the 6<sup>th</sup> order

102

Figure A.3: Magnitude and phase response of the 6<sup>th</sup> order Chebyshev filter

103

Figure A.4: Filter circuit

104

Figure A.5: Antialiasing filter-6<sup>th</sup> order Chebyshev filter

109

Figure A.6: Cascaded transfer functions for 6<sup>th</sup> order Chebyshev filter

110

Figure A.7: Location of poles for cascaded transfer functions for 6<sup>th</sup> order Chebyshev filter

111

Figure A.8: Magnitude response of 6 <sup>th</sup> order Chebyshev filter	112
Figure A.19: Phase response of 6 <sup>th</sup> order Chebyshev filter	113
Figure B.1: Input Voltage and Inrush Current when Switching Angle = 0°	115
Figure B.2: Input Voltage and Inrush Current when Switching Angle = 45°	116
Figure B.3: Input Voltage and Inrush Current when Switching Angle = 90°	117
Figure B.4: Input Voltage and Inrush Current when Switching Angle = 135°	118
Figure B.5: Input Voltage and Inrush Current when Switching Angle = 180°	119
Figure B.6: Input Voltage and Inrush Current when Switching Angle = 225°	120
Figure B.7: Input Voltage and Inrush Current when Switching Angle = 270°	121
Figure B8: Input Voltage and Inrush Current when Switching Angle = 315°	122
Figure B9: Input Voltage and Inrush Current when Switching Angle = 360°	123
Figure D.1: MATLAB Model for Harmonics Analysis	128
Figure D.2: Phase A to ground fault at Primary side, response of the three phases of differential current at no load power transformer and Response of electronic switch	129
Figure D.3: Phase B to ground fault at no load power transformer and response of electronic switch	130

Figure D.4: Phase B to ground fault at no load power transformer, harmonics and response of electronic switch	131
Figure D.5: Phase C to ground fault at no load power transformer and response of electronic switch	132
Figure D.6: Phase C to ground fault at no load power transformer, harmonics and response of electronic switch	133
Figure D.7: Phase A to ground fault-Primary side, responses of the three phases of differential current at equal resistive load (600 $\Omega$ ), power transformer and response of electronic switch.	134
Figure D.8: Phase B to ground fault at equal resistive load (600 $\Omega$ ) power transformer and response of electronic switch	135
Figure D.9: Phase B to ground fault at equal resistive load (600 $\Omega$ ) power transformer, harmonics and response of electronic switch.	136
Figure D.10: Phase C to ground fault at equal resistive load (600 $\Omega$ ) power transformer and response of electronic switch	137
Figure D.11: Phase C to ground fault at equal resistive load (600 $\Omega$ ) power transformer, harmonics and response of electronic switch	138

Figure D.12: Response of the three phases of differential currents at unequal resistive load (600/1200/2400 $\Omega$ ) power transformer and response of electronic switch	139
Figure D.13: Phase B to ground fault at unequal resistive load (600/1200/2400 $\Omega$ ), power transformer and response of electronic switch	140
Figure D.14: Phase B to ground fault at unequal resistive load (600/1200/2400 $\Omega$ ), power transformer, harmonics and response of electronic switch.	141
Figure D.15: Phase C to ground fault at unequal resistive load (600/1200/2400 $\Omega$ ), power transformer and response of electronic switch	142
Figure D.16: Phase C to ground fault at unequal resistive load (600/1200/2400 $\Omega$ ), power transformer, harmonics and response of electronic switch.	143
Figure D.17: Responses of the three phases of differential currents for phase to phase fault, secondary side open, power transformer and response of electronic switch	144
Figure D.18: Phase A to Phase B fault at primary side and secondary open and response of electronic switch	145
Figure D.19: Phase A to Phase B fault at primary side and secondary open, harmonics and response of electronic switch.	146

Figure D.20: Phase A to Phase B fault at primary side and secondary open and response of electronic switch	147
Figure D.21: Phase A to Phase B fault at primary side and secondary open, harmonics and response of electronic switch	148
Figure D.22: Response of the three phases of differential currents for inrush magnetizing inrush current when power transformer secondary side open and response of electronic switch	149
Figure D.23: Magnetizing Inrush Current in Phase B when secondary side of power transformer open and response of electronic switch	150
Figure D.24: Magnetizing Inrush Current in Phase B when secondary side of power transformer open, harmonics and response of electronic switch	151
Figure D.25: Response of the three phases of differential currents for inrush magnetizing inrush current when power transformer secondary side at equal resistive load ( $600\Omega$ ) and response of electronic switch	152
Figure D.26: Magnetizing Inrush Current in Phase B when secondary side of power transformer at equal resistive load ( $600\Omega$ ) and response of electronic switch.	153
Figure D.27: Magnetizing Inrush Current in Phase B when secondary side of power transformer at equal resistive load ( $600\Omega$ ) , harmonics and response of electronic switch	154

Figure D.28: Magnetizing Inrush Current in Phase C when secondary side of power transformer at equal resistive load ( $600\Omega$ ) and response of electronic switch. 155

Figure D.29: Magnetizing Inrush Current in Phase C when secondary side of power transformer at equal resistive load ( $600\Omega$ ), harmonics and response of electronic switch. 156

Figure D.30: Response of the three phases of differential currents for magnetizing inrush current when power transformer secondary side at variable resistive load ( $600/1200/2400\Omega$ ) and response of electronic switch 157

Figure D.31: Magnetizing Inrush Current in Phase A when secondary side of power transformer at variable resistive load ( $600/1200/2400\Omega$ ) and response of electronic switch. 158

Figure D.32: Magnetizing Inrush Current in Phase A when secondary side of power transformer at variable resistive load ( $600/1200/2400\Omega$ ), harmonics and response of electronic switch 159

Figure D.33: Magnetizing Inrush Current in Phase B when secondary side of power transformer at variable resistive load ( $600/1200/2400\Omega$ ) and response of electronic switch. 160

Figure D.34: Magnetizing Inrush Current in Phase B when secondary side of power transformer at variable resistive load (600/1200/2400 $\Omega$ ), harmonics and response of electronic switch	161
Figure D.35: Magnetizing Inrush Current in Phase C when secondary side of power transformer at variable resistive load (600/1200/2400 $\Omega$ ) and response of electronic switch.	162
Figure D.36: Magnetizing Inrush Current in Phase C when secondary side of power transformer at variable resistive load (600/1200/2400 $\Omega$ ), harmonics and response of electronic switch	163
Figure D.37: Response of the three phases of differential currents for phase to neutral fault when power transformer secondary side open and response of electronic switch	164
Figure D.38: Phase to neutral fault current (secondary side) in Phase A when secondary side of power transformer open and response of electronic switch	165
Figure D.39: Phase to neutral fault current (secondary side) in Phase A when secondary side of power transformer open, harmonics and response of electronic switch.	166
Figure D.40: Phase to neutral fault current (secondary side) in Phase B when secondary side of power transformer open and response of electronic switch.	167
Figure D.41: Phase to neutral fault current (secondary side) in Phase B when secondary side of power transformer open, harmonics and response of electronic switch.	168

Figure D.42: Phase to neutral fault current (secondary side) in Phase C when secondary side of power transformer open and response of electronic switch	169
Figure D.43: Phase to neutral fault current (secondary side) in Phase C when secondary side of power transformer open, harmonics and response of electronic switch.	170
Figure D.44: Response of the three phases of differential currents for phase to neutral fault when power transformer secondary side at equal resistive load (600 $\Omega$ ) and response of electronic switch.	171
Figure D.45: Phase to neutral fault current (secondary side) in Phase B when secondary side of power transformer at equal resistive load (600 $\Omega$ ) and response of electronic switch.	172
Figure D.46: Phase to neutral fault current (secondary side) in Phase B when secondary side of power transformer at equal resistive load (600 $\Omega$ ), harmonics and response of electronic switch.	173
Figure D.47: Phase to neutral fault current (secondary side) in Phase C when secondary side of power transformer at equal resistive load (600 $\Omega$ ) and response of electronic switch.	174
Figure D.48: Phase to neutral fault current (secondary side) in Phase C when secondary side of power transformer at equal resistive load (600 $\Omega$ ), harmonics and response of electronic switch.	175

Figure D.49: Response of the three phases of differential currents for phase to neutral fault when power transformer secondary side at unequal resistive load (600/1200/2400  $\Omega$ ) and response of electronic switch S. 176

Figure D.50: Phase to neutral fault current (secondary side) in Phase B when secondary side of power transformer at un-equal resistive load (600/1200/2400  $\Omega$ ) and response of electronic switch S. 177

Figure D.51: Phase to neutral fault current (secondary side) in Phase B when secondary side of power transformer at un-equal resistive load (600/1200/2400  $\Omega$ ) and response of electronic switch S. 178

Figure D.52: Phase to neutral fault current (secondary side) in Phase C when secondary side of power transformer at un-equal resistive load (600/1200/2400  $\Omega$ ) and response of electronic switch S. 179

Figure D.53: Phase to neutral fault current (secondary side) in Phase C when secondary side of power transformer at un-equal resistive load (600/1200/2400  $\Omega$ ) and response of electronic switch. 180

Figure D.54: Responses of the three phases of differential currents for phase to phase fault when power transformer secondary side open and response of electronic switch. 181

Figure D.55: Phase to Phase fault current (secondary side) in Phase B when secondary side of power transformer open and response of electronic switch S. 182

Figure D.56: Phase to Phase fault current (secondary side) in Phase B when secondary side of power transformer open and response of electronic switch S.	183
Figure D.57: Phase to Phase fault current (secondary side) in Phase C when secondary side of power transformer open and response of electronic switch S.	184
Figure D.58: Phase to Phase fault current (secondary side) in Phase C when secondary side of power transformer open and response of electronic switch.	185
Figure D.59: Responses of the three phases of differential currents for phase to phase fault when power transformer secondary side at equal resistive load (600 $\Omega$ ) and response of electronic switch.	186
Figure D.60: Phase to Phase fault current (secondary side) in Phase B when secondary side of power transformer at equal resistive load (600 $\Omega$ ) and response of electronic switch S.	187
Figure D.61: Phase to Phase fault current (secondary side) in Phase B when secondary side of power transformer at equal resistive load (600 $\Omega$ ) and response of electronic switch S.	188
Figure D.62: Phase to Phase fault current (secondary side) in Phase C when secondary side of power transformer at equal resistive load (600 $\Omega$ ) and response of electronic switch S.	189

Figure D.63: Phase to Phase fault current (secondary side) in Phase C when secondary side of power transformer at equal resistive load (600 $\Omega$ ) and response of electronic switch.	190
Figure D.64: Responses of the three phases of differential currents for phase to phase fault when power transformer secondary side different at resistive load (600/1200/2400 $\Omega$ ) and response of electronic switch.	191
Figure D.65: Phase to Phase fault current (secondary side) in Phase B when secondary side of power transformer at different resistive load (600/1200/2400 $\Omega$ ) and response of electronic switch S.	192
Figure D.66: Phase to Phase fault current (secondary side) in Phase B when secondary side of power transformer at different resistive load (600/1200/2400 $\Omega$ ) and response of electronic switch S.	193
Figure D.67: Phase to Phase fault current (secondary side) in Phase C when secondary side of power transformer at different resistive load (600/1200/2400 $\Omega$ ) and response of electronic switch S.	194
Figure D.68: Phase to Phase fault current (secondary side) in Phase C when secondary side of power transformer at different resistive load (600/1200/2400 $\Omega$ ) and response of electronic switch S.	195
Figure F.1.1: Pin Diagram for Microcontroller-16F877	201
Figure F.1.2: Block Diagram of Programmable Controller (PIC 16F877)	202

## List of Tables

5.1: Inrushes and faults at various operating conditions and responses of Triac Switch. 81

# Chapter 1

## Introduction

### 1.1 General

Digital protection has been an area of interest for the last three decades. In the early 1970's the use of the computer was proposed for the protection of power systems. Efforts are being made to increase the reliability, speed, economics and flexibility and to reduce the size of the protection system. Advancement of the microprocessor, like microcontroller, made it possible to achieve the objectives of the proposed protection of a power distribution transformer.

The protection of the power transformer poses a challenge to protection engineers, such as protection from magnetizing inrushes in power transformers made up of iron laminations during over-voltage excitation. Simple and ordinary electro-mechanical relays have failed to adequately fulfill these versatile requirements. These requirements include protection that identifies magnetizing inrush current, saturation and over-excitation. Magnetizing inrush occurs at the instance of switching on the power transformer, whereas over excitation is due to voltage surges at input or saturation of the iron laminated core of the power transformer. Differential current protection is the most popular technique for the protection of the transformer. In the ideal case, these differential currents are linear. However, the residual flux density and saturation of iron lamination make the inrush current non-linear and non-sinusoidal. The differential protection technique is used for digital protection of the power transformer. It requires

the sampling of the input current data and evaluation according to the algorithm used. These input sample data are digitally filtered by the algorithm in the processor and declares the fault or no fault like inrush.

## **1.2 Summary of Short Literature Review**

The power transformer is one of the most essential components of a power system. Power transformers are broadly classified as: (1) Generating transformer, (2) Transmission transformer, (3) Distribution transformer, in terms of power and voltage ratings. The generating transformer is connected to the generator directly and usually located just outside the generating building. The generator and the generating transformer are called the unit transformer. The generating transformer is a step up power transformer having ratings of 13.8 kV/ 132kV (Line to Line), etc. Transmission transformers are located in transmission substations. These are step up transformers having standard voltage ratings of 138kV/230kV/345kV/500kV/735kV. At the load center (substation) the transmission transformers are step down types having standard voltage ratings 132kV/66kV/33kV. The distribution transformers are typically low voltage types having standard voltage ratings of 33kV/12.47kV/4.16kV/575V/208V (L-L) and 110V (L-N). This thesis deals with the protection of distribution power transformers.

There are two types of major over current abnormalities in power transformers. The first one is the fault currents and the other one is magnetizing inrush currents. The objectives of all types of distribution transformer protection include the art and science of protecting against the faults in the transformer itself and against high magnetizing inrush

currents during the initial switching. The art of protection also lies on the intelligent decision to trip a circuit breaker against any fault, while restraining the trip of the circuit breaker during the inrush conditions. The discriminating features involve isolating the fault current but allowing the inrush currents for the first six cycles or hundred milliseconds of the sixty hertz (60Hz) power system as per IEEE standard.

Many analog and digital circuits are employed for protection of power transformers. There exist numerous papers and methods in the literature for power transformer protection. The earlier art of power transformer protection is mechanical or analog types over the years until the 1980s [1-18]. Systematic researches are being carried out at the Memorial University's Power Research Laboratory for developing and improving the digital protection of power transformer, as a part of worldwide research and development of techniques for protecting the power transformers [19-64]. A brief review of the literature would highlight the contribution of the researches to achieve these goals. In 1979, MUN undergraduate student, Eric Downton had successfully implemented the weighted least square algorithms for discriminating between inrush and fault currents in power transformers [22]. Gangopandhy, a MUN graduate student, did complete digital computer based simulation of the magnetizing inrush and fault currents in 1980 [30]. Rahman, Dash, Phadke, Jeyasurya and Yalla contributed significantly towards digital protection of power transformers by employing various techniques and methods for performing harmonic analyses [16, 22, 24, 30, 33, 38, and 40].

Ivi Harmanto, another MUN graduate student, was the first to use the microprocessor based protection of a power transformer in the late 1980s [21, 23 and 37]. In recent years, intelligent high speed digital relays have been introduced; employing artificial

neural networks, fuzzy logics and wavelet techniques based protection of power transformers. These newer intelligent techniques were investigated by many other MUN graduate students like Zaman, Hoque, Darwash, So and Saleh on different aspects for using computer relaying of power systems [47-50, 62]. The uses of microcontrollers are not well researched for distribution type power transformers. The microcontroller based digital relay is now considered as cheap and inexpensive for stand-alone protection of single and three phase power distribution transformers. These cost effective microcontroller relays are connected in parallel with the standard HRC (high interrupting capacity) English Electric fuses.

### **1.3 Pertinent and Brief Literature Review on Digital Protection**

Earlier protection schemes of power transformer protection are both electro-mechanical and analog electronic types. Since the 1960s research has moved towards computer relaying. The computer relaying in power transformer protection has been progressing in step with advances in high speed computing since the 1970s. The digital algorithms for power transformer protection have been the focus of the research in computer relaying. Rockefeller introduced a detailed digital scheme for fault protection in the joint Pacific Gas & Electric (PG&E) and Westinghouse sub-station project [9]. Digital relays for transformer protection are based on a harmonic restraint percentage differential current principle. The harmonic analysis is carried out for digital processing of the differential current samples. The primary design objective is to find a fast and accurate algorithm to quickly calculate the fundamental, second and higher, (particularly the fifth) harmonic components from the current samples. Sykes and Morrison attempted to extract the fundamental (1<sup>st</sup>) and second harmonic (2<sup>nd</sup>) components of differential current samples

using two recursive filters [14]. The ratio of 2<sup>nd</sup>/1<sup>st</sup> harmonics has been obtained to distinguish between the magnetizing inrush and fault currents of a power transformer using digital filters [12, 14]. Malik proposed the cross-correlation algorithm which involves computation of odd and even functions of any harmonics from the differential current samples [16]. The ratio of 2<sup>nd</sup>/1<sup>st</sup> harmonics has been used as a threshold value to declare the inrush condition, if it is more than 17%. Schweitzer used the finite impulse response (FIR) filter to estimate the harmonic components of the differential current of a power transformer protection to declare the fault, if the ratio of 2<sup>nd</sup>/1<sup>st</sup> harmonic magnitudes is less than 17% [17]. Degens used the least square curve-fitting technique to find the ratio of 2<sup>nd</sup>/1<sup>st</sup> harmonic components for restraining an inrush trip in a power transformer [20]. Rahman extended it to include the weighted least square algorithm for better restraint of the inrush trip in an over-excited power distribution transformer [22]. Ramamoorthy introduced the Fourier transform technique to extract the harmonic components of current from one cycle of inrush or fault current samples [11]. In these earlier digital protections of power transformers up to 16 current samples per cycle were used for simulations and field tests.

The rectangular transform algorithm involving computation of Fourier sine and cosine coefficients has been used by Rahman and Dash for fast but reliable protection of power transformers [24]. The response of the algorithm was reasonably fast because the calculation of the harmonic coefficients up to the 5<sup>th</sup> requires only a few additions and subtractions. It was both simulated and experimentally tested using an Intel 8085 microprocessor. These protection schemes for power transformers were implemented using 12 current samples per cycle [24]. Thorp and Phadke utilized a discrete Fourier

transform (DFT) algorithm for microprocessor based protection of power transformers using also 12 current samples per cycle [23].

Many other digital algorithms have been used for power transformer protection. These include the Kalman filtering technique [33, 38], spectral observer technique [31], Walsh functions [29], Haar function [27], artificial neural networks [51], wavelet packet transforms [55, 57], wavelet filter banks [58], a multi-resolution signal decomposition technique [53] and electromagnetic transient models [44], etc.

In both simulation and experimental testing of modern digital protection of power transformers following the IEEE standard of six cycles of the 60 Hz in North America. The 16 current samples per cycle which cover 100 ms for 6 cycles, are used because of the availability of high speed and large memory capabilities of modern computers.

A comparative analysis on various algorithms for differential protection of three phase power transformers has been made by Habib and Martin [32]. Performance indices have been calculated on the basis of computing time and sampling frequency using 16 samples per cycle. Rahman and Jeyasurya have systematically carried out another comparative study of six algorithms, namely discrete Fourier transform, rectangular transform, Walsh functions, Haar functions, finite impulse response and least square curve fitting techniques for the digital protection of power transformers using the same mainframe computer. The common sampling frequency was 960 Hz and 16 current samples per cycle were used. It has been established in both independent studies that the Discrete Fourier transform is the most efficient algorithm in terms of speed, accuracy

and reliability for the harmonic restraint differential protection of power transformers. A brief analysis of the popular DFT technique is presented in the next section.

### 1.3.1 Digital Algorithms for Power Transformer Protection

For power transformer protection, there exist many digital relay algorithms. Some of the algorithms are discussed in the above paragraph. Most of these are based on the harmonic restraint. Generally these are similar to each other. But the only difference is the method of calculating the harmonic components. It has been found that among these algorithms the discrete Fourier transform (DFT) is the best one in terms of speed, accuracy, memory requirements and reliability [11, 32 and 33]. A brief description of this technique is discussed in the section below.

### 1.3.2 Discrete Fourier Transform (DFT)

Ramamoorthy was the first researcher who proposed that the fundamental component of a current wave can be extracted from the fault transient by correlating the stored samples of sine and cosine waves [11]. Fourier series were used to develop this theory. Fourier series theory states that any periodic function  $f(t)$  having a finite number of discontinuities in the interval of  $(0,T)$  can be modeled in the interval as:

$$f(t) = \frac{a_0}{2} + \sum_{k=1}^{\infty} (C_k \cos(k\omega t) + S_k \sin(k\omega t)) \dots \dots \dots (1.1)$$

where

$$a_0 = \frac{2}{T} \int_0^T f(t) dt$$

$$S_k = \frac{2}{T} \int_0^T f(t) \sin(k\omega t) dt$$

$$C_k = \frac{2}{T} \int_0^T f(t) \cos(k\omega t) dt \dots\dots\dots (1.2)$$

$a_0$  is the dc component or average value and  $S_k$  and  $C_k$  are the sine and cosine functions of the Fourier coefficients, respectively. If the wave is sampled at equal time intervals and time space  $\Delta T$  then there is a total of  $N/\Delta T$  samples per cycle, the  $S_k$  and  $C_k$  can be represented as:

$$S_k = \frac{2}{N} \sum_{n=0}^{N-1} x(n) \sin\left(\frac{2\pi kn}{N}\right) \dots\dots\dots (1.3)$$

$$C_k = \frac{2}{N} \sum_{n=0}^{N-1} x(n) \cos\left(\frac{2\pi kn}{N}\right) \dots\dots\dots (1.4)$$

where  $x(n)$  is the sampled waveform at the nth instant.

A matrix presentation of the above equations is as follows:

$$S = C_s X \dots\dots\dots (1.5)$$

$$C = C_c X \dots\dots\dots (1.6)$$

where  $S$ ,  $C$  are the vectors containing sine and cosine components of the sampled waveforms, respectively.  $C_s$  and  $C_c$  are system matrices containing sine and cosine coefficients, respectively.  $X$  is the vector containing the sampled waveform to be analyzed. The dimension of the system matrices  $C_s$  and  $C_c$  are  $N \times N$  whereas vectors  $C$ ,  $S$  and  $X$  are of the length  $N$ . For the protection of the power transformer a data window of 16 sample per cycles ( $N=16$ ) is selected to get the all the required harmonics [37]. The cosine ( $C_c$ ) and sine ( $C_s$ ) system matrices are as following:

$$C_c = \begin{bmatrix} \cos\left(\frac{2 \times \pi \times 1 \times 1}{16}\right) & \cos\left(\frac{2 \times \pi \times 2 \times 1}{16}\right) & \dots & \cos\left(\frac{2 \times \pi \times 16 \times 1}{16}\right) \\ \cos\left(\frac{2 \times \pi \times 1 \times 2}{16}\right) & \cos\left(\frac{2 \times \pi \times 2 \times 2}{16}\right) & \dots & \cos\left(\frac{2 \times \pi \times 16 \times 2}{16}\right) \\ \vdots & \vdots & \ddots & \vdots \\ \cos\left(\frac{2 \times \pi \times 1 \times 16}{16}\right) & \cos\left(\frac{2 \times \pi \times 2 \times 16}{16}\right) & \dots & \cos\left(\frac{2 \times \pi \times 16 \times 16}{16}\right) \end{bmatrix} \dots \dots \quad (1.7)$$

$$C_s = \begin{bmatrix} \sin\left(\frac{2 \times \pi \times 1 \times 1}{16}\right) & \sin\left(\frac{2 \times \pi \times 2 \times 1}{16}\right) & \dots & \sin\left(\frac{2 \times \pi \times 16 \times 1}{16}\right) \\ \sin\left(\frac{2 \times \pi \times 1 \times 2}{16}\right) & \sin\left(\frac{2 \times \pi \times 2 \times 2}{16}\right) & \dots & \sin\left(\frac{2 \times \pi \times 16 \times 2}{16}\right) \\ \vdots & \vdots & \ddots & \vdots \\ \sin\left(\frac{2 \times \pi \times 1 \times 16}{16}\right) & \sin\left(\frac{2 \times \pi \times 2 \times 16}{16}\right) & \dots & \sin\left(\frac{2 \times \pi \times 16 \times 16}{16}\right) \end{bmatrix} \dots \dots \quad (1.8)$$

From the system matrices  $C_s$  and  $C_c$ , the amplitude of the nth harmonic can be computed

$$\text{as: } F_k = \sqrt{(S_k^2 + C_k^2)} \dots \dots \dots \quad (1.9)$$

where  $F_k$  is the kth harmonic Fourier coefficient and  $k = 1, 2, 3, \dots, N$ .

### 1.3.3 Application of Discrete Fourier Transform (DFT) in Power Distribution Transformer Protection

The DFT coefficients are of frequency selective filters and these coefficients are used to extract the frequency components from time domain signals. In the power distribution transformer protection, three such filters are used to extract the fundamental, second and fifth harmonic components. From the equation (1.9), these harmonics can be calculated. These are  $F_1$ ,  $F_2$  and  $F_5$  respectively.

In the case of magnetizing inrush current the ratio of  $F_2/F_1$  is greater than 17.7% and it is less than 17.7% for internal faults. For the magnetizing inrush current the magnitude is quite high for the first few cycles but the ratio  $F_2/F_1$  remains higher than the threshold level of 17.7% and thus the protection relay would restrain from operation for magnetizing inrush conditions. For the internal faults the ratio  $F_2/F_1$  is less than the

threshold level of 17.7% and thus operates the protection relay. In the over excitation and saturation cases the ratio  $F_2/F_1$  may fall below the threshold level of 17.7% and there exists no fault, then the ratio  $F_5/F_1$  is calculated and its threshold value is 6.5%. If the ratio is above than this level, then there is no fault condition and a restraint signal is given to the relay for not tripping.

#### **1.4 Purpose of This Thesis**

There are several techniques for realizing the microprocessor based digital protection of the power transformer. Each technique has offered some operational advantages like speed, accuracy, reliability and size. The performances of some differential protection techniques were investigated off-line while others were experimentally verified. Despite testing different transformers, which caused some performance variations, performance comparison between various protections techniques are reported in the literature.

The purpose of this thesis is to realize the microcontroller based digital protection system for a laboratory power transformer to achieve reliable, accurate, flexible and cost effective protection which is compact in size. The developed digital protective relay is based on harmonic analysis, which is realized employing the discrete Fourier transform (DFT). These current signals are passed through an anti-aliasing filter before being digitized by the analog to digital converters (ADC) on the input side of the microprocessor. The developed DFT-based harmonic analysis is designed to extract the 1<sup>st</sup>, 2<sup>nd</sup>, and 5<sup>th</sup> harmonics, present in the differential currents. The distinction between fault and magnetizing inrush currents is set based on the ratios of 2<sup>nd</sup> to 1<sup>st</sup> harmonics, as well as the 5<sup>th</sup> to 1<sup>st</sup> ones.

The hardware part consists of a current to voltage isolator as scaling circuits to acquire the current signal from current transformers on the primary and secondary sides of the tested power transformer in the MUN power research laboratory. Anti-aliasing filters are used to eliminate the unwanted signals. Certain threshold levels are predefined according to the transformer parameters. These levels are defined in the software. These parameters are verified according to the speed of the processor. All analog to digital conversions take place in the controller board. The Discrete Fourier Transform (DFT) is used in this protection system.

### **1.5 Outline of the thesis**

Chapter 1: It states the problem.

Chapter 2: It provides the non-linear behaviour of a power transformer through illustrating the magnetizing inrush phenomena, along with the magnetizing saturation of the core and current transformer. It also discusses over excitation in power transformers.

Chapter 3: It provides the details of hardware implementation. It includes scaling circuit analog filter microcontroller, electronic control circuit and electronic switch.

Chapter 4: It gives the details of software execution for fault and no fault conditions (inrush) by using harmonics ratios.

Chapter 5: Harmonics ratios are analyzed and tested for the no fault (inrush) and fault conditions. It provides the real time testing of software and hardware designs. These results are evaluated in MATLAB environment.

Chapter 6: It summarizes the conclusions and suggests future works.

## **Chapter 2**

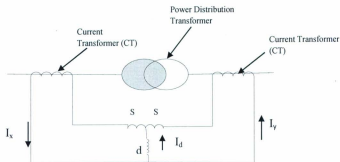
### **Power Transformer Protection Principles**

Among the different protection techniques the differential protection method is the most popular one. In the following sections this method is discussed.

#### **2.1 Differential Protection Technique**

The differential protection technique is based on extraction of information from differential currents, which are determined as the differences between the primary and secondary currents. In normal conditions the differential currents must have very small values. Figure 2.1 shows the schematic diagram for a basic biased differential circuit, where the net current flowing in the differential circuit is used for protection purposes.

The net current flow in the operating relay would operate the relay. Due to current transformer saturation or magnetizing inrush current, the unbiased protective system may operate and thus cause the unnecessary tripping of the system. Therefore the restraining coil is energised in the protection circuit to overcome this problem.



S=Restraint circuit coil

d=Operate circuit coil

Figure 2.1: Biased Transformer Differential Protection [61]

## 2.2 Tripping Characteristics of Differential Relay

The tripping actions of a differential relay are determined based on the differential current  $I_d$ .

$$I_d = I_x - I_y \quad (2.1)$$

This current represents the difference between the primary current  $I_x$  and secondary current  $I_y$ . The current  $I_d$  can also have a value due to:

1. Current transformers mismatch on primary and secondary side.
2. Saturation in the core of the main transformer or the current transformer.
3. Transient disturbances such as magnetizing inrush or fault currents, open supply and over-excitation.

In general, differential protection is used for protecting various components in power systems. This differential protection provides, with high selectivity of the protection

differential relay, from internal fault and shunt faults. This protection principle is used for the protection of generators, motors, power transformers and transmission lines.

For power transformers, we have to arrange special protection techniques, due to non linear characteristics of the transformer. That is the reason, the ratios of the 2<sup>nd</sup> and 5<sup>th</sup> harmonics to the fundamental component of the differential current are applied for restraining purposes [5]. Figure 2.2 shows the restraining and tripping area of the differential current with respect to the bias current [61].

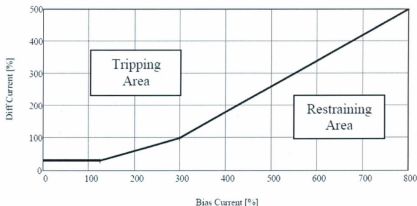


Figure 2.2: Differential Relay Tripping Characteristics [61]

### 2.3 Magnetizing Inrush Current

An internal fault causes significant current to operate the differential relay. But in the same time, magnetizing inrush, saturation of current transformer and over excitation of current transformer may also energize the trip coil of the differential relay.

The response of the inrush current depends upon the switching angle of the input voltage. Figure 2.3 shows the sample example of decreasing amplitude of the inrush current with time when switching angle of the input voltage is zero. The other responses, with the different switching angles of the input voltage are shown in the appendix B. This single phase simulation result of inrush current is obtained using Matlab. The residual flux in the lamination core of a 3-phase transformer is not considered.

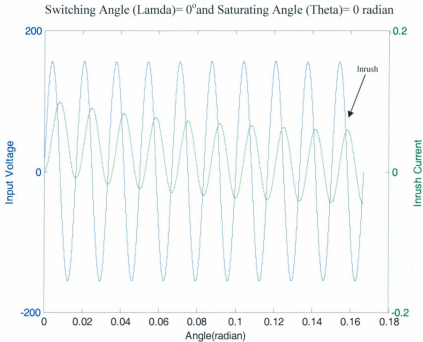


Figure 2.3: Input Voltage and Inrush Current when Switching Angle =  $0^\circ$

When the transformer is switched ON, the steady state flux enters in the core of transformer. Here the secondary of the transformer is open. The flux is quadrature with the input voltage, neglecting the resistance of the windings. The flux in the core has

the same shape but may have different in amplitude and phase shift. The starting point of the steady flux is also dependent on residual flux, Figure 2.4. Total flux at any instant would be the sum of steady state flux and residual flux. Transient flux at any instant is equal to the magnitude of residual flux. It is analogous to the dc transient component of asymmetrical faults currents. Inrush would be zero at point Y, as the instantaneous flux is the same as the residual flux. Magnetizing inrush current occurs when the polarity and magnitude of the residual flux do not agree with the polarity and magnitude of the instantaneous flux [5]. The amplitude of the inrush varies depending upon the switching angle and the residual flux. In the figure 2.4, the switch is closed at 0. The residual flux is in the positive direction. At point X the steady state flux is zero and at point Y the steady state flux is equal to the residual flux.

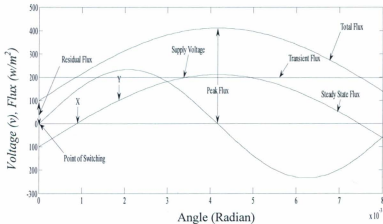


Figure 2.4: Voltage, flux and current during the magnetizing inrush current.

The transformer is energised at 0 degree of switching. If the transformer is energised at point Y, there would not be any inrush as the residual flux is equal to the steady state

flux. There would not be any transient flux at this point. If the transformer is energized at the  $180^\circ$  position, then the transient flux would be produced in the opposite direction [5]. The amount of the residual flux is determined by the hysteresis curve of the transformer. The excitation curve of figure 2.5 can be used to establish the inrush curve. Assume that sections OS and SP are straight lines. By extending the points on instantaneous flux at  $90^\circ$  degree, we get the point  $I_x$  and flux. Similarly extending other points we get the entire curve for inrush current.

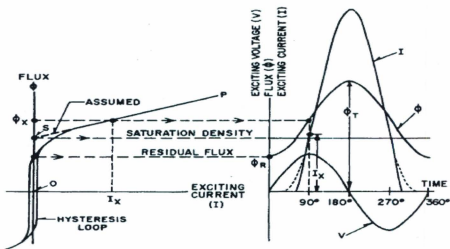


Figure 2.5: Derivation of magnetizing inrush current from the excitation characteristic [5]

If the residual flux is equal to the saturation density, the inrush current would be a sine wave while offsetting the negative cycle. Here the fault current cannot be distinguished from the inrush current. But practically the residual flux is always less than the saturation density. This inrush wave form is different from the fault current waveform.

In the figure 2.5 residual fluxes are taken to be 40% of the rated flux. In the modern steel core transformer the residual flux is 90% of the maximum rated flux.

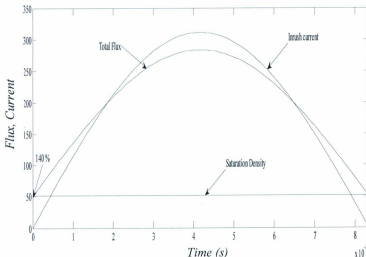


Figure 2.6: Effect of residual flux on inrush current, at saturation density [5]

The damping effect due to the resistance of the source and winding of the transformer would reduce the excitation voltage and thus reduce the inrush current. This damping effect is taken as a safety factor against the false tripping of differential relays. This is shown in figure 2.7. In modern steel the saturation density is fixed to 140% rated peak flux. The width of the inrush has reduced to 330° as compared to the figure 2.5 due to the damping effect. The harmonic contents of the inrush shown in the figure 2.6 are as follows [5]:

Fundamental=100%

Second Harmonic= 17.1%

Third harmonic= 7.4%

The minimum possible second harmonic component is 16 to 17% of the fundamental.

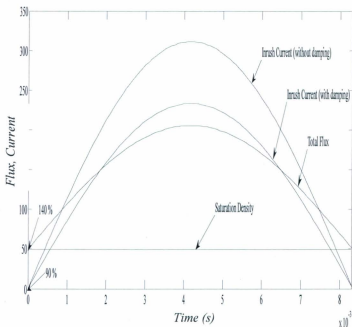


Figure 2.7: Effect of residual flux on inrush current, at 90% saturation density

Inrush current is complicated in the three-phase transformers. It can be in more than one phase. These phases can also be affected by the connections and magnetic coupling between the phases. The maximum amount of residual flux in each phase would be 90% of the rated flux.

The magnetizing inrush current is significantly dependent upon the residual flux in the core. As shown in figure 2.8 the transformer with the magnetic material, with a sharp knee point, has a flat magnetizing curve above the knee point. Two different types of the core materials are being used. The grain oriented electrical steel, (the newer type),

has a greater portion of the residual magnetization as compared to the non-oriented electrical steel (older type). The gap of maximum residual flux is along the y-intercept between the  $1.4 \text{ Wb/m}^2$  and  $1.8 \text{ Wb/m}^2$ .

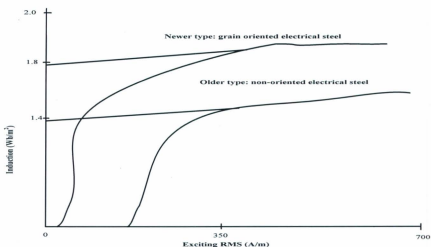


Figure 2.8: Magnetizing Curve for Steel Core Transformers [13]

## 2.4 Over-excitation

A common transformer with the standard iron lamination core is operated in the range of  $1.4 \text{ Wb/m}^2$  to  $1.8 \text{ Wb/m}^2$ . When this flux goes beyond this limit then the transformer is in an overexcited state and can cause transformer winding damage in a few seconds. This over excitation may be due to high input voltage, low frequency, clearance of the fault. Only the fuse can protect this type of fault. Under specification of the fuse may cause this fault. The third and fifth harmonics may distinguish the over-excitation and fault or load current. The third harmonic can be filtered out by the three phase current transformer with delta connection on Y-side. The 5<sup>th</sup> harmonic restraint is applied to

prevent the tripping from normal over excitation. 12 to 16 samples per cycle are required for good measurement of the 5<sup>th</sup> harmonic.

## **2.5 Current Transformer Saturation**

Current transformers are used to take the sample current for the differential relays. These transformers can be saturated when excessive current is conducted through them. This saturation occurs due to slow decaying dc components of internal and external faults. The dc component arises due to inductive behaviour of the coil of the current transformer. Percentage biasing of the differential relay is applied to overcome this problem [3].

## **2.6 Three Phase Transformer Protection**

Three phase differential protection is more difficult than the single phase transformer protection technique. Here, three phases are to be considered on both sides of the transformer.

### **2.6.1 Current Transformers (CTs)**

These are the sensing part of the test equipment. It takes the current from each phase for data analysis. Three CTs are used at the primary side and three are used on the secondary side of the transformer. In order to block the zero sequence current on external ground fault and to compensate for the 30 degree phase shift by Y/ $\Delta$  connection of the main transformer, the three transformers on the delta ( $\Delta$ ) side of the main transformer are connected in Y and Y side if the main transformer is connected in delta ( $\Delta$ ).

Figure 2.9 shows when an external ground fault exists. If CTs are connected in delta there would not be any zero sequence current and if these are in Y-configuration, it would trip the relay. The current in delta ( $\Delta$ ) connected CTs would have current  $(1/\sqrt{3})$  times the Y connected CTs. These CTs have to match the rated current of the transformer (as these current of the main transformer inverse ratio of current as comparing primary and secondary). If the transformer has tap changing then the differential protection system must fulfill the requirements.

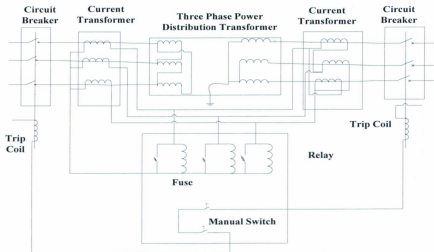


Figure 2.9 Differential Protection Scheme for Three Phase Power Transformer [4].

In this the power transformer is delta-star connected. On delta side the CTs are connected in star and on the star side the CTs are connected in delta as shown in the figure 2.9. Under normal working conditions the circulating currents caused by the primary and secondary load current in the relay circuit will balance; but under fault

conditions the balance will no longer be there and the relay will be energized to trip the circuit breakers on the primary and secondary side.

### 2.6.2 Harmonic Restraints for Differential Protection

Magnetic Inrush current appears as an internal fault current and it needs to be addressed. Normal biasing in the differential protection is ineffective. Harmonic restraint is required to prevent misoperation of relays. In the start, as shown in figure 2.10, harmonic restraint rectifies the inrush current and adds these in percentage restraint, through inductor- capacitor filtering. This is a single-phase protection system but it can be extended to a three-phase system. This relay is adjusted until the second harmonic crosses the certain predefined limit. Over-current protection is also provided as in the fault current, direct current offset and harmonics and fault current itself for safety purposes [7].

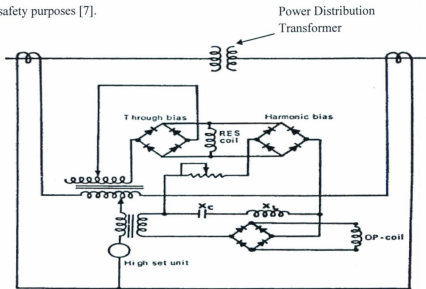


Figure 2.10: Basic circuit for harmonic restraint relay [7]

In figure 2.11, a separate blocking relay whose contacts are in series with differential relay, so that blocking relay would operate if the second harmonic is below the predefined limit [12].

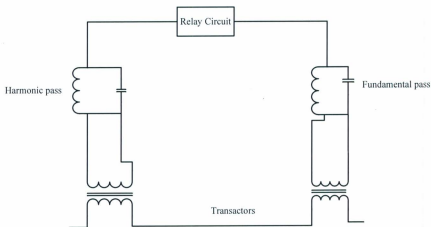


Figure 2.11: Basic circuit for harmonic blocking relay [12]

In conclusion, the basic elements of a modern power transformer relay are provided in this chapter. Here the inductor and capacitor are included to provide the restraint for the relay. In the next chapters, the harmonic ratios are used for the filtering of these harmonics from the faults. The discrete Fourier transform is used as an algorithm for the filtering.

## **Chapter 3**

# **Hardware Design of Microcontroller-based Protection of Three Phase Power Transformer**

### **3.1 Introduction**

Design of a hardware system is important for the power transformer protection. The design process involves both the electro-mechanical and electronic components for the successful protection of a power transformer. In chapter 2 the principle of protection against the inrush currents and the faults is explained. Figure 3.1 shows the electrical schematics of the laboratory 5kVA, 3-phase power transformer with tap changing provisions. The system block diagram is shown in figure 3.2. Holding circuit, multiplexing circuit, multiplexer and processor are included in the programmable controller card. The pertinent details are given in the following sections.

Three Phase 5kVA 230/550-575-600 V Delta/Wye Power Distribution Transformer

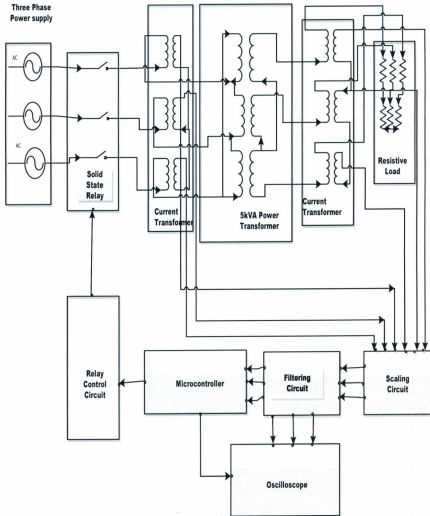


Figure 3.1: Experimental Set Up

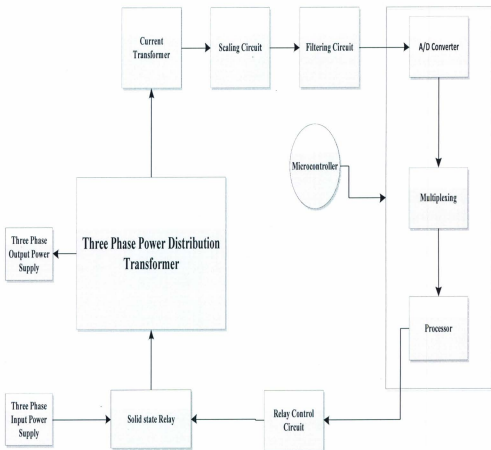


Figure 3.2: System Block Diagram

### Three Phase 5kVA 230/550-575-600 V Power Distribution Transformer-Testing Set-up

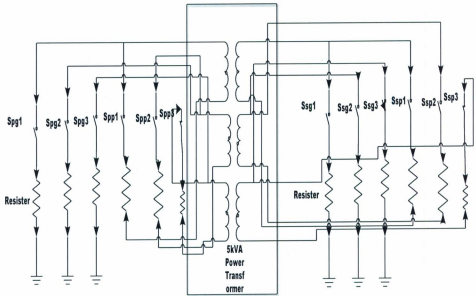


Figure 3.3: Experimental Set Up for Internal Faults Tests.

It is noted that  $S_{pg1}$ = Primary-side-Phase to ground switch 1,  $S_{pg2}$ = Primary-side-Phase to ground switch 2,  $S_{pg3}$ = Primary-side-Phase to ground switch 3,  $S_{pp1}$ = Primary-side-Phase to phase switch 1,  $S_{pp2}$ = Primary-side-Phase to phase switch 2,  $S_{pp3}$ = Primary-side-Phase to phase switch 3,  $S_{sg1}$ = Secondary -Phase to ground switch 1,  $S_{sg2}$ = Secondary -Phase to ground switch 2,  $S_{sg3}$ = Secondary -Phase to ground switch 3,  $S_{sp1}$ = Secondary -Phase to phase switch 1,  $S_{sp2}$ = Secondary -Phase to phase switch 2 and  $S_{sp3}$ = Secondary -Phase to phase switch 3.

### **3.2 Laboratory 3-phase Power Transformer**

The laboratory power transformer is provided by Siemens, Canada. It has the following specifications:

Power = 5kVA

Input Voltage = 230V

Output Voltages = 550V, 575V, 600V. 3 taps on the output side.

Input windings = Delta connected

Output windings = Y connected

Phase = 3 Phase

Type of cooling = Air cooling

### **3.3 Current Transformers**

A total of six current transformers (CTs) are used to sense input and output currents. One CT is connected in each phase for the primary and secondary sides, respectively. To overcome the zero sequence current, the primary side three current transformers are connected in a Wye configuration, whereas the secondary side of the laboratory test transformer, the three current transformers are connected in a Delta configuration. The shunt resistances at the output of the current transformers are included at both sides of the laboratory transformer. The values of the shunt resistances are  $0.3 \Omega$  for all current transformers, CTs.

The rating of the current transformer is as follows:

Input = 120 A

Output = 5 A

Cooling = Air Cooled

Shunt resistance =  $0.3 \Omega$

### **3.4 Relay Control Circuit**

The solid state relay is controlled through with the Darlington pair. Two NPN transistors are connected together to get the high current gain. The circuit diagram is shown in figure 3.4. Output is given to each solid state relay. So, three control circuits are utilized for the three phase power laboratory transformer protection system. Input for the control circuit is taken from the processor.

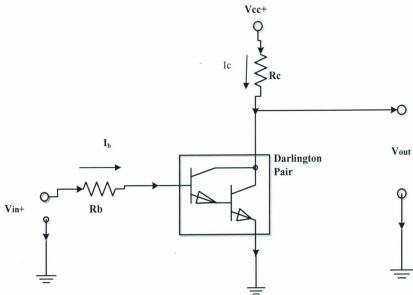


Figure 3.4: Relay Control Circuit

**Design Parameters:**

Darlington Pair of two NPN transistors

Model = 2N2222A

Turn On Time = 35ns

Turn Off Time = 285 ns

$V_{cc}$  = Collector Voltage = 5 V (DC)

$R_b$  = Base resistance = 1  $K\Omega$

$R_c$  = Collector resistance = 20 $\Omega$

$$I_c = V_{cc}/R_c = 250\text{mA}$$

$$I_b = V_{in}/R_b = 5/1000 = 5\text{mA}$$

For

$$V_{in} = 0\text{V}, V_{out} = 5\text{V or High}$$

$$V_{in} = 2-10\text{V dc}, V_{out} = 0\text{V or Low}$$

### 3.5 Solid State Relay

Crydom solid state relay is used for the switching. Its specifications are:

Model No. D2425

Input Voltage = 3-32V (DC)

Output Voltage-<sub>Max</sub> = 240 V (AC)

Output Current-<sub>Max</sub> = 25A

The equivalent circuit of the solid state relay is shown in figure 3.5. Two SCRs are coupled together. Gates are triggered from the opto-coupler. Three relays are used, one for each phase. Turn on time for this relay is .02 ms. It operates in less than half cycle of the input current.

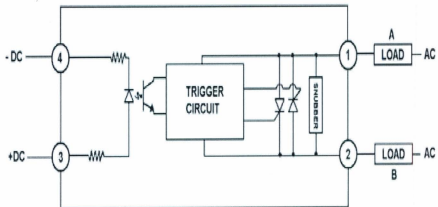


Figure 3.5: Equivalent circuit of Solid State Relay

### 3.6 Scaling Circuit

The current from the current transformer needs to be sensed and to be converted in dc voltage level for further evaluation. For this purpose, LM324 fourteen pins chip is selected. It has four Op-amps, each consists with the high gain and internally frequency compensated. The circuit diagram for this Quad Operational Amplifier is shown in figure 3.6.

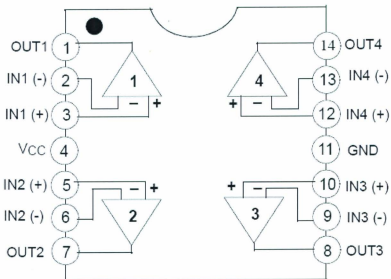


Figure 3.6: Quad Operational Amplifier

The gain of this amplifier is calculated as following:

$$Gain = \frac{V_o}{v_{in}} = 1 + \frac{R_A}{R_B}$$

where

$$R_A = 0 \text{ to } 5k\Omega$$

$$V_{cc} = 32V \text{ (dc)}$$

$$R_B = 5k\Omega$$

The circuit diagram for the scaling circuit is shown in figure 3.7. The response of the scaling circuit with different variable resistances ( $R_A$ ) is shown in figure 3.8, figure 3.9 and figure 3.10 respectively.

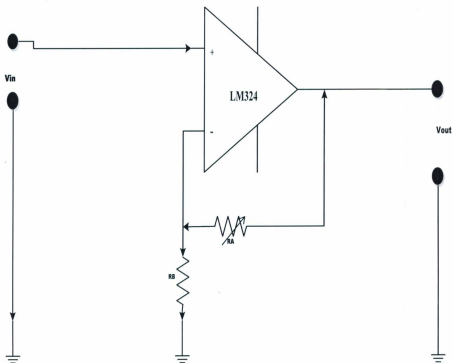


Figure 3.7: Scaling circuit

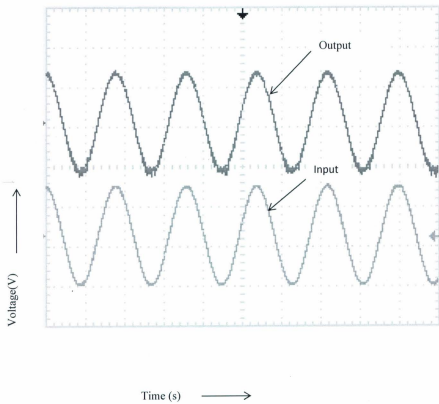


Figure 3.8: Scaling circuit when Low gain,  $R_A = 0$

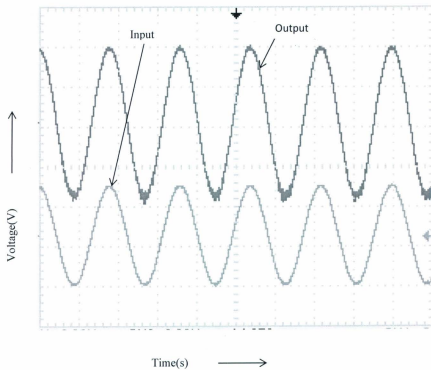


Figure 3.9: Scaling circuit when medium gain,  $R_A = 2.5K\Omega$

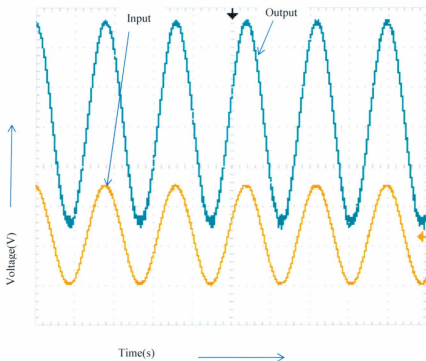


Figure 3.10: Scaling circuit when high gain,  $R_A = 5K\Omega$

The scaling circuit is tested for each phase of the 3-phase laboratory power transformer, both at primary side and secondary side. The output results are found to be perfect. A total of six scaling circuits are required to get six inputs to be analyzed.

### 3.7 Filtering Circuit

Whenever the sampling frequency is less than the twice the cut off frequency the phenomenon of the downward frequency translation occurs and it is called aliasing. Due to this effect the data in the sampled frequency cannot be linearly related with an input

continuous signal. To eliminate this error in the sampled frequency the input continuous signal must be filtered out to get the required signal.

For the power transformer differential protection, the design must detect the magnetizing inrush current by detecting the second harmonic component, and for over excitation the 5<sup>th</sup> harmonic component. To avoid the aliasing effect and preserve the fundamental component at 60Hz, second harmonic at 120Hz, and 5<sup>th</sup> harmonic at 300Hz, a low pass anti-aliasing filter is proposed. A cut off frequency ( $f_c$ ) of 350Hz and band stop frequency ( $f_s$ ) of 450 Hz are found to be practical. To get all three frequency components and to accommodate the differential protection algorithm, a sampling frequency of 960 Hz was chosen.

The Chebyshev filter was used for the anti-aliasing filter. It has a steep roll off characteristic near the cut off frequency. Referring to the filter specifications [46], minimum attenuation in the pass band is 0.3dB and maximum attenuation in stop band is 20dB. The Chebyshev low pass filter specifications are shown in figure 3.11.

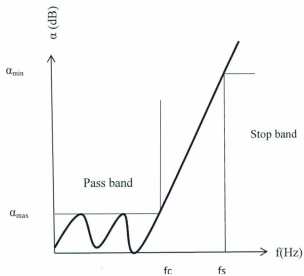


Figure 3.11: Chebyshev low pass filter specifications [46]

$\alpha_{max}$  = decibel attenuation in pass band

$\alpha_{min}$  = decibel attenuation in stop band

$f_c$  = Frequency at which  $\alpha_{max}$  occurs

$f_s$  = Frequency at which  $\alpha_{min}$  occurs

An anti-aliasing filter is required to overcome the aliasing effects, whenever the sampling frequency is less than the twice the frequency of the cut off frequency. To overcome these effects, the 6<sup>th</sup> order Chebyshev filter is proposed. Details of the design are given in the appendix A. The circuit diagram for the 6<sup>th</sup> order Chebyshev filter is shown in figure 3.12.

Design parameters are as follows:

$$\alpha_{\min} = 20\text{dB}$$

$$\alpha_{\max} = 0.3\text{ dB}$$

Cut Off Frequency = 350 Hz

Fundamental Frequency = 60 Hz

2<sup>nd</sup> Harmonic = 120 Hz

5<sup>th</sup> Harmonic = 300 Hz

Stop Band Frequency = 450 Hz

Order of Chebyshev filter (n) is given as:

$$n = \cosh^{-1} \left\{ \sqrt{\frac{\frac{\alpha_{\min}}{10^{\frac{\alpha_{\min}}{10}}} - 1}{\frac{\alpha_{\max}}{10^{\frac{\alpha_{\max}}{10}}} - 1}} \right\} \cosh^{-1} \left( \frac{\omega_s}{\omega_c} \right) \quad (3.1)$$

$$n = 6$$

The transfer function of the 6<sup>th</sup> order Chebyshev filter is:

$$T_s(6) = \frac{1.322 \cdot 10^{19}}{s^6 + 2925s^5 + 1.154 \cdot 10^7 s^4 + 2.039 \cdot 10^{10} s^3 + 3.257 \cdot 10^{13} s^2 + 1.368 \cdot 10^{16}} \quad (3.2)$$

Using this transfer function the frequency and phase response are found by simulation. The results of the simulation are shown in figure 3.13. The filter response shows that the cut off frequency is 2199 rad/sec (350 Hz), which ensures that all three harmonics pass through the filter and higher frequency components will be eliminated. The phase response is also linear for pass band. The program and detailed calculations are given in the appendix A. Six LM324 chips for all the three phases at primary and secondary side, respectively are used for the laboratory testing.

### Stage 1 (3.3)

$$\omega_{c1} = 9.4798 \cdot 10^2 \text{ rad/s}$$

$$C_1 = C_2 = 1 \mu\text{F}$$

$$R_1 = R_2 = 10.55 \text{ K}\Omega$$

$$R_{A1} = 1 \text{ k}\Omega$$

$$R_{B1} = 3.45 \text{ k}\Omega$$

### Stage 2 (3.4)

$$\omega_{c2} = 1.7315 \cdot 10^3 \text{ rad/s}$$

$$C_3 = C_4 = 1 \mu\text{F}$$

$$R_3 = R_4 = 5.775 \text{ K}\Omega$$

$$R_{A2} = 1k\Omega$$

$$R_{B2} = 4.38k\Omega$$

**Stage 3**

(3.5)

$$\omega_{c3} = 2.254 * 10^3 \text{rad/s}$$

$$C_5 = C_6 = 1 \mu\text{F}$$

$$R_5 = R_6 = 4.3K\Omega$$

$$R_{A3} = 1k\Omega$$

$$R_{B3} = 4.8k\Omega$$

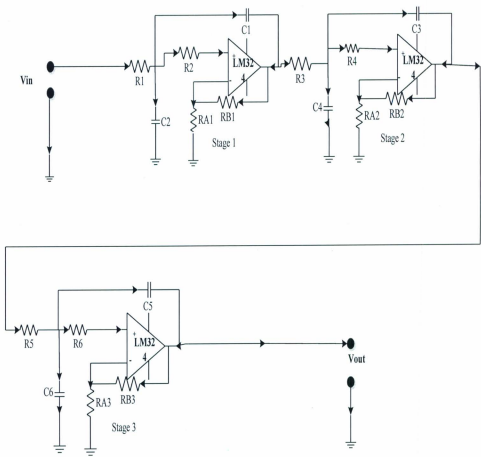


Figure 3.12: Circuit diagram for 6<sup>th</sup> order Chebyshev filter (anti-aliasing filter)

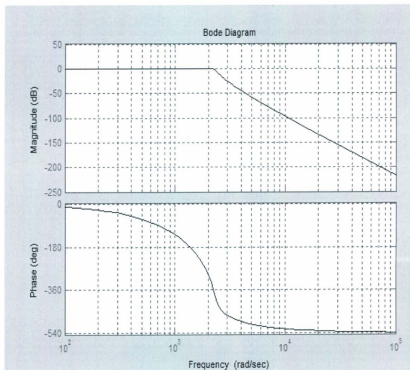


Figure 3.13: Output of Chebyshev filter

### 3.8 Microcontroller

After filtering the analog signal, it needs to be analyzed for decision making for fault and no fault conditions. The filtered analog signal is processed in the microcontroller. It is a 28/40-Pin, 8 bits CMOS flash Microcontroller PIC 16F877, which has been used for the experimental prototype digital relay. The scaled, filtered, sampled signal has to be presented to the analog-to-digital converter for conversion to form a number, which can be read by the microprocessor. An 8-channel 10-bit A/D convertor is within the microcontroller, making it ideal for real-time implementation in the experimental relay.

Multiplexing of the large amount of information in single line is done in the multiplexer in the controller. The microcontroller performs the power transformer differential protection functions and other tasks defined in the software. Port A is used for three input differential (filtered and scaled) currents and port B is used for the output. The same three inputs are used to analyze the data at the oscilloscope. The pin diagram of the used microcontroller is shown in figure. F 1.1 and the block diagram is shown in figure F.1.2 of the Appendix F. The main features of the microcontroller are as follows:

8K\*14 Words Flash Program Memory

368\*8 Bytes of data memory (RAM)

256\*8 Bytes of EEPROM data memory

A Compaq Laptop with 2G RAM and 80 G hard drive is used for writing the programme in the C language and it is downloaded to the processor via an RS232C cable through a PIC down loader. At any instant after scaling and filtering the three differential current signals are fed to the microcontroller where analog to digital conversion and then multiplexing of the signals are done. The signal is analyzed according to the discrete Fourier transform algorithm and a decision is taken for fault or no fault condition as specified in the software. This software operation will discuss in the next chapter.

## Chapter 4

# Software Design of Microcontroller-based Three Phase Power Transformer Protection

### 4.1 Introduction

In modern relays the use of analog and digital electronic circuit cards as well as computers is common. For laboratory testing, a 5kVA 230/550-575-600V,  $\Delta$ -Y connected three phase power transformer is analyzed.

$$I_{\text{rated,primary}} = \left( \frac{5000}{\sqrt{3} \cdot 230} \right) = 12.55 \text{ A} \quad (4.1)$$

### 4.2 Software Design

There are three input differential currents to the programmable controller. These are  $I_{da}$ ,  $I_{db}$ , and  $I_{dc}$ . The processor is doing the calculations for the fundamental, 2<sup>nd</sup> and 5<sup>th</sup> harmonic components. The discrete Fourier transform technique is used to get the harmonics. Data format and scaling are required for laboratory 5kVA power transformer protection. A flow chart for the power transformer differential relay is shown in figure 4.1. A stop for loop is applicable whenever there is interrupt signal, applied externally to the microcontroller.

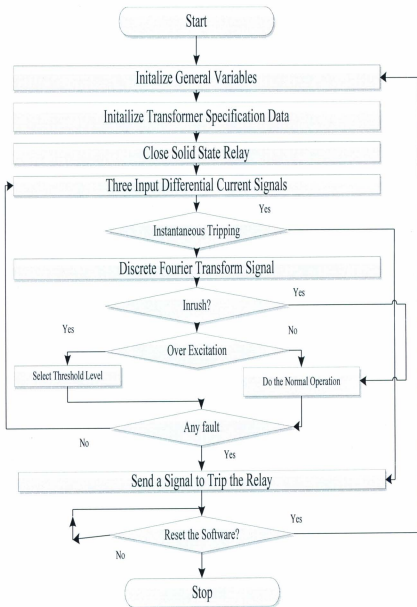


Figure 4.1: Flow Chart for Differential Relay Protection

#### 4.2.1 DFT Method for Harmonics Calculation

Detailed calculations of the Fourier coefficients are given in the Appendix C.

S = Sine function

C = Cosine function

$$S_j = \frac{2}{N} \sum_{i=1}^{i=N} \left( I_{dk} * \left( \sin \frac{2 * \pi * j * i}{N} \right) \right) \quad (4.1)$$

$$C_j = \frac{2}{N} \sum_{i=1}^{i=N} \left( I_{dk} * \left( \cos \frac{2 * \pi * j * i}{N} \right) \right) \quad (4.2)$$

N = 16

$\pi = 3.14 \dots$

j = 1, 2 and 5

k = a, b and c are differential phases

I<sub>d</sub> = Differential current

For Fundamental Component:

$$H_1^2 = S_{1a}^2 + S_{1b}^2 + S_{1c}^2 + C_{1a}^2 + C_{1b}^2 + C_{1c}^2 \quad (4.3)$$

For Second Harmonic:

$$H_2^2 = S_{2a}^2 + S_{2b}^2 + S_{2c}^2 + C_{2a}^2 + C_{2b}^2 + C_{2c}^2 \quad (4.4)$$

For 5<sup>th</sup> Harmonic:

$$H_5^2 = S_{5a}^2 + S_{5b}^2 + S_{5c}^2 + C_{5a}^2 + C_{5b}^2 + C_{5c}^2 \quad (4.5)$$

The flow chart of the subroutine for this algorithm is shown in the figure 4.2.

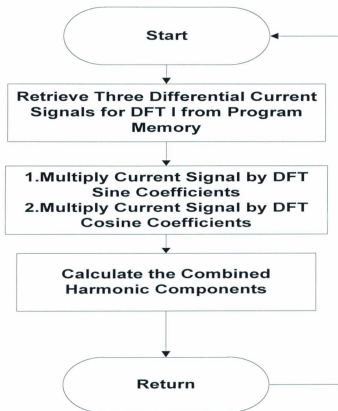


Figure 4.2: Flow Chart for Harmonic Calculations -Discrete Fourier Transform Method

## 4.2.2 Criteria for Harmonic Calculations

For Magnetizing Inrush Current:

$$\frac{H_2}{H_1} \geq 0.177 \quad (4.6)$$

Then no fault

For over excitation:

$$\frac{H_5}{H_1} \geq 0.065 \quad (4.7)$$

As the current to voltage isolator has a range from 0 to 10V dc, the reference voltage for instantaneous tripping of the digital relay 5V dc is taken as reference to save the test equipment. For Instantaneous tripping of the circuit breakers, voltage level setting for each phase is as follows:

$$V_a \geq 5V \quad (4.8)$$

$$V_b \geq 5V \quad (4.9)$$

$$V_c \geq 5V \quad (4.10)$$

where

$V_a$  =Reference voltage for phase A,

$V_b$  =Reference voltage for phase B

and  $V_c$  =Reference voltage for phase C

### 4.3 Protection Scheme

Differential current samples are taken and fed to the memory for reference. A DFT scheme is applied for the calculation of Fourier coefficients. In normal operations the digital relay is on and the transformer is in operation. The electronic relay gives the tripping signal whenever there is short circuiting or an internal fault. Equations (4.7) and (4.8) are used for inrush current conditions. The microcontroller is checking these conditions continuously. If these conditions are not met, then it concludes that it is a fault condition, and trips the relay. The input baud rate is 9600 samples per second and the window size for calculating the harmonics is 16 per cycle. The code for the microcontroller is given in appendix E. The system layout for analyzing the data in MATLAB is shown in figure 3.1. A four channel oscilloscope is used to observe the three input differential currents and the response of the electronic relay. Some sample results are discussed in chapter 5.

## Chapter 5

# Experimental Testing For Digital Protection of Power Transformer

### 5.1 Introduction

This chapter presents the experimental setup for testing a laboratory 3-phase power transformer. The 5kVA, three-phase power distribution transformer is used for the real time testing. Electronic control circuit and solid state relay are implemented on one circuit board. Three parallel light bulbs are also added with the electronic relays to see the continuous operation of the transformer and the digital switching actions. Both the circuits are tested separately, and give satisfactory results. No fault and fault conditions are analyzed and tested on the basis of harmonics over fundamental ratio criteria. High magnetizing inrush current is not a fault condition, and hence the digital protection scheme treats it as no fault condition. This is done by taking the ratio of magnitude of the 2<sup>nd</sup> harmonic component over fundamental, ( $2^{nd}/1^{st}$ ) greater than 17.7%. In the fault conditions, it would be less than this ratio value. However, for the over excitation case, if the ratio of 5<sup>th</sup> harmonic over fundamental, ( $5^{th}/1^{st}$ ) is less than 6.5%, then it would be considered also as no fault condition. The microcontroller checks both conditions almost instantaneously, and declares fault or no fault conditions, and initiates appropriate protective actions. In the next sections of this chapter, these no fault and fault conditions

are experimentally tested in a laboratory environment. The photograph of the experimental set up is shown in figure 5.1. Some sample results are presented below. More detailed results are given in appendix D.

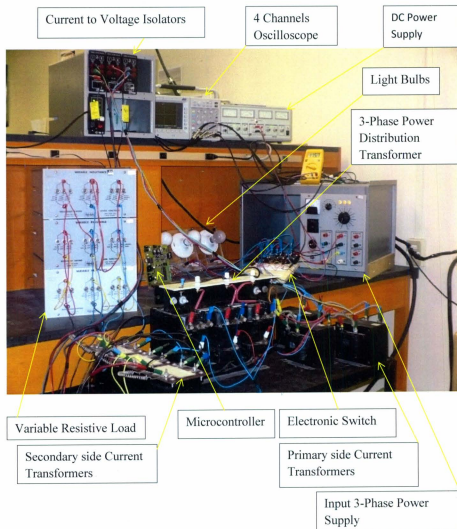


Figure 5.1: Photograph of Experimental Set up

## 5.2 Magnetizing Inrush Current Tests

This test was carried out without load, fixed resistive load ( $600\Omega$ ) and different resistive load ( $600/1200/2400\ \Omega$ ) and  $120V$  is applied. An electronic circuit breaker with the triac switch for the electronic relay for each phase of primary and secondary sides of the 3-phase transformer was employed for testing. While continuously switching the input power supply, the magnetizing inrush current phenomenon was observed. The differential current ( $I_{da}$ ) of phase A, its harmonics and the no tripping response of the electronic switch are shown in figures 5.2, 5.3 and 5.4, respectively. The following results are obtained during the inrush from the differential currents. The harmonic magnitudes and their ratios over fundamental are obtained in MATLAB from the inrush waveform of figure 5.3. The other two phases (phase B and phase C) with harmonics are given in appendix D as shown in figures D.22 to D.36. The noise in the response of the electronic switch is observed in fig.5.4 due to the interference of high frequency around the microcontroller.

Magnetizing Inrush Current at No load

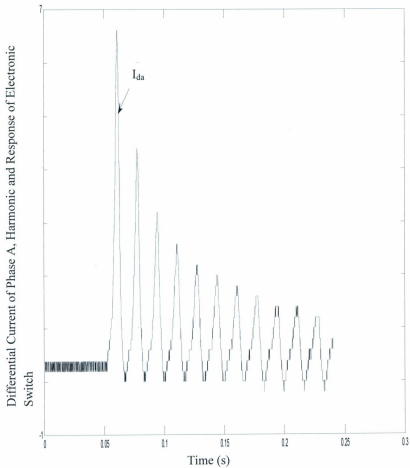


Figure 5.2: Experimental inrush current response for phase A

$I_{da}$ =Differential current of phase A

### Harmonics Analysis: Magnetizing Inrush

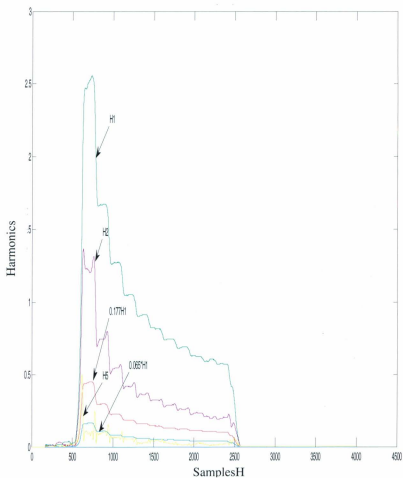


Figure 5.3: Experimental current harmonics in phase A

$H_1$  = Fundamental Harmonic,  $H_2$  = 2<sup>nd</sup> Harmonic and  $H_5$  = 5<sup>th</sup> harmonic

In figure 5.3, during the time scaled samples (500 to 2500) of the magnetizing inrush currents, the following results are observed:

$$H_2 > 0.177 * H_1 \quad (5.1)$$

$$H_5 < 0.065 * H_1$$

It is to be noted that there is no trip signal for the magnetizing current even at 9 cycles.

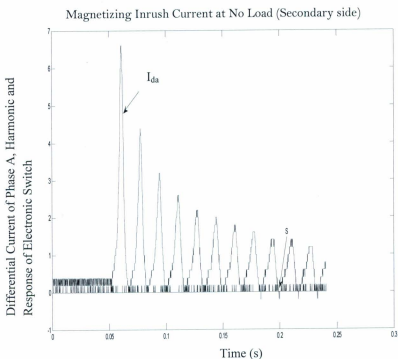


Figure 5.4: Experimental magnetizing inrush current and response of electronic switch

$I_{da}$  = Differential Current of Phase A,      S = Response of Electronic Switch

There is some noise at the bottom of the experimental response due to high frequency

### **5.3 Internal Fault Tests**

Controlled internal faults were tested in the laboratory. These tests are as following:

Primary side:

Phase to Neutral fault

Phase to Phase fault

Phase to Ground fault

Secondary side:

Phase to Neutral fault

Phase to Phase fault

Phase to Ground fault

An electronic switch is connected in series of each phase on both sides of the transformer.

A short circuit was imposed for a short duration of time while the input to the transformer was maintained at 50% of its rated value (60V).

#### **5.3.1 Phase to Ground Fault (Primary side-secondary unloaded)**

This fault was created by pressing switch  $s_{pg1}/s_{pg2}/s_{pg3}$ , as shown in figure 3.3. The switch responded in 0.045 seconds. The following results were observed: The fault was initiated at 0.11s, the fault current in phase A is increased, and within 3 cycles the trip signal was successfully activated to isolate the faulted phase A as shown in figure 5.5.

Phase A to Ground Fault at Primary side and Secondary side Open

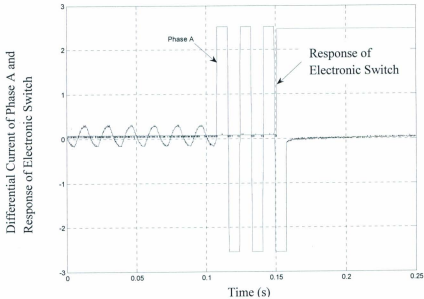


Figure 5.5: Experimental phase to ground fault and response of the electronic switch

In figure 5.6, during the fault in phase A, the following conditions were observed:

$$H_2 < 0.177 * H_1 \quad (5.2)$$

$$H_5 > 0.065 * H_1$$

The microcontroller gives the instruction to trip the circuit breaker switch, and isolate the fault of the power transformer as shown in fig. 5.5. Differential current, harmonics and ratios are given in figure 5.6.

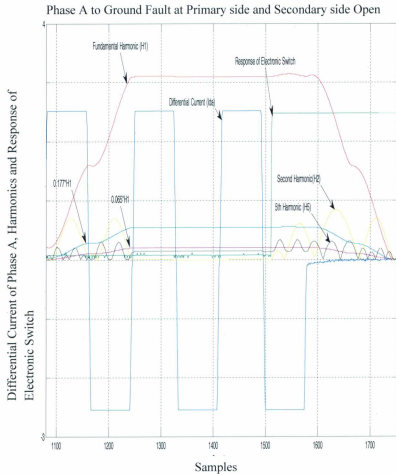


Figure 5.6: Phase A to ground fault at no load power transformer, harmonics and response of electronic switch.

Appendix D contains the fault results at no load of the phase B and phase C cases, as shown in figures D.2-D.6.

### 5.3.2 Phase to Ground Fault (Primary side-secondary at equal resistive load)

This fault was created by pressing switch  $s_{pg1}/s_{pg2}/s_{pg3}$ , as shown in figure 3.3. Equal resistive loads of  $600 \Omega$  are connected to each phase of the delta connected system. The switch responds in 0.04 seconds. It is to be noted from figure 5.7 that at 0.12 sec, the fault was applied, and it is cleared within 3 cycles (50ms).

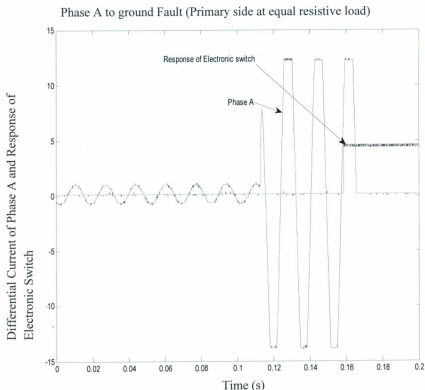


Figure 5.7: Phase A to ground fault at equal resistive load ( $600 \Omega$ ), power transformer and response of electronic switch.

Phase A to Ground Fault at Primary side and Secondary side at  
Equal Resistive Load

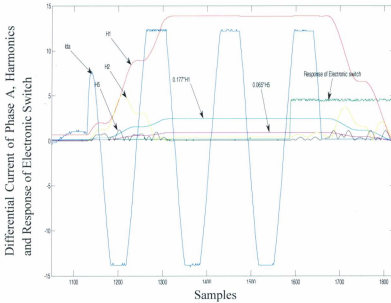


Figure 5.8: Phase A to ground fault at equal resistive load (600  $\Omega$ )-power transformer, harmonics and response of electronic switch.

$I_{da}$  = Differential Current of Phase A,  $H_1$ = Fundamental Harmonic,  $H_2$ = 2<sup>nd</sup> Harmonic and  $H_5$  = 5<sup>th</sup> harmonic, S = Response of Electronic Switch

In figure 5.8, the harmonics, the ratios and Phase A to ground fault currents at 600  $\Omega$  resistive load are given. In figure 5.8, during the fault in phase A, the following conditions were observed:

$$H_2 < 0.177 * H_1 \quad (5.3)$$

$$H_5 > 0.065 * H_1$$

Appendix D contains the fault results at 600  $\Omega$  load of the phase B and phase C cases, as shown in figures D.7-D.11.

### 5.3.3 Phase to Ground Fault (Primary side-secondary at different resistive load)

This fault was created by pressing switch  $s_{pg1}/s_{pg2}/s_{pg3}$ , as shown in figure 3.3. Phase A is connected to 600  $\Omega$ , phase B is connected to 1200  $\Omega$  and phase C is connected to 2400  $\Omega$ . The switch responded quickly. It is to be noted from figure 5.9 that at 0.12 sec, the fault was applied, and it is cleared within 3 cycles (50ms). A trip signal was issued. For the other two phases B and C the responses are given in appendix D as shown in figures D.12 to D.16.

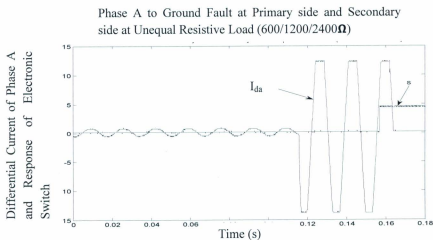


Figure 5.9: Phase A to ground fault at unequal resistive load (600/1200/2400  $\Omega$ ), power transformer and response of electronic switch

$I_{da}$  = Differential Current of Phase A, S = Response of Electronic Switch

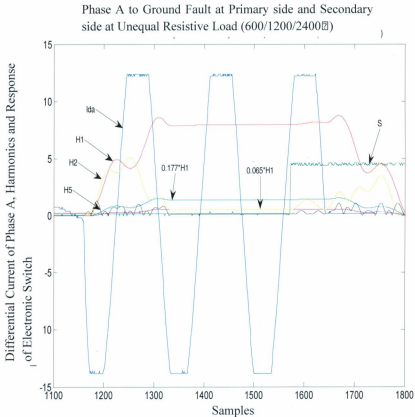


Figure 5.10: Phase A to ground fault at unequal resistive load (600/1200/2400  $\Omega$ ), power transformer, harmonics and response of electronic switch.

$I_{da}$  = Differential Current of Phase A,  $H_1$ = Fundamental Harmonic,  $H_2$ = 2<sup>nd</sup> Harmonic and  $H_5$  = 5<sup>th</sup> harmonic, S = Response of Electronic Switch

In figure 5.10, the harmonics, the ratios and Phase A to ground fault currents at 600/1200/2400  $\Omega$  resistive load are given.

The following conditions were established.

Results:

$$H_2 < 0.177 * H_1 \quad (5.4)$$

$$H_5 > 0.065 * H_1$$

Current harmonics and ratios are given in figure 5.10.

#### **5.3.4 Phase to Phase Fault (Primary side secondary at no load)**

This fault was created by pressing switch  $s_{pp1}/s_{pp2}/s_{pp3}$ , as shown in figure 3.3. The switch responded quickly. The fault was initiated at 0.115s, the fault current in phase A increased, and within 3 cycles the trip signal was successfully activated to isolate the faulted phase A as shown in figure 5.11. For the phase B and phase C cases, the responses are given in appendix D in figures D.17 to D.21.

Phase to Phase Fault at Primary side and  
Secondary side Open

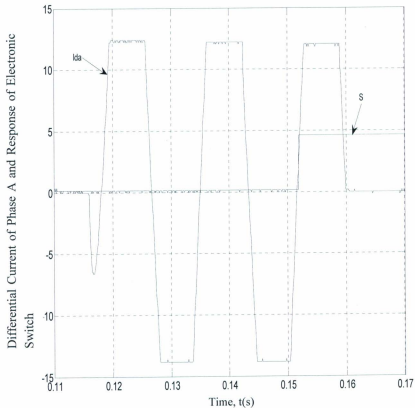


Figure 5.11: Phase A to Phase B fault primary side and secondary open and response of electronic switch

$I_{da}$  = Differential Current of Phase A,  $S$  = Response of Electronic Switch

Phase to Phase Fault at Primary side and  
Secondary side Open

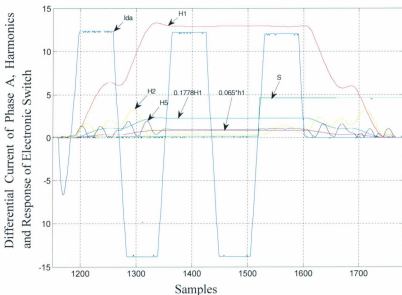


Figure 5.12: Phase A to Phase B fault primary side and secondary open, harmonics and response of electronic switch

$I_{da}$  = Differential Current of Phase A,  $H_1$  = Fundamental Harmonic,  $H_2$  = 2<sup>nd</sup> Harmonic and  $H_5$  = 5<sup>th</sup> harmonic,  $S$  = Response of Electronic Switch

Results:

$$H_2 < 0.177 * H_1 \quad (5.5)$$

$$H_5 > 0.065 * H_1$$

Current harmonics and ratios are given in figure 5.12.

### 5.3.5 Phase to Neutral Fault (Secondary side-secondary at equal resistive load)

This fault was created by pressing switch  $s_{sg1}/s_{sg2}/s_{sg3}$ , as shown in figure 3.3. Equal resistive loads of  $600 \Omega$  were connected to each phase and in delta connection. The switch responded quickly. The fault was initiated at  $0.11s$ , the fault current in phase A increased, and within 3 cycles the trip signal was successfully activated to isolate the faulted phase A as shown in figure 5.13. For the phase B and phase C cases, the responses are given in appendix D, figures D.44 to D.48.

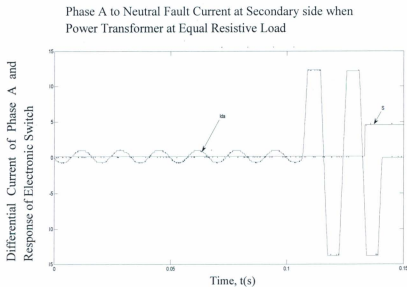


Figure 5.13: Phase to neutral fault current (secondary side) in Phase A when secondary side of power transformer at equal resistive load ( $600 \Omega$ ) and response of electronic switch.

$I_{da}$  = Differential Current of Phase A, S = Response of Electronic Switch

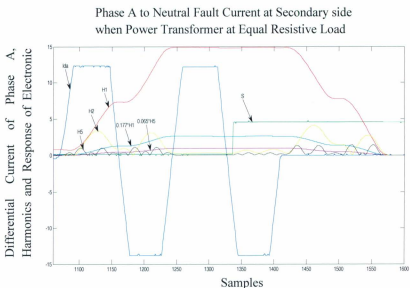


Figure 5.14: Phase to neutral fault current (secondary side) in Phase A when secondary side of power transformer at equal resistive load ( $600\Omega$ ), harmonics and response of electronic switch.

$I_{da}$  = Differential Current of Phase A,  $H_1$  = Fundamental Harmonic,  $H_2$  = 2<sup>nd</sup> Harmonic and  $H_5$  = 5<sup>th</sup> harmonic,  $S$  = Response of Electronic Switch

The following conditions were established.

Results:

$$H_2 < 0.177 * H_1 \quad (5.6)$$

$$H_5 > 0.065 * H_1$$

Current harmonics and ratios are given in figure 5.14.

### 5.3.6 Phase to Neutral Fault (Secondary side-secondary at different resistive load)

This fault was created by pressing switch  $s_{sg1}/s_{sg2}/s_{sg3}$ , as shown in figure 3.3. Phase A is connected to  $600 \Omega$ , phase B is connected to  $1200 \Omega$  and phase C is connected to  $2400 \Omega$ . The switch responded quickly. The fault was initiated at  $0.113s$ , the fault current in phase A increased, and within 3 cycles the trip signal was successfully activated to isolate the faulted phase A as shown in figure 5.15. For the phase B and phase C, the responses are given in appendix D as shown in figures D.49 to D.53.

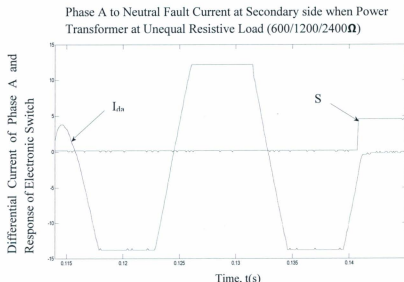


Figure 5.15: Phase to neutral fault current (secondary side) in Phase A when secondary side of power transformer at unequal resistive load ( $600/1200/2400 \Omega$ ) and response of electronic switch.

$I_{da}$  = Differential Current of Phase A, S = Response of Electronic Switch

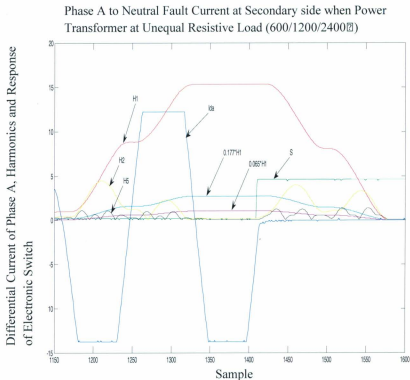


Figure 5.16: Phase to neutral fault current (secondary side) in Phase C when secondary side of power transformer at unequal resistive load (600/1200/2400 $\Omega$ ) and response of electronic switch.

$I_{da}$  = Differential Current of Phase A,  $H_1$  = Fundamental Harmonic,  $H_2$  = 2<sup>nd</sup> Harmonic and  $H_5$  = 5<sup>th</sup> harmonic, S = Response of Electronic Switch

The following conditions were established.

Results:

$$H_2 < 0.177 * H_1 \quad (5.7)$$

$$H_5 > 0.065 * H_1$$

Current harmonics and ratios are given in figure 5.16.

### **5.3.7 Phase to Phase Fault (Secondary side-secondary-open)**

This fault was created by pressing switch  $s_{sp1}/s_{sp2}/s_{sp3}$ , as shown in figure 3.3. The switch responded quickly. The fault was initiated at 0.105s, the fault current in phase A increased, and within 3 cycles the trip signal was successfully activated to isolate the faulted phase A as shown in figure 5.17. For the phase B and phase C, the responses are given in appendix D as shown in figures D.54 to D.58.

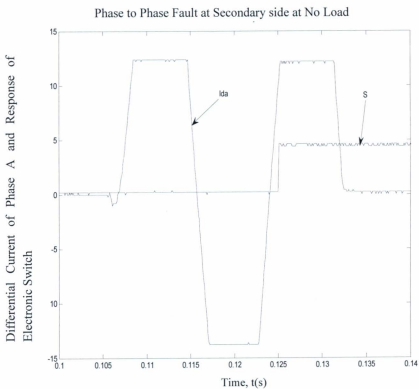


Figure 5.17: Phase to Phase fault current (secondary side) in Phase A when secondary side of power transformer open and response of electronic switch.

$I_{da}$  = Differential Current of Phase A, S = Response of Electronic Switch

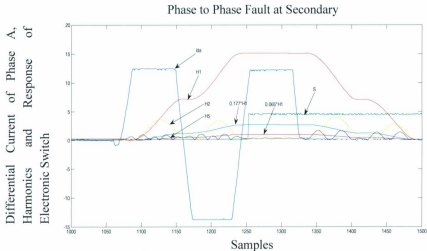


Figure 5.18: Phase to Phase fault current (secondary side) in Phase A when secondary side of power transformer open and response of electronic switch.

$I_{da}$  = Differential Current of Phase A,  $H_1$  = Fundamental Harmonic,  $H_2$  = 2<sup>nd</sup> Harmonic and  $H_5$  = 5<sup>th</sup> harmonic, S = Response of Electronic Switch

The following conditions were established.

Results:

$$H_2 < 0.177 * H_1 \quad (5.8)$$

$$H_5 > 0.065 * H_1$$

Current harmonics and ratios are given in figure 5.18.

### 5.3.8 Phase to Phase Fault (Secondary side-secondary at equal resistive load)

This fault was created by pressing switch  $s_{sp1}/s_{sp2}/s_{sp3}$ , as shown in figure 3.3. The switch responded quickly. The fault was initiated at 0.14s, the fault current in phase A is increased, and within 3 cycles the trip signal was successfully activated to isolate the faulted phase A as shown in figure 5.19. For all three phases responses are given in the appendix D figure D.59 to D.63.

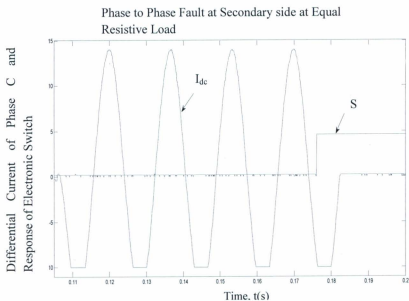


Figure 5.19: Phase to Phase fault current (secondary side) in Phase C when secondary side of power transformer at equal resistive load (600  $\Omega$ ) and response of electronic switch.

$I_{dc}$  = Differential Current of Phase C, S = Response of Electronic Switch.

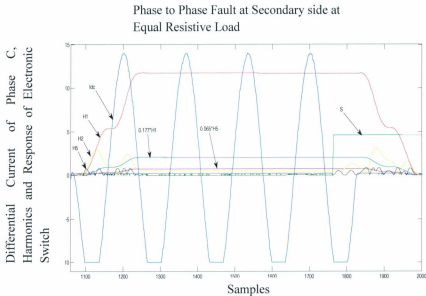


Figure 5.20: Phase to Phase fault current (secondary side) in Phase C when secondary side of power transformer at equal resistive load (600  $\Omega$ ) and response of electronic switch.

$I_{dc}$  = Differential Current of Phase A,  $H_1$  = Fundamental Harmonic,  $H_2$  = 2<sup>nd</sup> Harmonic and  $H_5$  = 5<sup>th</sup> harmonic,  $S$  = Response of Electronic Switch

The following conditions were established.

Results:

$$H_2 < 0.177 * H_1 \quad (5.9)$$

$$H_5 > 0.065 * H_1$$

Current harmonics and ratios are given in figure 5.20.

### 5.3.9 Phase to Phase Fault (Secondary side-secondary at different resistive load)

This fault was created by pressing switch  $s_{sp1}/s_{sp2}/s_{sp3}$ , as shown in figure 3.3. Phase A is connected to  $600 \Omega$ , phase B is connected to  $1200 \Omega$  and phase C is connected to  $2400 \Omega$ . The switch responded quickly. The fault was initiated at  $0.14s$ , the fault current in phase A increased, and within 2 cycles (33.3ms), the trip signal was successfully activated to isolate the faulted phase A as shown in figure 5.21. For the phase B and phase C, the responses are given in appendix D as shown in figure D.64 to D.68.

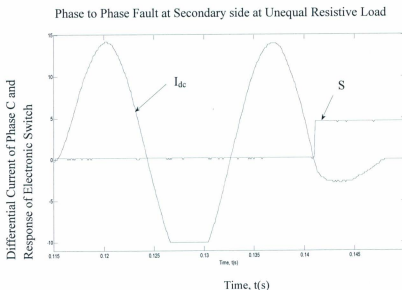


Figure 5.21: Phase to Phase fault current (secondary side) in Phase C when secondary side of power transformer at different resistive load ( $600/1200/2400 \Omega$ ) and response of electronic switch.

$I_{dc}$  = Differential Current of Phase C, S = Response of Electronic Switch

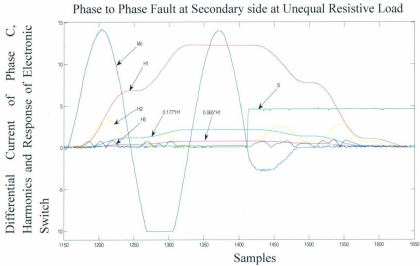


Figure 5.22: Phase to Phase fault current (secondary side) in Phase C when secondary side of power transformer at different resistive load (600/1200/2400  $\Omega$ ) and response of electronic switch.

$I_{dc}$  = Differential Current of Phase A,  $H_1$  = Fundamental Harmonic,  $H_2$  = 2<sup>nd</sup> Harmonic and  $H_5$  = 5<sup>th</sup> harmonic, S = Response of Electronic Switch

The following conditions were established.

Results:

$$H_2 < 0.177 * H_1 \quad (5.10)$$

$$H_5 > 0.065 * H_1$$

Current harmonics and ratios are given in figure 5.22.

## 5.4 Summary of Experimental Results

This chapter provided experimental test results of protection of a three phase laboratory distribution transformer. The magnetising inrush current and faults have been distinguished using the discrete Fourier transform algorithm. A discrete Fourier transform (DFT) technique is used to filter out the harmonic ratios. The 2<sup>nd</sup> to fundamental harmonic ratio 17.7% is used to declare the fault and no fault condition. For no fault conditions involving magnetising inrush currents and normal full load current including switching transient condition, it remained higher than this ratio value of 17.7%. For various fault conditions, it remained always lower than this ratio. This condition was experimentally checked for different faults for the laboratory test power transformer and the maximum response time for the triac switch for any fault was within 50ms ( 3 cycles). Details of all the faults and their response times are given in table 5.1. For no fault condition like magnetizing inrush current, it did not trip the circuit breaker and hence did not interrupt the operation of the transformer. It is shown in the first row of table 5.1. The precise values of these ratios were found appropriate for quick and appropriate decisions for the switch to distinguish between the fault and inrush currents. It is evident from table 5.1 that in every case, the designed protective relay operated correctly. The details of experimental inrush conditions in phase B and phase C are given in appendix D. The details of the faults in phase B and phase C involving various operating conditions are also given in appendix D.

S.No	Conditions	Inrush / Fault	Response Time Triac Switch (s)
1.	$H_2 > 0.177 \cdot H_1$ $H_5 < 0.065 \cdot H_1$	No Fault: Magnetizing Inrush Current	No tripping
2.	$H_2 < 0.177 \cdot H_1$ $H_5 > 0.065 \cdot H_1$	Phase to Ground Fault (Primary side-secondary unloaded)	0.045 Within 3 cycles
3.	$H_2 < 0.177 \cdot H_1$ $H_5 > 0.065 \cdot H_1$	Phase to Ground Fault (Primary side-secondary equal resistive load)	0.04 Within 3 cycles
4.	$H_2 < 0.177 \cdot H_1$ $H_5 > 0.065 \cdot H_1$	Phase to Ground Fault (Primary side-secondary-different resistive load)	0.14 Within 3 cycles
5.	$H_2 < 0.177 \cdot H_1$ $H_5 > 0.065 \cdot H_1$	Phase to Phase Fault (Primary side-secondary unloaded)	0.03 Within 3 cycles
6.	$H_2 < 0.177 \cdot H_1$ $H_5 > 0.065 \cdot H_1$	Phase to Neutral Fault (Secondary side-secondary equal resistive load)	0.04 Within 3 cycles
7.	$H_2 < 0.177 \cdot H_1$ $H_5 > 0.065 \cdot H_1$	Phase to Neutral Fault (Secondary side-secondary-different resistive load)	0.025 Within 3 cycles
8.	$H_2 < 0.177 \cdot H_1$ $H_5 > 0.065 \cdot H_1$	Phase to Phase Fault (Secondary side-secondary-open)	0.019 Within 3 cycles
9.	$H_2 < 0.177 \cdot H_1$ $H_5 > 0.065 \cdot H_1$	Phase to Phase Fault (Secondary side-secondary-open)	0.025 Within 3 cycles

Table 5.1: Inrushes and faults at various operating conditions and responses of Triac Switch.

## Chapter 6

### Conclusions and Future Works

#### 6.1 Conclusion

This thesis contains the experimental investigations of protection for a stand-alone power distribution transformer utilizing a microcontroller. A three phase 5kVA power transformer has been tested in the laboratory of Memorial University of Newfoundland. Detailed derivation is provided to extract the harmonic contents of the differential current for both inrushes and faults. Criteria for protection of power transformers are obtained for both magnetizing inrush currents including over excitation and faults. The designed relay differentiated the inrush currents from internal fault currents of the transformer. It successfully protected the transformer against inrush currents without tripping the circuit breaker. The faults are created for different conditions and observed on the four channels digital scope. It is experimentally confirmed that the second harmonic is responsible for magnetizing inrush current and the 5<sup>th</sup> harmonic is for over-excitation condition. If the ratio of 2<sup>nd</sup> harmonic over fundamental is greater than 0.177 and ratio of 5<sup>th</sup> harmonic over fundamental is less than 0.065, then the transformer is experiencing inrush current conditions. The designed relay protects the transformer from misoperation due to inrush currents. If this criterion is not met, then the transformer has internal fault condition. The relay will energize the operate coil and trip the circuit breaker after a delay time of 100 ms (6 cycles). Software is written in C language to give the predefined threshold for the

harmonics ratios. A programmable microcontroller is used to execute these instructions. The designed digital relay has been found acceptable for power distribution transformers. Extensive tests are carried out in the laboratory for various operating conditions. In all cases, the designed relay worked successfully. This set up can be used for protection of power distribution transformers having standard and new core lamination materials. The transformer specifications are given for the software design. This digital relay protection system can be useful for single phase pole-mounted power distribution transformers.

## **6.2 Future Works**

The present experimental relay set up was tested only for the Discrete Fourier Transform algorithm. However, it can be tested for the other algorithms. For these cases, only the coefficients in the software need to be changed. Due to the availability of inexpensive and fast microcontroller, there would be no problem of data storage and processing time requirements for any type of algorithm.

The remote protection with this type of digital relay can be applied for all types of power network. Local Area Network (LANs) and Wide Area Network (WANs) can be utilized to integrate with the proposed digital protection of power system in smart grid.

## References

- [1] Kennedy, L.F. and Hayward, C.D., "Harmonic-Current Restrained Relays for Differential Protection", Transactions of the AIEE, Vol. 57, 1938, pp.262-271.
- [2] Blume, L.F., Camilli, G., Farnham, S.B. and Peterson, H.A., "Transformer Magnetizing Inrush Currents and Influence on System Operation", Transactions of the AIEE, Vol. 63, 1944, pp.366-375.
- [3] Finzi, L.A. and Muttschler, W.H., "The Inrush Magnetizing Current in Single Phase Transformers", Transactions of the AIEE, Vol. 70, 1951, pp.1436-1438.
- [4] Mathews, C.A., "Improved Transformer Differential Relay", Transactions of the AIEE, Vol. 73, 1954, pp. 645-649.
- [5] Sonnemann, W.K., Wanger, C.L. and Rockefeller, G.D., "Magnetizing Inrush Phenomenon in Transformer Banks", Transactions of the AIEE, Vol. 77, 1958, pp.884-892.
- [6] Sharp, R.L. and Glassburn, W.E., "A Transformer Differential Relay with Second Harmonic Restraint", Transactions of the AIEE, Vol. 77, 1958, pp.913-918.
- [7] Warrington, A.R. Van C., "Protective Relays Their Theory and Practice", Volume 1, Chapman and Hall Ltd, Great Britain, 1968, pp.380-412.
- [8] Specht, T.R., "Transformer Inrush and Rectifier Transient Current", IEEE Transactions on Power Apparatus and Systems, Vol. PAS 88, No. 4, 1969, pp.269-276.

- [9] Rockefeller, G.D., "Fault Protection with a Digital Computer", IEEE Transactions on Power Apparatus and Systems, Vol. PAS 88, No. 4, 1969, pp.438-461.
- [10] Mann, B.L. and Morrison, I.F., "Digital Calculation of Impedance for Transmission Line Protection", IEEE Transactions on Power Apparatus and Systems, Vol. PAS 90, No. 1, 1971, pp.270-279.
- [11] Ramamoorthy, M, "Application of Digital Computer for Power System Protection", Journal of Institute of Engineers (India), Vol. 52 No. 10, 1972 pp.235-238.
- [12] Sykes, J.A., and Morrison, I.F., "A Proposed Method of Harmonic Restraint Differential Protection of Transformers by Digital Computer", IEEE Transactions on Power Apparatus and Systems, Vol. PAS 91, No. 3, 1972, pp.1266-1272.
- [13] Einval, C.H. and Linders, J.R., "A Three Phase Differential Relay for Power Transformer Protection", IEEE Transactions on Power Apparatus and Systems, Vol. PAS 94, No. 6, 1975, pp.1971-1980.
- [14] Dash, P.K. and Khincha, H.P., "Crosscorrelation Technique for Differential-Protection Schemes with a Digital Computer", Transactions of the AIEE, Vol. 123, 1976, pp. 170 - 171.
- [15] J. W. Horton, "Walsh Functions for Digital Impedance Relaying of Power Lines", IBM J. RES. Develop., 1976, pp. 530-541.

- [16] Malik, O.P., Dash, P.K. and Hope, G.S., "Digital Protection of Power Transformer", IEEE Power Engineering Society Summer Meeting, Paper A 77510-1, Mexico City, Mexico, 1977.
- [17] Schweitzer, E.O., Larson, R.R. and Flechsig, A.J., "An Efficient Inrush Current-detection Algorithm for Digital Computer Relay Protection of Transformers", IEEE Power Engineering Society Summer Meeting, Paper A 77510-1, Mexico City, Mexico, 1977.
- [18] Larson, R.R., Flechsig, A.J. and Schweitzer, E.O., "The Design and Test of a Digital Relay for Transformer Protection", IEEE Transactions on Power Apparatus and Systems, Vol. PAS 98, No. 3, 1979, pp.795-804.
- [19] Sachdev, M.S., and Baribeau, M.A., "A new Algorithm for Digital Impedance Relays", IEEE Transactions on Power Apparatus and Systems, Vol. PAS 98, No. 6, 1979, pp. 2232-2240.
- [20] Degens, A.J., "Algorithm for a Digital Transformer Differential Protection Based on Least Square Curve Fitting", IEE Proceedings, Vol. 128, Part C, 1981, pp. 155-161.
- [21] Degens, A.J., "Microprocessor-Implemented Digital Filters for Inrush Current Detection", Electrical Power and Energy Systems, Vol. 4, No. 3, 1982, pp.196-205.

- [22] Rahman, M. A., Dash, P.K. and Downton, E.R., "Digital Protection of Power Transformer Based on Weighted Least Square Algorithm ", IEEE Transactions on Power Apparatus and Systems, Vol. PAS 101, No. 11, 1982, pp.4204-4210.
- [23] Throp, J.S. and Phadke, A.G., "A Microprocessor Based Three Phase Transformer Differential Relay", IEEE Transactions on Power Apparatus and Systems, Vol. PAS 101, No. 2, 1982, pp.426-432.
- [24] Rahman, M. A., and Dash, P.K. "Fast Algorithm for Digital Protection of Power Transformer ", IEE Proceedings, Vol. 129, Part C, No. 2, 1982, pp. 79-85.
- [25] Throp, J.S. and Phadke, A. G., "A Microprocessor Based Voltage Restrained Three Phase Power Transformer Differential Relay", Proceedings of the South Eastern Symposium on System Theory, 1982, pp. 312-316.
- [26] Throp, J.S. and Phadke, A. G., "A New Computer Based, Flux Restrained, Current Differential Relay for Power Transformer Protection", IEEE Transactions on Power apparatus and Systems, Vol. PAS-102, No. 11, 1983, pp. 3264-3269.
- [27] Fakruddin, D.B., Parthasarathy, K., Jenkins, L. and Hogg, B.W., "Application of Haar Function for Transmission Line and Transformer Differential Protection", Electrical Power and Energy Systems, Vol. 6, No. 3, 1984, pp. 525-533.
- [28] Gangopadyay, A., "An analysis for Digital Protection of Transformers", Master's thesis, Memorial University of Newfoundland, St. John's, NF, 1984.

- [29] Rahman, M. A., and Jeyasurya, B., "Application of Walsh Functions for Microprocessor- Based Transformer Protection ", IEEE Transactions on Electromagnetic Compatibility, Vol. EMC-27, No. 4, 1985, pp. 221-225.
- [30] Rahman, M. A. and Gangopadhyay, A., "Digital Simulation of Magnetizing Inrush Current in Three Phase Transformers ", IEEE Transactions on Power delivery, Vol. PWRD-1, No. 4 1986, pp. 232-242.
- [31] Dash, P.K. and Rahman, M.A., "A New Algorithm for Digital Protection of Power Transformers", Canadian Electrical Association Transactions, Section 90-SP-150, 1987,pp.1-25.
- [32] Habib, M. and Martin, M.A., "A Comparative Analysis of Digital Relaying Algorithms for Differential Protection of Three Phase Power Transformer", IEEE Transactions on Power System, Vol. 3, No. 3, 1988, pp. 1378-1384.
- [33] Rahman, M. A., and Jeyasurya, B., "A State of art Review of Transformer Protection Algorithms ", IEEE Transactions on Power delivery, Vol. 3, No. 2, 1988, pp. 534-544.
- [34] Murty, Y. V. V. S. and Somlinski, W. J., "Design and Implementation of Digital Differential Relay for Three Phase Power Transformer Based on Kalman Filtering Theory", IEEE Transactions on Power Delivery, Vol. 3, No. 2, 1988, pp. 525-533.
- [35] Liu, P., Malik, O.P., Chen, D. and Hope, G.S., "Study of Non- Operation for Internal Faults of Second Harmonic Restraint Differential Protection of Power

- Transformers", Transaction of the Engineering and Operating Division of Canadian Electrical Association Power System Planning and Operation Section, Vol. 89-sp-141, 1989.
- [36] Sidhu, T.S., Sachdev, M.S. and Wood, H.C., "A Digital relaying algorithm for Detecting Transformer Winding Faults", IEEE Transactions on Power Delivery, Vol. 4, 1989, pp. 1638-1648.
- [37] Hermanto, Ivi., "Design, Development and Testing of Microprocessor Based Prototype Relay Protection of Power Transformer", Master's thesis, Memorial University of Newfoundland, St. John's, NF, 1990.
- [38] Murty, Y. V. V. S. and Somlinski, W. J., "A Kalman Filter Based Digital Percentage Differential and Ground Fault for Three Phase Power Transformer", IEEE Transactions on Power Delivery, Vol. 5, No. 3, 1990, pp. 1299-1308.
- [39] Sachdev, M.S. and Sidhu, T.S., "A Least Squares Technique and Differential Protection of Three Phase Power Transformers", Transaction of The Engineering and Operating Division of Canadian Electrical Association Power System Planning and Operation Section, Vol. 90-sp-158, 1990.
- [40] Rahman, M.A. , Hermanto, I. and Murty, Y. V. V. S., "A Stand Alone Digital Protective Relay for Power Transformers", IEEE Transactions on Power Delivery, Vol. 6, No. 1, 1991, pp. 85-95.
- [41] Rahman , M.A. , Lihua, H., Yilin, Y., Chan, D.T.W. and Ong, P. K. S., " A Novel algorithm for Digital Protection of Power Transformers", Transaction of

The Engineering and Operating Division of Canadian Electrical Association  
Power System Planning and Operation Section, Vol. 92-sp-165, 1992.

- [42] Sachdev, M.S. and Sidhu, T.S., "Online Identification of Magnetizing Inrush and Internal Faults in Three Phase Power Transformers", IEEE Transactions on Power Delivery, Vol. 7, No. 4, 1992, pp. 1885-1891.
- [43] Vaessen, P.M. and Hanique, E., Sachdev, "A New Frequency Response Analysis Method for Power Transformer", IEEE Transactions on Power Delivery, Vol. 7, No. 1, 1992, pp. 384-391.
- [44] Leon, F. and Semylen, A., "Efficient Calculation of Electromagnetic Parameters of Transformer", IEEE Transactions on Power Delivery, Vol. 7, No. 4, 1992, pp. 376-383.
- [45] Leon, F. and Semylen, A., "Complete Transformer Model for Electromagnetic Transients", IEEE Transactions on Power Delivery, Vol. 7, No. 1, 1992, pp. 361-369.
- [46] So, B., "Experimental Testing of Stand-Alone Digital Relay for Power Transformers", Master's thesis, Memorial University of Newfoundland, St. John's, NF, 1993.
- [47] Leon, F. and Semylen, A., "Reduced order Model of Transformer Transients", IEEE Transactions on Power Delivery, Vol. 9, No. 1, 1994, pp. 231-239.

- [48] Rahman, M. A. and Zaman, M. R., "Online Implementation of the Artificial Neural Network Based Protection of Power Transformer", NECEC 96 Proceedings, St John's, NF, Canada, 1996, pp. 5-11.
- [49] Zaman, M.R., "Artificial Neural Network Based Protection of Power Transformer.", PhD thesis, Memorial University of Newfoundland, St. John's, NF, 1996.
- [50] Rahman, M. A., So, B. and Zaman, M. R., "Testing of Algorithms for a Stand-Alone Digital Relay for Power Transformers", IEEE Transactions on Power Delivery, Vol. 13, No. 2, 1998, pp. 374-385.
- [51] Rahman, M. A. and Zaman, M. R., "Experimental Testing of the Artificial Neural Network Based Protection of Power Transformer", IEEE Transactions on Power Delivery, Vol. 13, No. 2, 1998, pp. 510-517.
- [52] Rahman, M. A., So, B., Zaman, M. R. and Hoque, M.A., "Testing of Algorithms for a Stand-Alone Digital Relay for Power Transformer", IEEE Transactions on Power Delivery, Vol. 13, No. 2, 1998, pp. 374-385.
- [53] Pandy, S. K. and Satish, L., "Multiresolution Signal Decomposition: A new Tool for Fault Detection in Power Transformers During Impulse Tests", IEEE Transactions on Power Delivery, Vol. 13, No. 4, 1998, pp. 1194-1200.
- [54] Rahman, M.A. and Saleh, S. A., "Transient Model for Power Transformer Using Wavelet-Filter-Bank", LESCOPE02 Proceedings, Halifax, NS, Canada, 2002, pp. 47-54.

- [55] Youssef, O. S., "A wavelet-Based Technique for Discrimination between Fault and Inrush Currents in Transformers", IEEE Power Engineering Society summer Meeting, Paper PE-027PRD (03-2002), Chicago, IL, 2002.
- [56] Saleh, A. S., "A Wavelet Packet Transform Based technique for Three Phase Power Transformer Protection", M. Eng. Thesis, Memorial University of Newfoundland, St. John's, NF, 2003.
- [57] Saleh, A. S. and Rahman, M. A., "Modeling and Protection of a Three Phase Power Transformer Using Wavelet Packet Transform", IEEE Transactions on Power Delivery, Vol. 20, No. 2, Part II, 2005, pp. 1273-1282.
- [58] Saleh, A. S. and Rahman, M. A., "A New Transient Model for Three Phase Power Transformer Using Wavelet Filter Bank", IEEE Transactions on Power Delivery, Vol. 20, No. 1, Part II, 2005, pp. 1409-1419.
- [59] Saleh, A. S. and Rahman, M. A., "Real Time Testing of a WPT-Based Protection Algorithm for Three Phase Power Transformers", IEEE Transactions on Industry Applications, Vol. 41, No. 4, 2005, pp. 1125-1132.
- [60] Rahman, M. A. , Ozgonenel, O. , Killic, E. and Khan, M. A. S. K. , "A New Method of Fault Detection and Identification of Incipient Fault in Power Transformer", Journal of Electric Power Components and Systems, Vol. 36, 2008., pp.126-1244.
- [61] Zoran Gagic, "Differential Protection for Arbitrary Three Phase Power Transformer", PhD thesis, Lund University, 2008.

- [62] Saleh, A. S. and Rahman, M. A., "Testing of a Wavelet-Packet-Transform-Based Differential Protection for Resistance-Grounded Three-Phase Transformers", IEEE Transactions on Industry Applications, Vol. 56, No. 3, 2010, pp. 1109-1117.
- [63] Saleh, A. S., Scaplen, B. and Rahman, M. A., "A New Implementation Method of Wavelet-Packet-Transform Differential Protection for Power Transformers", IEEE Transactions on Industry Applications, Vol. 47, No. 2, 2011, pp. 1003-1012.
- [64] Rolf Schaumann and Mac E. Van Valkenburg, "Design of Analog Filter", chapter 7, 2001, pp. 277-296.

# Appendices

## Appendix A

### Design of Chebyshev Filter for Anti-aliasing

For the analysis of three signals of frequency 60Hz, 120Hz and 300Hz, a chebyshev filter is designed to filter out unwanted signal in the band 0-350Hz

#### Design parameters:

For fundamental frequency  $f = 60$  Hz

$$\omega = 2\pi f$$

$$\omega = 2 * 3.14 * 60 = 376.8 \text{ rad/sec}$$

$$2^{\text{nd}} \text{ harmonic } \omega_2 = 2 * 3.14 * 60 * 2 = 753.6 \text{ rad/sec}$$

$$5^{\text{th}} \text{ harmonic } \omega_5 = 2 * 3.14 * 60 * 5 = 1885 \text{ Hz}$$

Let cut off frequency  $f_c = 350$  Hz

Therefore

$$\omega_c = 2 * \pi * f_c$$

$$\omega_c = 2 * 3.14 * 350 = 2199 \text{ rad/sec}$$

Let band stop frequency  $f_s = 450$  Hz

Therefore

$$\omega_s = 2 * \pi * f_s$$

$$\omega_s = 2 * 3.14 * 450$$

$$\omega_s = 2827 \text{ rad/sec}$$

$$\text{Normalized frequency } \omega = \frac{\omega_s}{\omega_c}$$

$$\omega = 2826/2198 = 1.29$$

Order of Chebyshev filters (n):

$$n = \cosh^{-1} \left\{ \sqrt{\frac{\frac{\alpha_{min}}{10^{\frac{\alpha_{min}}{10}}} - 1}{\frac{\alpha_{max}}{10^{\frac{\alpha_{max}}{10}}} - 1}} \right\} \cosh^{-1} \left( \frac{\omega_s}{\omega_c} \right) \quad (\text{A.1})$$

Let attenuation for band stop filter ( $\alpha_{min}$ ) and band pass filter ( $\alpha_{max}$ ) respectively for low pass filter be as follows:

$$\alpha_{min} = 20 \text{ dB}$$

$$\alpha_{max} = 0.3 \text{ dB}$$

By substituting the values of  $\alpha_{min}$ ,  $\alpha_{max}$ ,  $\omega_s$  and  $\omega_c$  in equation (A.1)

$$n = 5.78$$

Taking the next higher number

$$n = 6$$

**Ripple factor ( $\xi$ ):**

$$\xi = \sqrt{10^{\frac{\sigma_{max}}{20}} - 1} \quad (\text{A.2})$$

$$\xi = 0.27$$

$\xi$  = Ripple in dB

$$\xi = 20 \log_{10} \left( \frac{1}{\sqrt{1+\xi^2}} \right) \quad (\text{A.3})$$

$$\xi = 20 \text{Log}_{10}(0.96)$$

$$\xi = 20(-0.017)$$

$$\xi = -0.35 \text{dB}$$

$$a = \frac{\sinh^{-1}\left(\frac{1}{k}\right)}{n} \quad (\text{A.4})$$

$$b = \frac{\cosh^{-1}\left(\frac{1}{k}\right)}{n} \quad (\text{A.5})$$

By substituting the values of  $n$  and  $\xi$  in equation (A.4).

$$a = \frac{2.02}{6} = 0.34$$

By substituting the values of  $n$  and  $\xi$  in equation (A.5).

$$b = \frac{1.98}{6} = 0.33$$

$$\text{Cosh}(b) = 1.06$$

$$\text{Sinh}(a) = 0.35$$

**For Poles Locations:**

$$P_k = -w_c \sin\left(\frac{2k-1}{n} \cdot \left(\frac{\pi}{2}\right)\right) \cdot \sinh\left(\frac{1}{n} \cdot \sinh^{-1}\frac{1}{\xi}\right) + jw_c \cos\left(\frac{2k-1}{n} \cdot \left(\frac{\pi}{2}\right)\right) \cdot \cosh\left(\frac{1}{n} \cdot \cosh^{-1}\frac{1}{\xi}\right)$$

(A.6)

where

$$a = \left(\frac{1}{n} \cdot \sinh^{-1}\frac{1}{\xi}\right)$$

(A.7)

$$b = \left(\frac{1}{n} \cdot \cosh^{-1}\frac{1}{\xi}\right)$$

(A.8)

MATLAB Program for Chebyshev 6<sup>th</sup> Order Filter

```
clear all
```

```
close all
```

```
format short e;
```

```
[n,wn]=cheblord(2*pi*350,2*pi*450,.3,20,'s');
```

```

[num,den]=cheby1(n,3,2*pi*350,'s');
sys=tf(num,den);
figure(1);
bode(sys),grid;
r=roots(den);
figure(2);
pzmap(num,den),sgrid;
f1=conv([1 -r(1,1)],[1 -r(2,1)]);
f2=conv([1 -r(3,1)],[1 -r(4,1)]);
f3=conv([1 -r(5,1)],[1 -r(6,1)]);
t1=tf([8.9867e5],[1 1.4645e3 8.9867e5]);
t2=tf([2.998e6],[1 1.0721e3 2.998e6]);
t3=tf([5.0869e6],[1 3.942e2 5.0869e6]);
figure(3);
bode(t1,t2,t3);
figure(4);
bode(t1*t2*t3);
%Quality factors Q1, Q2 and Q3 where:Q1<Q2<Q3
Q1=sqrt(8.9867e5)/1.4645e3;
Q2=sqrt(2.998e6)/1.0721e3;
Q3=sqrt(5.0869e6)/3.942e2;
%Cut off frequency for first stage=wc1
wc1=sqrt(8.9867e5);
%let C1=0.1uF
c1=0.1e-6;
%wc1=1/R1*C1;
R1=1/(wc1*c1);
R2=R1;
%n-1/Q1=1+RB1/RA1
%RA1=lkohms or 1e3
RA1=1e3;
RB1=RA1*((n-(1/Q1))-1);
%Cut off frequency for second stage=wc2
wc2=sqrt(2.998e6);
%let C3=0.1uF
c3=0.1e-6;

```

```

c4=c3;
%wc2=1/R3*C3;
R3=1/(wc2*c3);
R4=R3;
%n-1/Q1=1+RB1/RA1
%RA2=1kohms or 1e3
RA2=1e3;
RB2=RA2*((n-(1/Q2))-1);
%Cut off frequency for second stage=wc3
wc3=sqrt(5.0869e6);
%let C3=0.1uF
c5=0.1e-6;
c6=c5;
%wc3=1/R5*C5;
R5=1/(wc3*c5);
R6=R5;
%n-1/Q1=1+RB1/RA1
%RA2=1kohms or 1e3
RA3=1e3;
RB3=RA3*((n-(1/Q3))-1);

```

By MATLAB programme we have following complex roots for  $k=1,2,3... 6$ .

$$P_1 = -1.9621e+002 + 2.2469e+003i$$

$$P_2 = -1.9621e+002 - 2.2469e+003i$$

$$P_3 = -5.3606e+002 + 1.6448e+003i$$

$$P_4 = -5.3606e+002 - 1.6448e+003i$$

$$P_5 = -7.3227e+002 + 6.0204e+002i$$

$$P_6 = -7.3227e+002 - 6.0204e+002i$$

Since all the roots are the left side of the vertical axis ( $j\omega$ ), therefore the filter is stable.

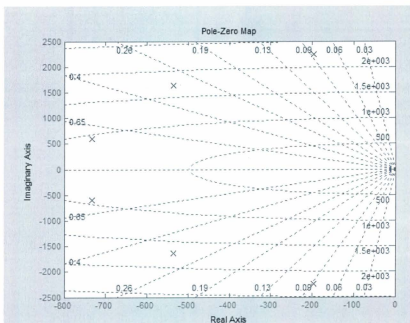


Figure A.1: Poles location for the 6<sup>th</sup> order Chebyshev filter

For the transfer functions following formula is used [64] :

$$T_s(n) = \frac{w_c^n}{s^{n+2} + 2^{(n-1)}(s-c_1)(s-c_2)(s-c_3)\dots(s-c_n)} \quad (\text{A.9})$$

By MATLAB programme, there are three transfer functions as follows:

$$T_s(1) = \frac{898670}{s^2 + 1465s + 898670} \quad (\text{A.10})$$

$$T_s(2) = \frac{2.998 \cdot 10^6}{s^2 + 1072s + 2.998 \cdot 10^6} \quad (\text{A.11})$$

$$T_s(3) = \frac{5.087 \cdot 10^6}{s^2 + 394.2s + 5.087 \cdot 10^6} \quad (\text{A.12})$$

The magnitude and phase responses of these three transfer functions are shown in figure A.2.

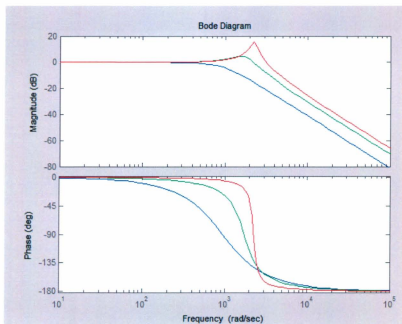


Figure A.2: Magnitude and phase response of three transfer functions separately for the 6<sup>th</sup> order Chebyshev filter

$$T_s(6) = T_s(1) * T_s(2) * T_s(3) \quad (\text{A.13})$$

$$T_s(6) = \frac{1.322 \cdot 10^{19}}{s^6 + 2925 \cdot s^5 + 1.154 \cdot 10^7 \cdot s^4 + 2.039 \cdot 10^{10} \cdot s^3 + 3.257 \cdot 10^{13} \cdot s^2 + 1.368 \cdot 10^{19}} \quad (\text{A.14})$$

The magnitude and phase response of the 6<sup>th</sup> order Chebyshev filter is given in figure A.3.

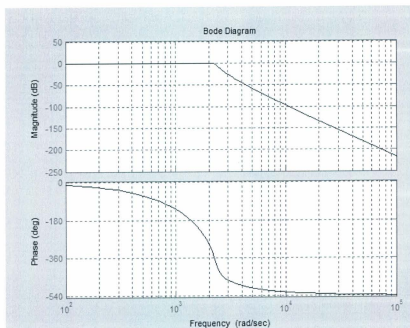


Figure A.3: Magnitude and phase response of the 6<sup>th</sup> order Chebyshev filter.

## Hardware Design of 6<sup>th</sup> Order Chebyshev Filter

Basic RC low pass filter circuit is proposed with LM324 quad amplifier. Same is shown in figure A.4. There are three stages for 6<sup>th</sup> order Chebyshev filter. Each stage contains two capacitors and four resistors.

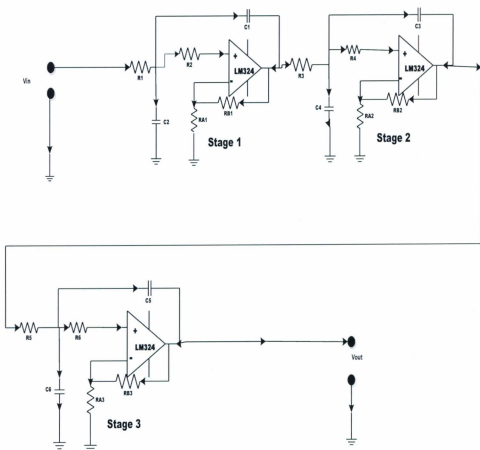


Figure A.4: Filter circuit

Stage 1

$$w_{c1} = \sqrt{\text{Numerator of } T_1(s)} \quad (\text{A.15})$$

$$w_{c1} = 9.4798 * 10^2$$

$$w_{c1} = \frac{1}{R_1 * C_1} \quad (\text{A.16})$$

Let  $C_1 = C_2 = 1 \mu\text{F}$

$$R_1 = R_2 = 10.55 \text{K}\Omega$$

$$n - \frac{1}{Q_1} = 1 + \frac{R_{B1}}{R_{A1}} \quad (\text{A.17})$$

where  $Q_1$  is quality factor of stage 1

$$Q_1 = \frac{\sqrt{\text{Numerator of } T_1(s)}}{\text{Coefficient of } S \text{ in denominator of } T_1(s)} \quad (\text{A.18})$$

$$Q_1 = 0.642$$

Let  $R_{A1} = 1 \text{k}\Omega$

By equation A.17

$$R_{A1} = 3.45 \text{k}\Omega$$

In the circuit diagram A.5, at node A, By Kirchoff's current law, we have:

$$((v_{out} - v_A)R_2 + v_{out} * sC_2) = 0 \quad (A.7)$$

At node B, by Kirchoff's current Law:

$$(v_A - v_{out})\frac{1}{R_2} + c_1(v_A - v_{out})s + (v_A - v_{in})\frac{1}{R_1} = 0 \quad (A.8)$$

$$\left(\frac{1}{R_1} + \frac{1}{R_2} + c_1 s\right) v_A = \frac{v_{in}}{R_1} + \left(\frac{1}{R_2} + c_1 s\right) v_{out} \quad (A.9)$$

Equation A.7 is rearranged as follows:

$$\left(\frac{1}{R_2}\right) v_A = \left(\left(\frac{1}{R_2}\right) + c_2 s\right) v_{out} \quad (A.10)$$

Substituting value of  $v_A$  from equation A.10 to equation A.9, to get

$$T_1(s) = \frac{\frac{1}{R_1 R_2 c_1 c_2}}{s^2 + \left(\frac{1}{R_1 c_1} + \frac{1}{R_2 c_1}\right)s + \frac{1}{R_1 R_2 c_1 c_2}} \quad (A.11)$$

where

$$\frac{v_{out}}{v_{in}} = T_1(s)$$

$$T_1(s) = \frac{1}{R_1 R_2 c_1 c_2 s^2 + (R_1 + R_2) c_2 s + 1} \quad (A.12)$$

Similarly for stages 2 and stage 3 respectively for 6<sup>th</sup> order Chebyshev filter transfer functions are as follows:

$$T_2(s) = \frac{1}{R_3 R_4 c_3 c_4 s^2 + (R_3 + R_4) c_4 s + 1} \quad (\text{A.13})$$

$$T_3(s) = \frac{1}{R_5 R_6 c_5 c_6 s^2 + (R_5 + R_6) c_6 s + 1} \quad (\text{A.14})$$

To make the 6<sup>th</sup> order chebyshev filter three, second order filters need to be cascaded as shown in figure A.6.

$$T(s) = (T_1(s) * T_2(s) * T_3(s)) \quad (\text{A.14})$$

Substituting the values of  $T_1(s)$ ,  $T_2(s)$  and  $T_3(s)$

$$T(s) = \left( \frac{1}{R_1 R_2 c_1 c_2 s^2 + (R_1 + R_2) c_2 s + 1} * \frac{1}{R_3 R_4 c_3 c_4 s^2 + (R_3 + R_4) c_4 s + 1} * \frac{1}{R_5 R_6 c_5 c_6 s^2 + (R_5 + R_6) c_6 s + 1} \right) \quad (\text{A.15})$$

$$\text{Let } R_1 = R_2 = R_3 = R_4 = R_5 = R_6 = 2 K \Omega \quad (\text{A.16})$$

The values of  $c_1$ ,  $c_2$ ,  $c_3$ ,  $c_4$ ,  $c_5$  and  $c_6$  can be calculated by iteration method. These values are also given in [46] for 6<sup>th</sup> order Chebyshev filter. These values are un-

scaled and are as follows:

$$c_{1\text{unscaled}} = 2.5530$$

$$c_{2\text{unscaled}} = 1.7760$$

$$c_{3\text{unscaled}} = 3.4870$$

$$c_{4unscaled} = 0.4917$$

$$c_{5unscaled} = 9.5310$$

$$c_{6unscaled} = 0.1110$$

$$\text{Scale factor} = \frac{1}{2 \cdot \pi \cdot R \cdot f_c} \quad (\text{A.17})$$

Substituting values of  $R=2 \text{ K}\Omega$  and  $f_c = 350 \text{ Hz}$  in equation A.17

$$\text{Scale factor} = 2.27 \cdot 10^{-7}$$

By multiplying the un-scaled capacitance values with the scale factors we have required values for the capacitors. These are as follows:

$$c_1 = 0.579 \mu\text{F}$$

$$c_2 = 0.4031 \mu\text{F}$$

$$c_3 = 0.792 \mu\text{F}$$

$$c_4 = 0.112 \mu\text{F}$$

$$c_5 = 2.1 \mu\text{F}$$

$$c_6 = 0.0251 \mu\text{F}$$

Due to unavailability of the exact values as designed above, for actual hardware implementation nearest values of the capacitances are used. Transfer functions  $T_1(s)$ ,  $T_2(s)$  and  $T_3(s)$ , are cascaded and simulated in MATLAB. Cascaded transfer function is

shown in figure A.6, its pole locations is shown in figure A.7, its magnitude and phase response is shown in figure A.8 and figure A.9 respectively.

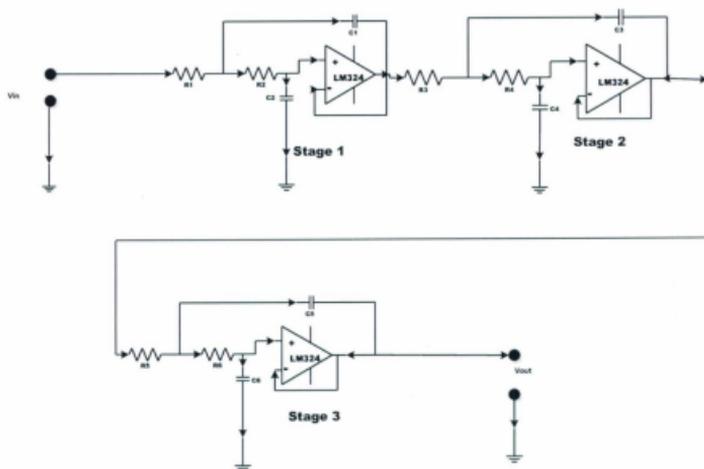


Figure A.5: Anti-aliasing filter-6<sup>th</sup> order Chebyshev Filter

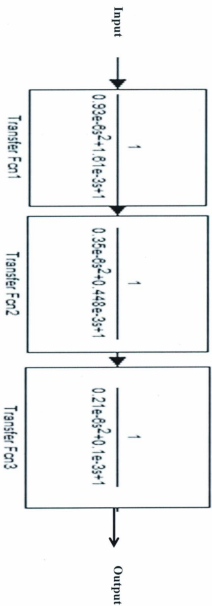


Figure A.6: Cascaded transfer functions for 6<sup>th</sup> order Chebyshev

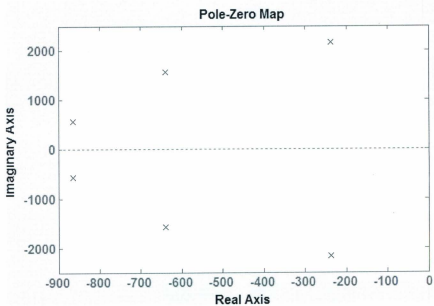


Figure A.7: Location of poles for cascaded transfer functions for 6<sup>th</sup> order Chebyshev filter

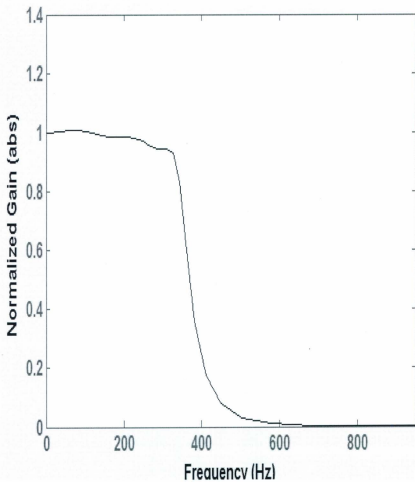


Figure A.8: Magnitude response of 6<sup>th</sup> order Chebyshev filter

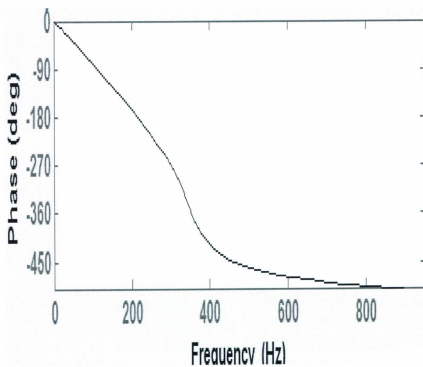


Figure A.9: Phase response of 6<sup>th</sup> order Chebyshev filter

## Appendix B

### MATLAB Program for Inrush Analysis

```
clear all
close all
clc
f=60;
w=2*pi*f;
T=1/f;
t=(0:T/200:10*T);
%Programme-Inrush_Analysis.m
%y1=Input Voltage=e
E=110;
y1=sqrt(2)*(E*sin(w*t));
R=100;
X=30*R;
%X=wl=2*pi*f*1
Z=sqrt(R^2+X^2);
%phi=Inverse(tan(X/R))
phi=1.54;
%theta=Saturating angle
theta=0;
%y2=Inrush current=Im
%lamda= Switching angle
lamda=0;
y2=(((sqrt(2))*E)/Z)*((sin(w*t-phi))-(exp(-(w*t)+theta-
lamda)*R/X).*sin(theta+lamda-phi)));
[At,H1,H2]=plotyy(t,y1,t,y2,'plot');
set(get(At(1),'Ylabel'),'String','Input Voltage');
set(get(At(2),'Ylabel'),'String','Inrush Current');
xlabel('Angle (radian)');
title ('Switching(Lamda)=0 & Saturating Angle(Thetta)= 0 radian');
```

Switching Angle ( $\lambda$ )= 0 and Saturating Angle ( $\theta$ )= 0 radian

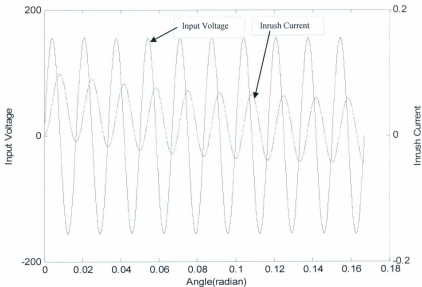


Figure B.1: Input Voltage and Inrush Current when Switching Angle =  $0^\circ$

Switching Angle ( $\lambda$ ) =  $45^\circ$  and Saturating Angle ( $\theta$ ) = 0 radian

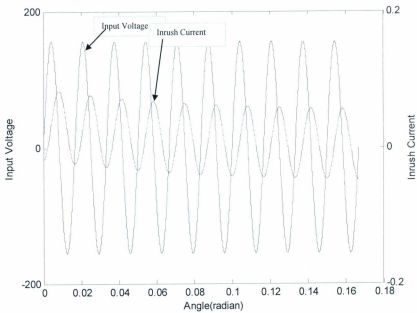
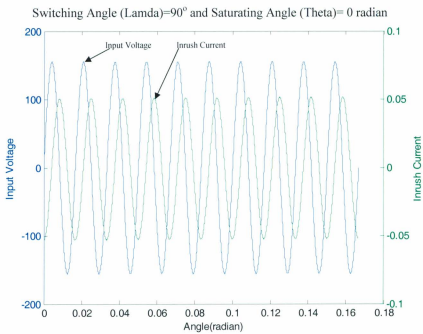


Figure B.2: Input Voltage and Inrush Current when Switching Angle =  $45^\circ$



FigureB.3: Input Voltage and Inrush Current when Switching Angle =  $90^\circ$

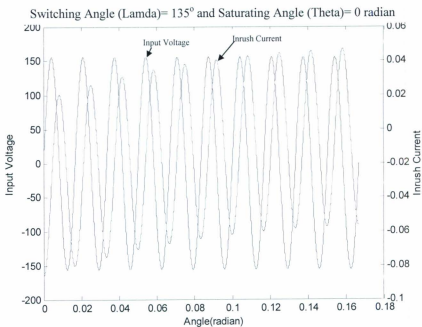


Figure B.4: Input Voltage and Inrush Current when Switching Angle =  $135^\circ$

Switching Angle ( $\lambda$ ) =  $180^\circ$  and Saturating Angle ( $\theta$ ) = 0 radian

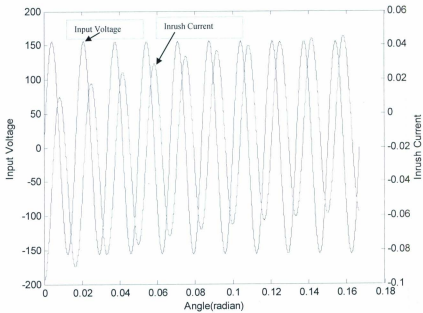


Figure B.5: Input Voltage and Inrush Current when Switching Angle =  $180^\circ$

Switching Angle ( $\lambda$ ) =  $225^\circ$  and Saturating Angle ( $\theta$ ) = 0 radian

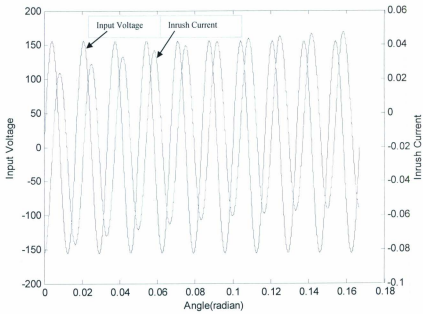


Figure B.6: Input Voltage and Inrush Current when Switching Angle =  $225^\circ$

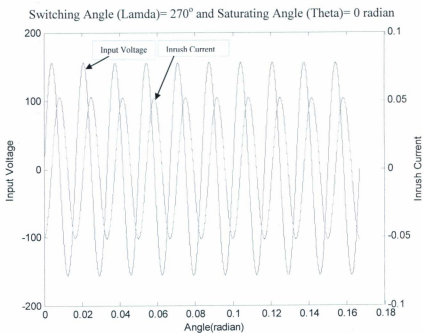


Figure B.7: Input Voltage and Inrush Current when Switching Angle =  $270^\circ$

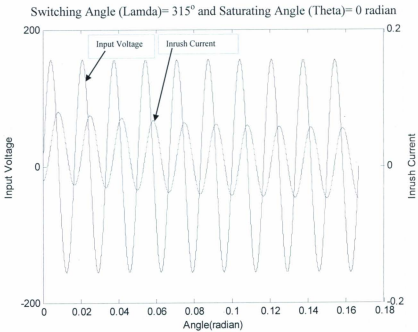


Figure B.8: Input Voltage and Inrush Current when Switching Angle =  $315^\circ$

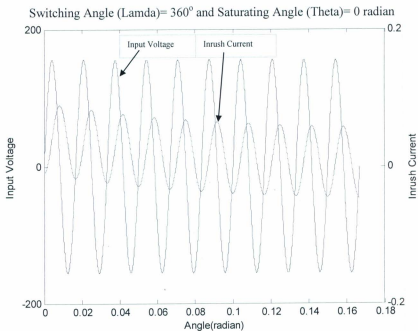


Figure B.9: Input Voltage and Inrush Current when Switching Angle =  $360^\circ$

## Appendix C

### Discrete Fourier Transform (DFT) Algorithm

A continuous signal of an interval can be checked through Fourier series. Let  $g(t)$  be any continuous function for an interval  $(0, T)$ , Then we have

$$g(t) = \frac{a_0}{2} + \sum_{j=1}^{\infty} c_j * \cos(j * w * t) + s_j * \sin(j * w * t) \quad (C.1)$$

where

$$a_0 = \frac{2}{T} * \int_0^T g(t) * dt \quad (C.2)$$

$$s_j = \frac{2}{T} * \int_0^T g(t) * \sin_j(w * t) dt \quad (C.3)$$

$$c_j = \frac{2}{T} * \int_0^T g(t) * \cos_j(w * t) dt \quad (C.4)$$

where

$a_0$  = Average value or DC Component

$s_j$  = Sine component for Fourier Series

$c_j$  = Cosine component for Fourier Series

If  $t_j$  is the sampling time and  $\Delta t$  is the time separation of two sampling signals, then total number of samples is:

$$N = \frac{t_i}{\Delta T} \quad (C.5)$$

Equation C.3 applies:

$$s_j = \frac{2}{N} * \sum_{i=j}^N g(t_i) * \sin\left(\frac{2*\pi*j*i}{N}\right) \quad (C.6)$$

$$c_j = \frac{2}{N} * \sum_{i=j}^N g(t_i) * \cos\left(\frac{2*\pi*j*i}{N}\right) \quad (C.7)$$

For our case analysis:

$$g(t) = I(t_j) \quad (C.8)$$

Equations (C.6) and (C.7) become:

$$s_j = \frac{2}{N} * \sum_{i=j}^N I(t_j) * \sin\left(\frac{2*\pi*j*i}{N}\right) \quad (C.9)$$

$$c_j = \frac{2}{N} * \sum_{i=j}^N I(t_j) * \cos\left(\frac{2*\pi*j*i}{N}\right) \quad (C.10)$$

where

$$N=16$$

$$i = 1, 2, 3...16$$

$$j = 1, 2, 3...16$$

Each sample makes an array of 16\*1. So, a total of two 16\*16 matrices for both sine and cosine functions are developed.

**MATLAB Programme for the values of  $C_j$  and  $S_j$ :**

```
>>i=[1:1:16];
```

```
>>j=[1:1:16];
```

```
>>j*I;
```

```
>>N=16;
```

```
>>s_j=2/N*(sin(2*pi*j*i));
```

```
>>c_j=2/N*(sin(2*pi*j*i));
```

For harmonic analysis of single phase system:

$$H_j = \sqrt{(s_j^2 + c_j^2)} \quad (\text{C.11})$$

The fundamental ( $H_1$ ), second ( $H_2$ ) and 5<sup>th</sup> ( $H_5$ ) harmonics of single phase differential currents are as follows:

$j= 1, 2$  and  $5$

$$H_1 = \sqrt{(s_1^2 + c_1^2)} \quad (\text{C.12})$$

$$H_2 = \sqrt{(s_2^2 + c_2^2)} \quad (\text{C.13})$$

$$H_5 = \sqrt{(s_5^2 + c_5^2)} \quad (\text{C.14})$$

The fundamental ( $H_1$ ), second ( $H_2$ ) and 5<sup>th</sup> ( $H_5$ ) harmonics of three phase differential currents are as follows:

$$H_1 = \sqrt{(s_{1a}^2 + s_{1b}^2 + s_{1c}^2 + c_{1a}^2 + c_{1b}^2 + c_{1c}^2)} \quad (\text{C.15})$$

$$H_2 = \sqrt{(s_{2a}^2 + s_{2b}^2 + s_{2c}^2 + c_{2a}^2 + c_{2b}^2 + c_{2c}^2)} \quad (\text{C.16})$$

$$H_5 = \sqrt{(s_{5a}^2 + s_{5b}^2 + s_{5c}^2 + c_{5a}^2 + c_{5b}^2 + c_{5c}^2)} \quad (\text{C.17})$$

where a, b and c are three phases of the system.

For magnetizing inrush condition (No fault condition):

$$\frac{H_2}{H_1} \geq 0.177 \quad (\text{C.18})$$

For over-excitation condition (No fault condition):

$$\frac{H_5}{H_1} \geq 0.065 \quad (\text{C.19})$$

## Appendix D

### Real Time Testing

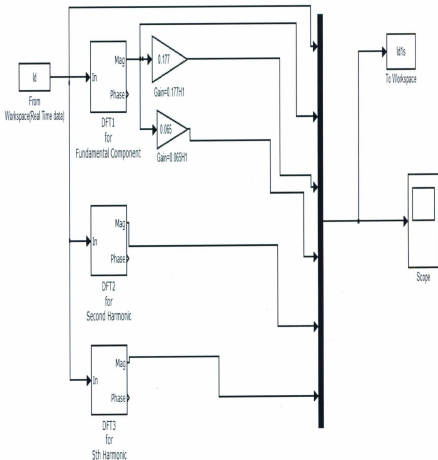


Figure D.1: MATLAB Model for Harmonics Analysis

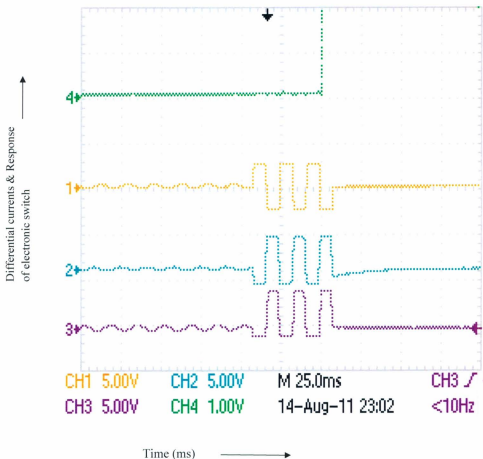


Figure D.2: Phase A to ground fault at Primary side, responses of the three phases of differential current at no load power transformer and response of electronic switch

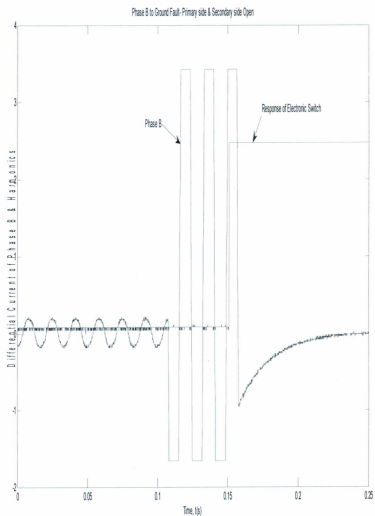


Figure D.3: Phase B to ground fault at no load power transformer and response of electronic switch

Phase B to Ground Fault at Primary side and Secondary side Open

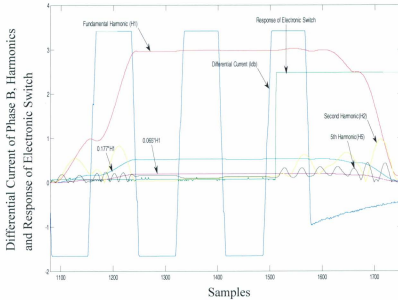


Figure D.4: Phase B to ground fault at no load power transformer, harmonics and response of electronic switch

$I_{dB}$  = Differential current of phase B,  $H_1$  = Fundamental Harmonic,  $H_2$  = 2<sup>nd</sup> Harmonic,

$H_5$  = 5<sup>th</sup> harmonic and S = Response of Electronic Switch.

Results:

$$H_2 < 0.177 * H_1 \quad (D.1)$$

$$H_5 > 0.065 * H_1$$

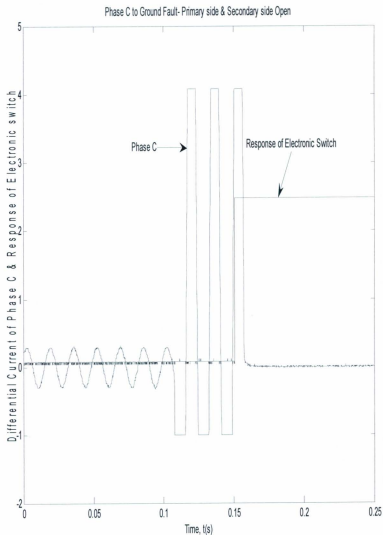


Figure D.5: Phase C to ground fault at no load power transformer and response of electronic switch

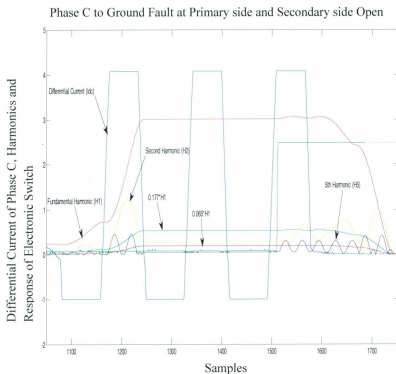


Figure D.6: Phase C to ground fault at no load power transformer, harmonics and response of electronic switch

$I_{dc}$  = Differential current of phase C,  $H_1$  = Fundamental Harmonic,  $H_2$  = 2<sup>nd</sup> Harmonic,

$H_5$  = 5<sup>th</sup> harmonic and  $S$  = Response of Electronic Switch.

Results:

$$H_2 < 0.177 * H_1 \quad (D.2)$$

$$H_5 > 0.065 * H_1$$

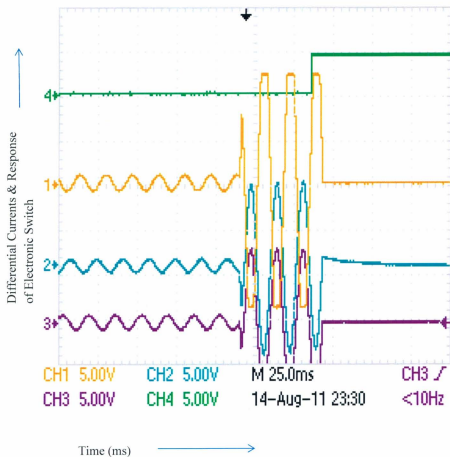


Figure D.7: Phase A to ground fault primary side, responses of the three phases of differential current at equal resistive load ( $600\Omega$ ), power transformer and response of electronic switch.

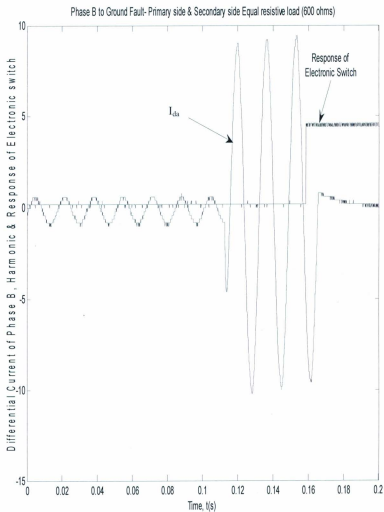


Figure D.8: Phase B to ground fault at equal resistive load (600  $\Omega$ ) power transformer and response of electronic switch

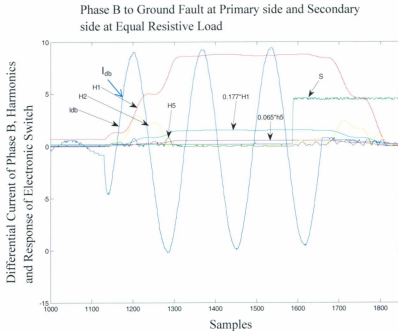


Figure D.9: Phase B to ground fault at equal resistive load (600V) power transformer, harmonics and response of electronic switch.

$I_{gb}$  = Differential current of phase B,  $H_1$  = Fundamental Harmonic,  $H_2$  = 2<sup>nd</sup> Harmonic,

$H_5$  = 5<sup>th</sup> harmonic and S = Response of Electronic Switch.

Results:

$$H_2 < 0.177 * H_1 \quad (D.3)$$

$$H_5 > 0.065 * H_1$$

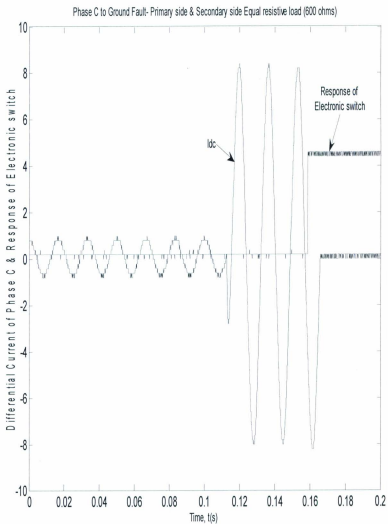


Figure D.10: Phase C to ground fault at equal resistive load ( $600\Omega$ ) power transformer and response of electronic switch

Phase C to Ground Fault at Primary side and Secondary side at Equal Resistive Load

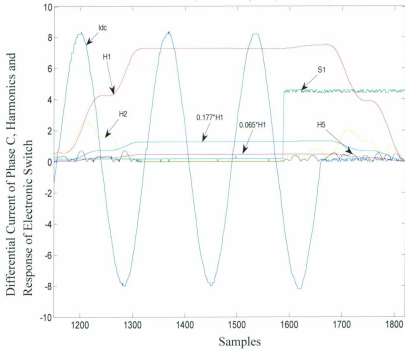


Figure D.11: Phase C to ground fault at equal resistive load (600Ω) power transformer, harmonics and response of electronic switch.

$I_{dc}$  = Differential current of phase C,  $H_1$  = Fundamental Harmonic,  $H_2$  = 2<sup>nd</sup> Harmonic,

$H_5$  = 5<sup>th</sup> harmonic and S = Response of Electronic Switch.

Results:

$$H_2 < 0.177 * H_1 \quad (D.4)$$

$$H_5 > 0.065 * H_1$$

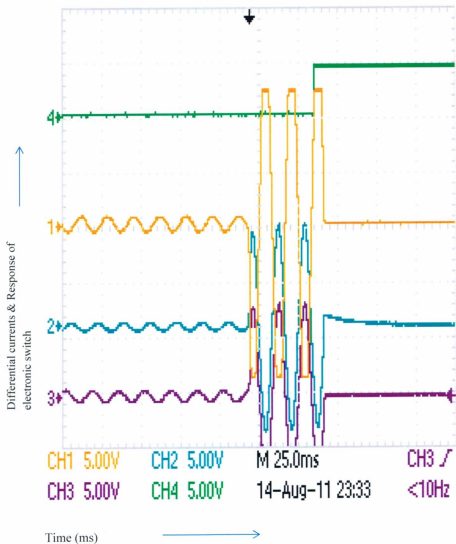


Figure D.12: Response of the three phases of differential currents at unequal resistive load (600/1200/2400 $\Omega$ ) power transformer and response of electronic switch

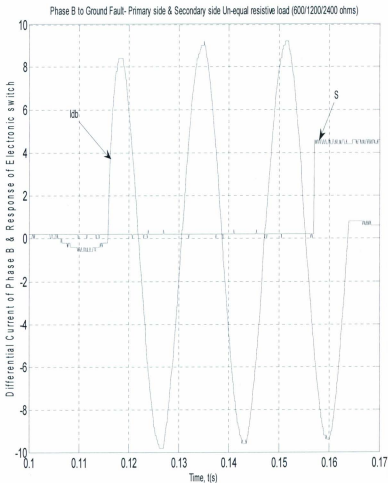


Figure D.13: Phase B to ground fault at unequal resistive load (600/1200/2400  $\Omega$ ), power transformer and response of electronic switch

$I_{db}$  = Differential Current of Phase B, S = Response of Electronic Switch

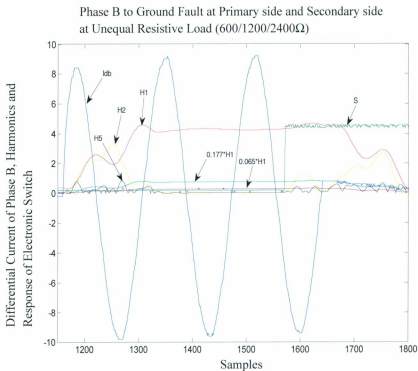


Figure D.14: Phase B to ground fault at unequal resistive load (600/1200/2400  $\Omega$ ), power transformer, harmonics and response of electronic switch

$I_{ab}$  = Differential current of phase B,  $H_1$  = Fundamental Harmonic,  $H_2$  = 2<sup>nd</sup> Harmonic,

$H_5$  = 5<sup>th</sup> harmonic and S = Response of Electronic Switch.

Results:

$$H_2 < 0.177 * H_1 \quad (D.5)$$

$$H_5 > 0.065 * H_1$$

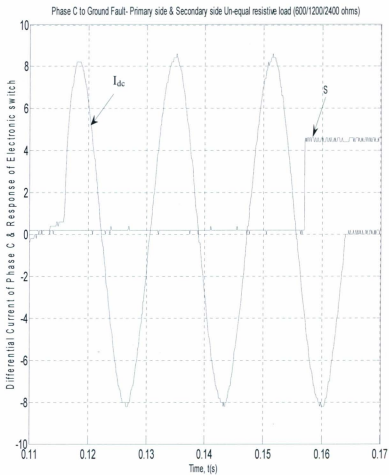


Figure D.15: Phase C to ground fault at unequal resistive load (600/1200/2400  $\Omega$ ), power transformer and response of electronic switch

$I_{dc}$  = Differential Current of Phase C, S = Response of Electronic Switch

Phase C to Ground Fault at Primary side and Secondary side at Unequal Resistive Load (600/1200/2400Ω)

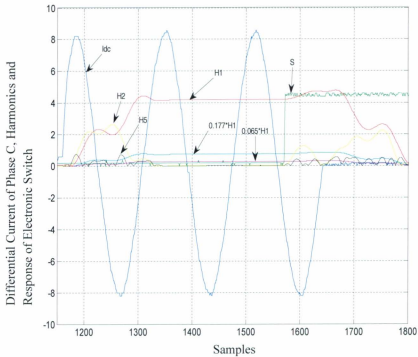


Figure D.16: Phase C to ground fault at unequal resistive load (600/1200/2400 Ω), power transformer, harmonics and response of electronic switch

$I_{dc}$  = Differential current of phase C,  $H_1$  = Fundamental Harmonic,  $H_2$  = 2<sup>nd</sup> Harmonic,

$H_3$  = 5<sup>th</sup> harmonic and S = Response of Electronic Switch.

Results:

$$H_2 < 0.177 * H_1 \quad (D.6)$$

$$H_5 > 0.065 * H_1$$

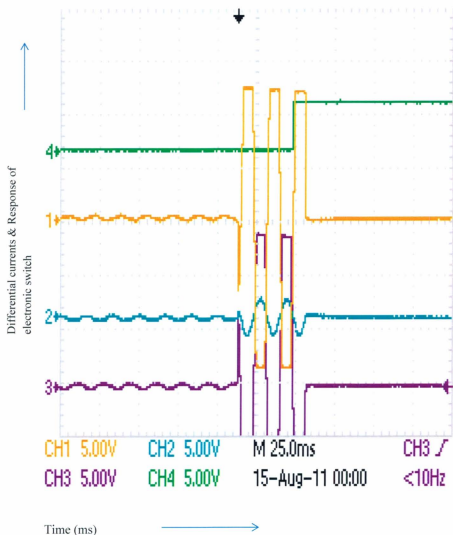


Figure D.17: Responses of the three phases of differential currents for phase to phase fault, secondaryside open, power transformer and response of electronic switch

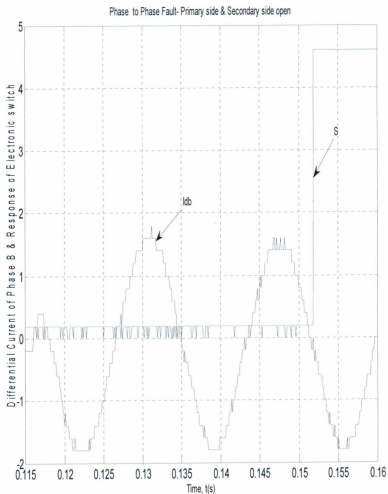


Figure D.18: Phase A to Phase B fault at primary side when secondary open and response of electronic switch

$I_{db}$  = Differential Current of Phase B, S = Response of Electronic Switch

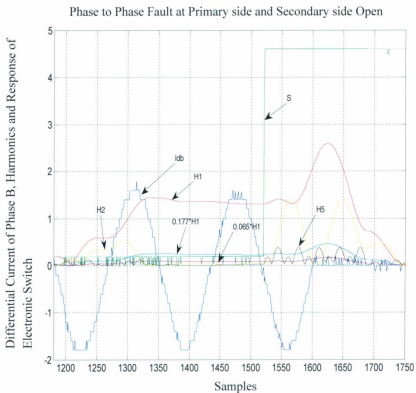


Figure D.19: Phase A to Phase B fault at primary side when secondary side open, harmonics and response of electronic switch.

$I_{db}$  = Differential current of phase B,  $H_1$  = Fundamental Harmonic,  $H_2$  = 2<sup>nd</sup> Harmonic,

$H_5$  = 5<sup>th</sup> harmonic and  $S$  = Response of Electronic Switch.

Results:

$$H_2 < 0.177 * H_1 \quad (D.7)$$

$$H_5 > 0.065 * H_1$$

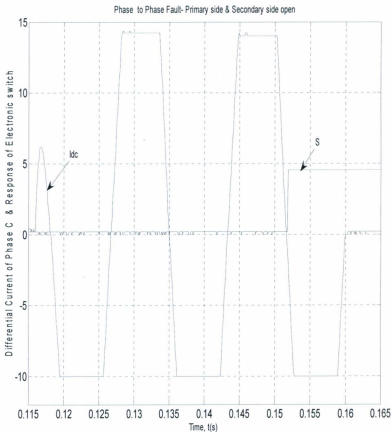


Figure D.20: Phase A to Phase B fault at primary side when secondary side open and response of electronic switch

$I_{dc}$  = Differential Current of Phase C, S = Response of Electronic Switch

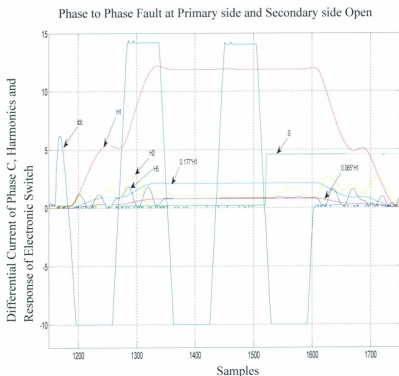


Figure D.21: Phase A to Phase B fault at primary side and secondary open, harmonics and response of electronic switch.

$I_{dc}$  = Differential current of phase C,  $H_1$  = Fundamental Harmonic,  $H_2$  = 2<sup>nd</sup> Harmonic,

$H_5$  = 5<sup>th</sup> harmonic and S = Response of Electronic Switch.

Results:

$$H_2 < 0.177 * H_1 \quad (D.8)$$

$$H_5 > 0.065 * H_1$$

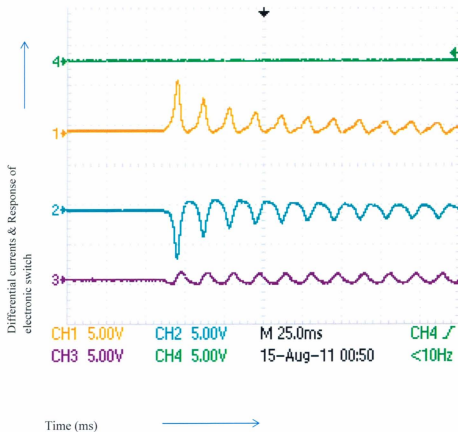


Figure D.22: Response of the three phases of differential currents for inrush magnetizing inrush current when power transformer secondary side open and response of electronic switch

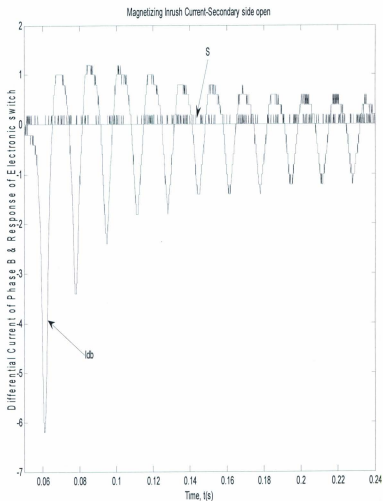


Figure D.23: Magnetizing Inrush Current in Phase B when secondary side of power transformer open and response of electronic switch.

$I_{db}$  = Differential Current of Phase B, S = Response of Electronic Switch

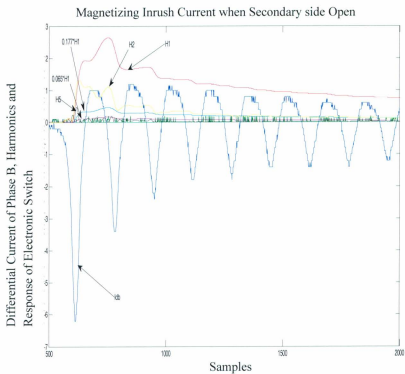


Figure D.24: Magnetizing Inrush Current in Phase B when secondary side of power transformer open, harmonics and response of electronic switch

$I_{db}$  = Differential current of phase B,  $H_1$ = Fundamental Harmonic,  $H_2$ = 2<sup>nd</sup> Harmonic,  $H_5$  = 5<sup>th</sup> harmonic and S= Response of Electronic Switch.

Results:

$$H_2 > 0.177 * H_1 \tag{D.9}$$

$$H_5 < 0.065 * H_1$$

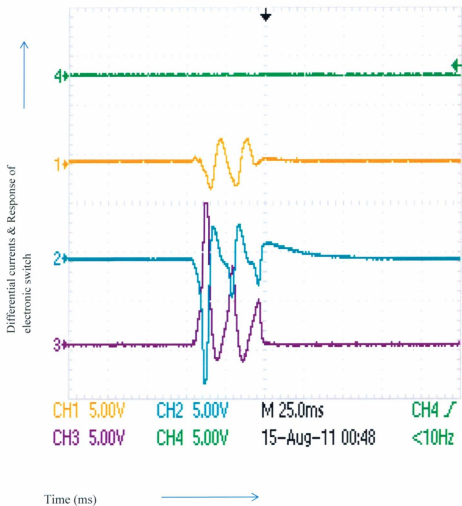


Figure D.25: Response of the three phases of differential currents for magnetizing inrush current when power transformer secondary side at equal resistive load (600Ω) and response of electronic switch

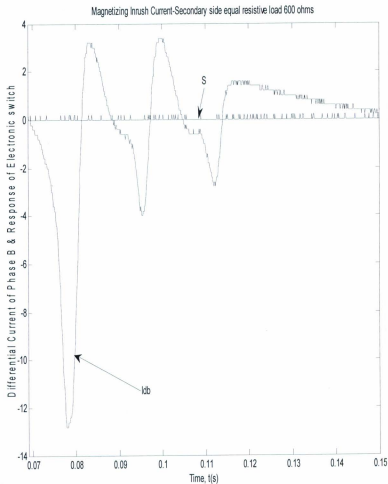


Figure D.26: Magnetizing Inrush Current in Phase B when secondary side of power transformer at equal resistive load ( $600\ \Omega$ ) and response of electronic switch.

$I_{db}$  = Differential Current of Phase B, S = Response of Electronic Switch

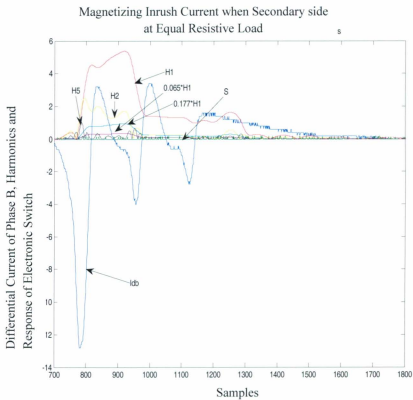


Figure D.27: Magnetizing Inrush Current in Phase B when secondary side of power transformer at equal resistive load ( $600\Omega$ ), harmonics and response of electronic switch

$I_{db}$  = Differential current of phase B,  $H_1$  = Fundamental Harmonic,  $H_2$  = 2<sup>nd</sup> Harmonic,

$H_5$  = 5<sup>th</sup> harmonic and S = Response of Electronic Switch.

Results:

$$H_2 > 0.177 * H_1 \quad (D.10)$$

$$H_5 < 0.065 * H_1$$

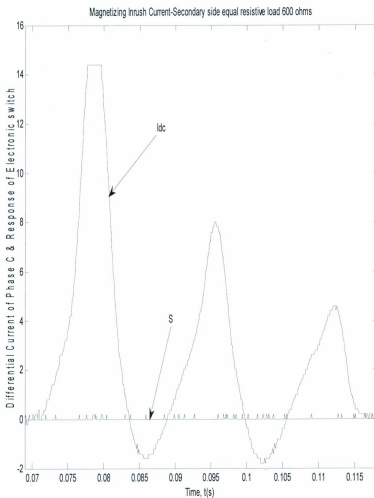


Figure D.28: Magnetizing Inrush Current in Phase C when secondary side of power transformer at equal resistive load ( $600\Omega$ ) and response of electronic switch.

$I_{dc}$  = Differential Current of Phase C, S = Response of Electronic Switch

Magnetizing Inrush Current when Secondary side at  
Equal Resistive Load

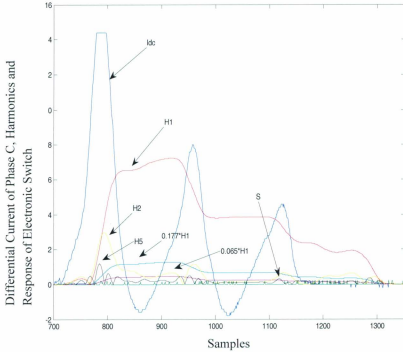


Figure D.29: Magnetizing Inrush Current in Phase C when secondary side of power transformer at equal resistive load ( $600\Omega$ ), harmonics and response of electronic switch

$I_{dc}$  = Differential current of phase C,  $H_1$  = Fundamental Harmonic,  $H_2$  = 2<sup>nd</sup> Harmonic,

$H_5$  = 5<sup>th</sup> harmonic and S = Response of Electronic Switch.

Results:

$$H_2 > 0.177 * H_1 \quad (D.11)$$

$$H_5 < 0.065 * H_1$$

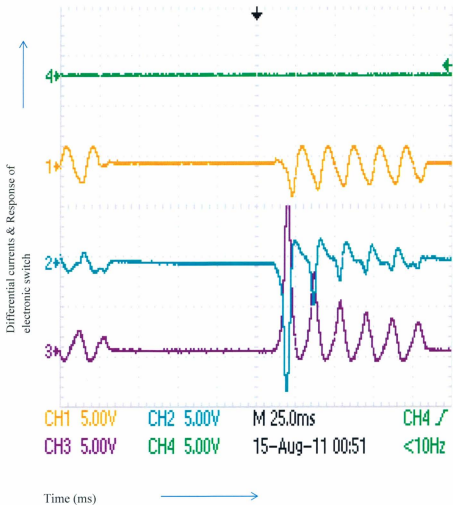


Figure D.30: Response of the three phases of differential currents for magnetizing inrush current when power transformer secondary side variable resistive load (600/1200/2400  $\Omega$ ) and response of electronic switch

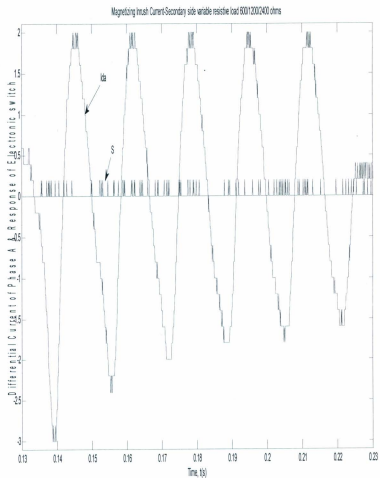


Figure D.31: Magnetizing Inrush Current in Phase A when secondary side of power transformer at variable resistive load (600/1200/2400  $\Omega$ ) and response of electronic switch

$I_{da}$  = Differential Current of Phase A, S = Response of Electronic Switch

Magnetizing Inrush Current when Secondary side at  
Variable Resistive Load (600/1200/2400  $\Omega$ )

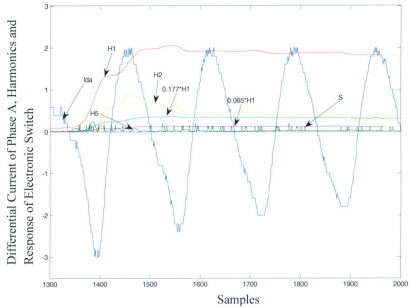


Figure D.32: Magnetizing Inrush Current in Phase A when secondary side of power transformer at variable resistive load (600/1200/2400  $\Omega$ ), harmonics and response of electronic switch

$I_{0a}$  = Differential current of phase A,  $H_1$  = Fundamental Harmonic,  $H_2$  = 2<sup>nd</sup> Harmonic,

$H_5$  = 5<sup>th</sup> harmonic and S = Response of Electronic Switch.

Results:

$$H_2 > 0.177 * H_1 \quad (D.12)$$

$$H_5 < 0.065 * H_1$$

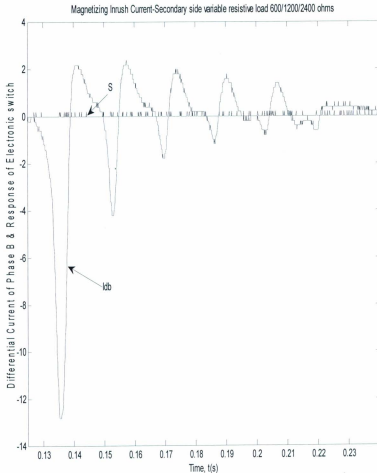


Figure D.33: Magnetizing Inrush Current in Phase B when secondary side of power transformer at variable resistive load (600/1200/2400  $\Omega$ ) and response of electronic switch.

$I_{db}$  = Differential Current of Phase B, S = Response of Electronic Switch

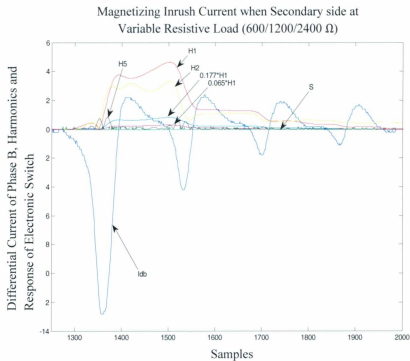


Figure D.34: Magnetizing Inrush Current in Phase B when secondary side of power transformer at variable resistive load (600/1200/2400 $\Omega$ ), harmonics and response of electronic switch

$i_{db}$  = Differential current of phase B,  $H_1$ = Fundamental Harmonic,  $H_2$ = 2<sup>nd</sup> Harmonic,

$H_5$  = 5<sup>th</sup> harmonic and S= Response of Electronic Switch.

Results:

$$H_2 > 0.177 * H_1 \quad (D.13)$$

$$H_5 < 0.065 * H_1$$

Magnetizing Inrush Current when Secondary side at  
Variable Resistive Load (600/1200/2400  $\Omega$ )

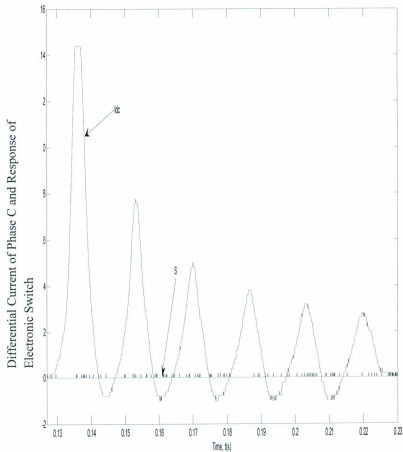


Figure D.35: Magnetizing Inrush Current in Phase C when secondary side of power transformer at variable resistive load (600/1200/2400  $\Omega$ ) and response of electronic switch.

$I_{dc}$  = Differential Current of Phase C, S = Response of Electronic Switch

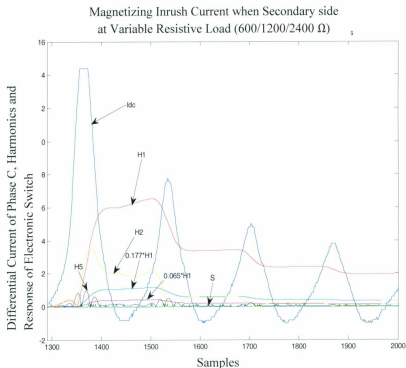


Figure D.36: Magnetizing Inrush Current in Phase C when secondary side of power transformer at variable resistive load (600/1200/2400 $\Omega$ ), harmonics and response of electronic switch

$I_{bc}$  = Differential current of phase B,  $H_1$ = Fundamental Harmonic,  $H_2$ = 2<sup>nd</sup> Harmonic,

$H_5$  = 5<sup>th</sup> harmonic and S= Response of Electronic Switch.

Results:

$$H_2 > 0.177 * H_1 \quad (D.14)$$

$$H_5 < 0.065 * H_1$$

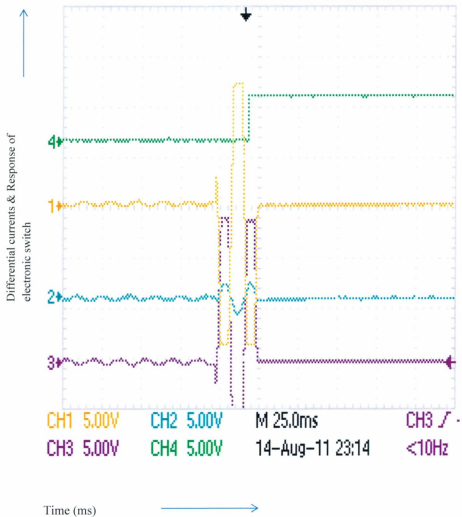


Figure D.37: Response of the three phases of differential currents for phase to neutral fault when power transformer secondary side open and response of electronic switch

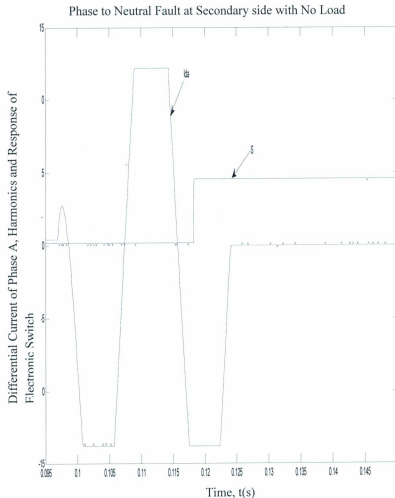


Figure D.38: Phase to neutral fault current (secondary side) in Phase A when secondary side of power transformer open and response of electronic switch.

$I_{da}$  = Differential Current of Phase A, S = Response of Electronic Switch

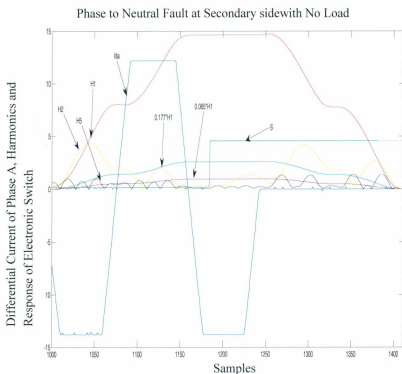


Figure D.39: Phase to neutral fault current (secondary side) in Phase A when secondary side of power transformer open, harmonics and response of electronic switch.

$I_{da}$  = Differential current of phase A,  $H_1$  = Fundamental Harmonic,  $H_2$  = 2<sup>nd</sup> Harmonic,

$H_5$  = 5<sup>th</sup> harmonic and S = Response of Electronic Switch.

Results:

$$H_2 < 0.177 * H_1 \quad (D.15)$$

$$H_5 > 0.065 * H_1$$

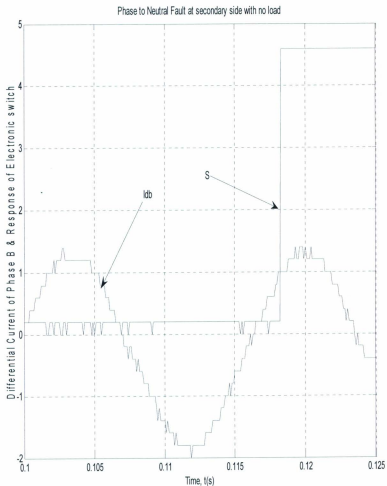


Figure D.40: Phase to neutral fault current (secondary side) in Phase B when secondary side of power transformer open and response of electronic switch.

$I_{db}$  = Differential Current of Phase B, S = Response of Electronic Switch

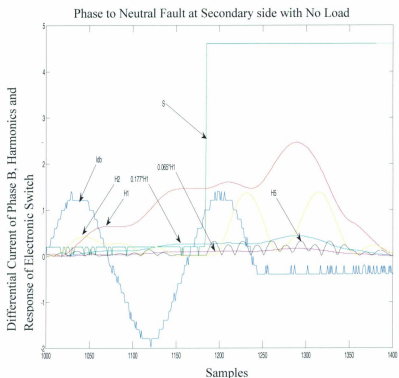


Figure D.41: Phase to neutral fault current (secondary side) in Phase B when secondary side of power transformer open, harmonics and response of electronic switch.

$I_{db}$  = Differential current of phase B,  $H_1$  = Fundamental Harmonic,  $H_2$  = 2<sup>nd</sup> Harmonic,

$H_5$  = 5<sup>th</sup> harmonic and  $S$  = Response of Electronic Switch.

Results:

$$H_2 < 0.177 * H_1 \quad (D.16)$$

$$H_5 > 0.065 * H_1$$

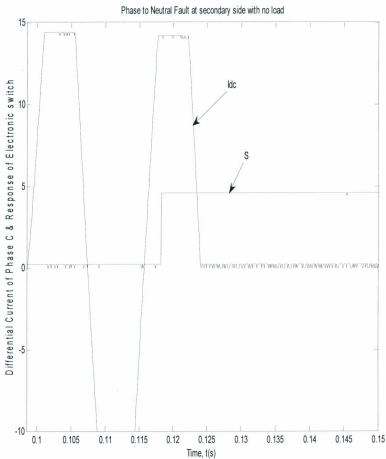


Figure D.42: Phase to neutral fault current (secondary side) in Phase C when secondary side of power transformer open and response of electronic switch.

$I_{dc}$  = Differential Current of Phase C, S = Response of Electronic Switch

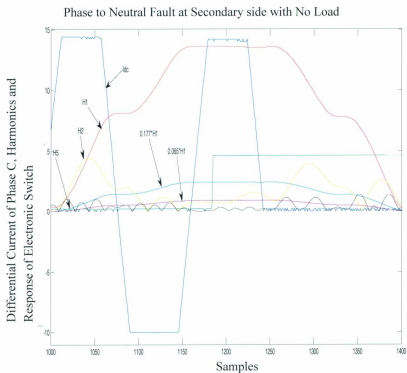


Figure D.43: Phase to neutral fault current (secondary side) in Phase C when secondary side of power transformer open, harmonics and response of electronic switch.

$I_{dc}$  = Differential current of phase C,  $H_1$  = Fundamental Harmonic,  $H_2$  = 2<sup>nd</sup> Harmonic,

$H_5$  = 5<sup>th</sup> harmonic and S = Response of Electronic Switch.

Results:

$$H_2 < 0.177 * H_1 \quad (D.17)$$

$$H_5 > 0.065 * H_1$$

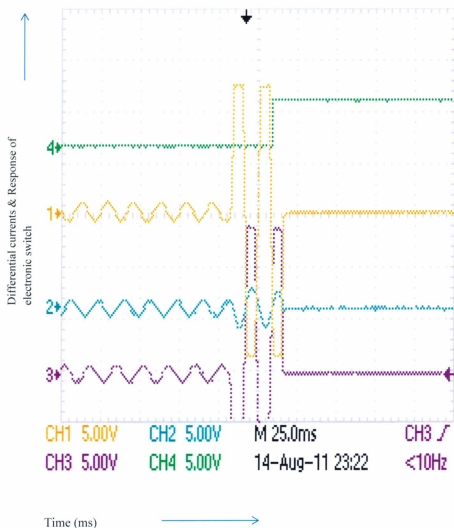


Figure D.44: Response of the three phases of differential currents for phase to neutral fault when power transformer secondary side at equal resistive load ( $600\ \Omega$ ) and response of electronic switch.

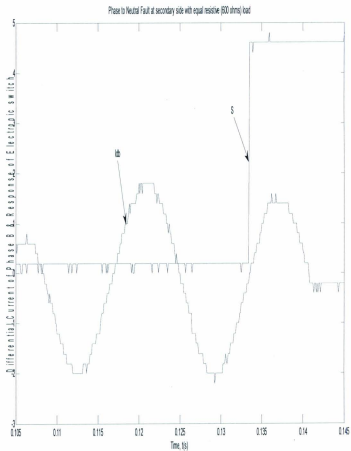


Figure D.45: Phase to neutral fault current (secondary side) in Phase B when secondary side of power transformer at equal resistive load ( $600\Omega$ ) and response of electronic switch.

$I_{db}$  = Differential Current of Phase B, S = Response of Electronic Switch

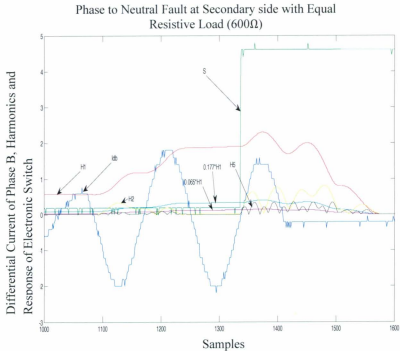


Figure D.46: Phase to neutral fault current (secondary side) in Phase B when secondary side of power transformer at equal resistive load, harmonics and response of electronic switch.

$I_{ab}$  = Differential current of phase B,  $H_1$  = Fundamental Harmonic,  $H_2$  = 2<sup>nd</sup> Harmonic,

$H_5$  = 5<sup>th</sup> harmonic and S = Response of Electronic Switch.

Results:

$$H_2 < 0.177 * H_1 \quad (D.18)$$

$$H_5 > 0.065 * H_1$$

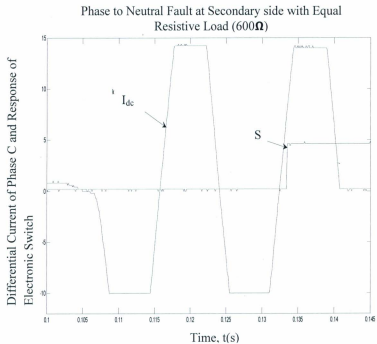


Figure D.47: Phase to neutral fault current (secondary side) in Phase C when secondary side of power transformer at equal resistive load ( $600\Omega$ ) and response of electronic switch.

$I_{dc}$  = Differential Current of Phase C, S = Response of Electronic Switch

Phase to Neutral Fault at Secondary side with Equal Resistive Load (600Ω)

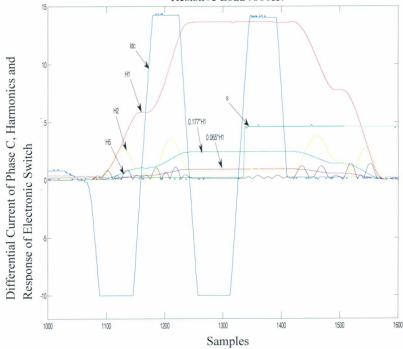


Figure D.48: Phase to neutral fault current (secondary side) in Phase C when secondary side of power transformer at equal resistive load (600Ω), harmonics and response of electronic switch.

$I_{dc}$  = Differential current of phase C,  $H_1$  = Fundamental Harmonic,  $H_2$  = 2<sup>nd</sup> Harmonic,

$H_5$  = 5<sup>th</sup> harmonic and S = Response of Electronic Switch.

Results:

$$H_2 < 0.177 * H_1 \quad (D.19)$$

$$H_5 > 0.065 * H_1$$

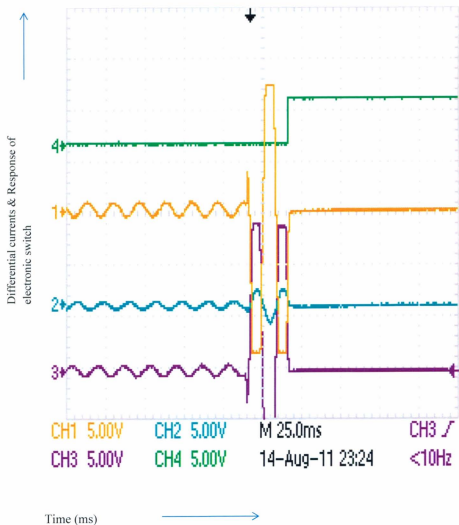


Figure D.49: Response of the three phases of differential currents for phase to neutral fault when power transformer secondary side at unequal resistive load (600/1200/2400  $\Omega$ ) and response of electronic switch S.

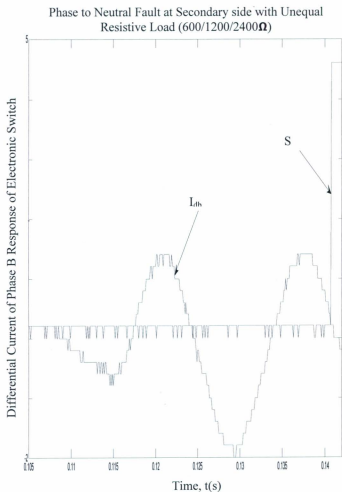


Figure D.50: Phase to neutral fault current (secondary side) in Phase B when secondary side of power transformer at un-equal resistive load (600/1200/2400  $\Omega$ ) and response of electronic switch S.

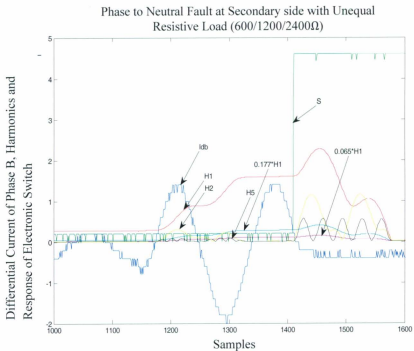


Figure D.51: Phase to neutral fault current (secondary side) in Phase B when secondary side of power transformer at un-equal resistive load (600/1200/2400 Ω) and response of electronic switch S.

$I_{db}$  = Differential current of phase B,  $H_1$  = Fundamental Harmonic,  $H_2$  = 2<sup>nd</sup> Harmonic,

$H_5$  = 5<sup>th</sup> harmonic and S = Response of Electronic Switch.

Results:

$$H_2 < 0.177 * H_1 \quad (D.20)$$

$$H_5 > 0.065 * H_1$$

Phase to Neutral Fault at Secondary side with Unequal Resistive Load (600/1200/2400 $\Omega$ )

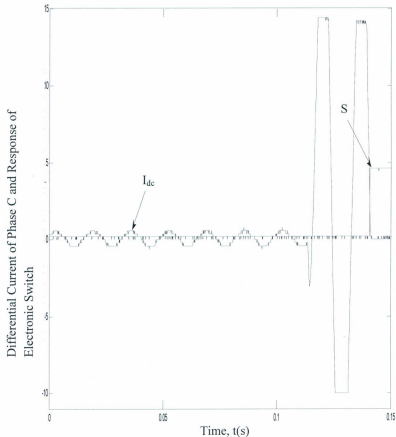


Figure D.52: Phase to neutral fault current (secondary side) in Phase C when secondary side of power transformer at un-equal resistive load (600/1200/2400  $\Omega$ ) and response of electronic switch S.

$I_{dc}$  = Differential Current of Phase C, S = Response of Electronic Switch

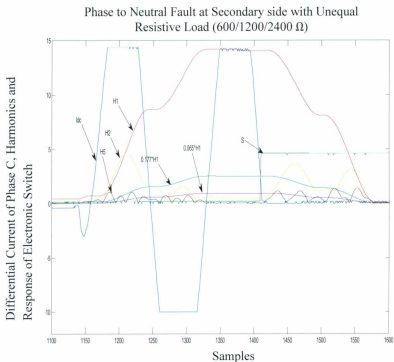


Figure D.53: Phase to neutral fault current (secondary side) in Phase C when secondary side of power transformer at un-equal resistive load (600/1200/2400  $\Omega$ ) and response of electronic switch.

$I_{dc}$  = Differential current of phase C,  $H_1$  = Fundamental Harmonic,  $H_2$  = 2<sup>nd</sup> Harmonic,

$H_5$  = 5<sup>th</sup> harmonic and S = Response of Electronic Switch.

Results:

$$H_2 < 0.177 * H_1 \quad (D.21)$$

$$H_5 > 0.065 * H_1$$

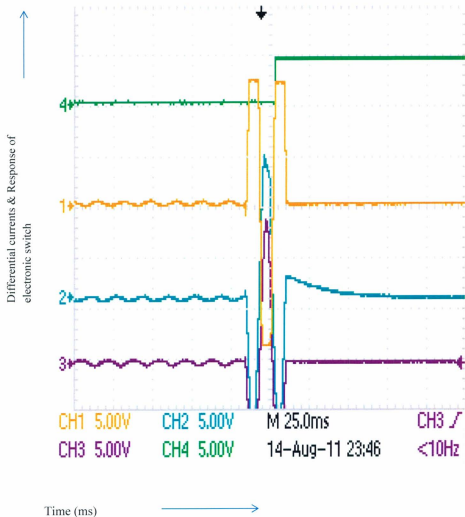


Figure D.54: Responses of the three phases of differential currents for phase to phase fault when power transformer secondary side open and response of electronic switch.

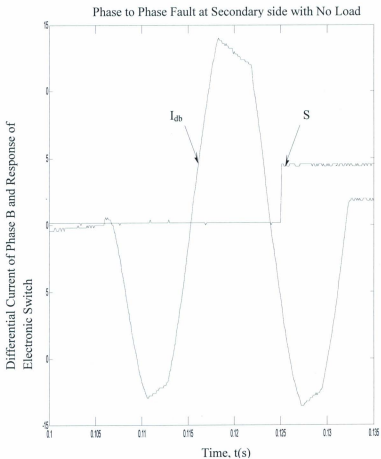


Figure D.55: Phase to Phase fault current (secondary side) in Phase B when secondary side of power transformer open and response of electronic switch.

$I_{db}$  = Differential Current of Phase B, S = Response of Electronic Switch

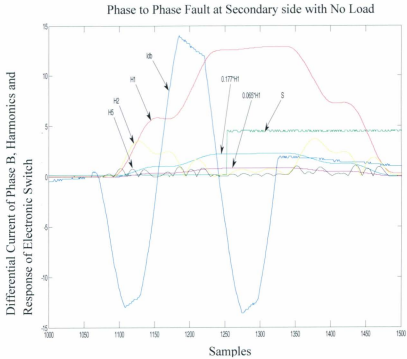


Figure D.56: Phase to Phase fault current (secondary side) in Phase B when secondary side of power transformer open and response of electronic switch S.

$i_{\Delta B}$  = Differential current of phase B,  $H_1$ = Fundamental Harmonic,  $H_2$ = 2<sup>nd</sup> Harmonic,

$H_5$  = 5<sup>th</sup> harmonic and S= Response of Electronic Switch.

Results:

$$H_2 < 0.177 * H_1 \quad (D.22)$$

$$H_5 > 0.065 * H_1$$

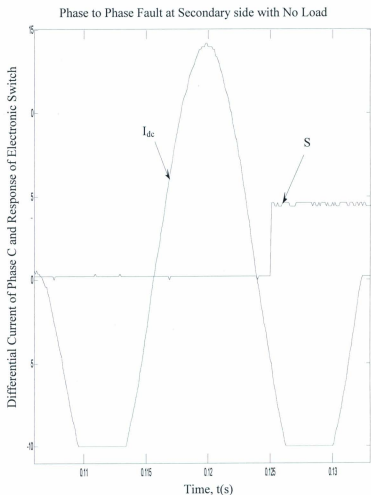


Figure D.57: Phase to Phase fault current (secondary side) in Phase C when secondary side of power transformer open and response of electronic switch S.

$I_{dc}$  = Differential Current of Phase C, S = Response of Electronic Switch

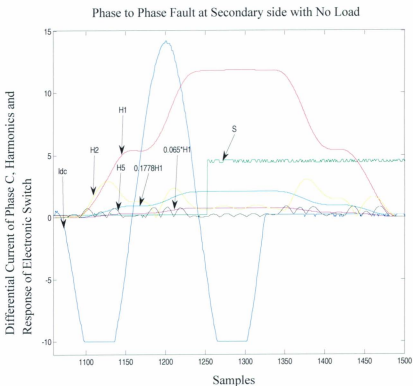


Figure D.58: Phase to Phase fault current (secondary side) in Phase C when secondary side of power transformer open and response of electronic switch.

$I_{dc}$  = Differential current of phase C,  $H_1$  = Fundamental Harmonic,  $H_2$  = 2<sup>nd</sup> Harmonic,  $H_5$  = 5<sup>th</sup> harmonic and S = Response of Electronic Switch.

Results:

$$H_2 < 0.177 * H_1 \quad (D.23)$$

$$H_5 > 0.065 * H_1$$

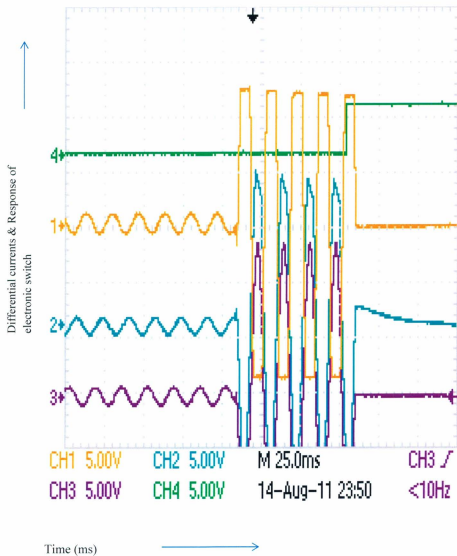


Figure D.59: Responses of the three phases of differential currents for phase to phase fault when power transformer secondary side at equal resistive load ( $600\ \Omega$ ) and response of electronic switch.

Phase to Phase Fault at Secondary side with Equal Resistive Load ( $600\Omega$ )

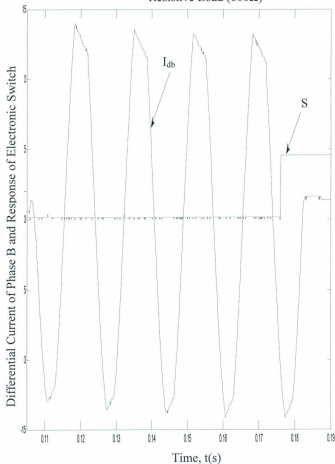


Figure D.60: Phase to Phase fault current (secondary side) in Phase B when secondary side of power transformer at equal resistive load ( $600\Omega$ ) and response of electronic switch S.

$I_{db}$  = Differential Current of Phase B, S = Response of Electronic Switch

Phase to Phase Fault at Secondary side with Equal Resistive Load (600  $\Omega$ )

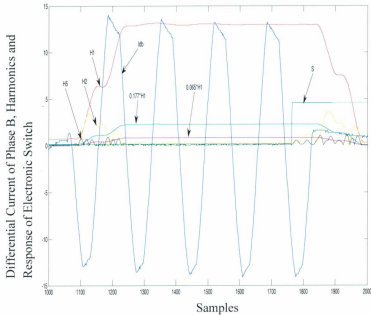


Figure D.61: Phase to Phase fault current (secondary side) in Phase B when secondary side of power transformer at equal resistive load (600  $\Omega$ ) and response of electronic switch S.

$I_{\Delta B}$  = Differential current of phase B,  $H_1$ = Fundamental Harmonic,  $H_2$ = 2<sup>nd</sup> Harmonic,

$H_5$  = 5<sup>th</sup> harmonic and S= Response of Electronic Switch.

Results:

$$H_2 < 0.177 * H_1 \quad (D.24)$$

$$H_5 > 0.065 * H_1$$

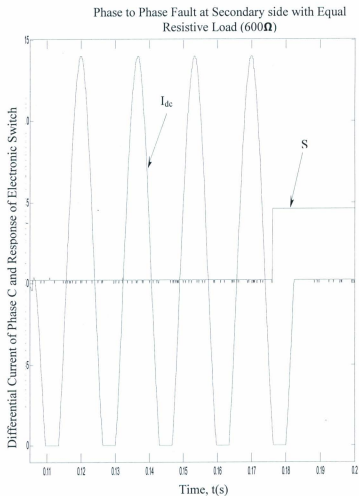


Figure D.62: Phase to Phase fault current (secondary side) in Phase C when secondary side of power transformer at equal resistive load ( $600\Omega$ ) and response of electronic switch S.

$I_{dc}$  = Differential Current of Phase C, S = Response of Electronic Switch

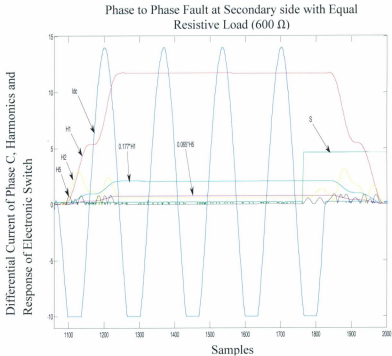


Figure D.63: Phase to Phase fault current (secondary side) in Phase C when secondary side of power transformer at equal resistive load (600  $\Omega$ ) and response of electronic switch.

$I_{dc}$  = Differential current of phase C,  $H_1$ = Fundamental Harmonic,  $H_2$ = 2<sup>nd</sup> Harmonic,

$H_5$  = 5<sup>th</sup> harmonic and S= Response of Electronic Switch.

Results:

$$H_2 < 0.177 * H_1 \quad (D.25)$$

$$H_5 > 0.065 * H_1$$

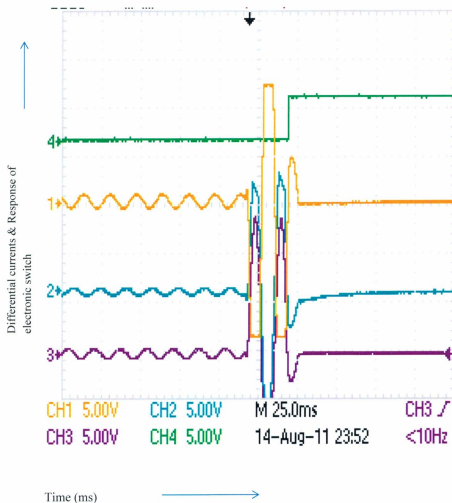


Figure D.64: Responses of the three phases of differential currents for phase to phase fault when power transformer secondary side different resistive load (600/1200/2400  $\Omega$ ) and response of electronic switch.

Phase to Phase Fault at Secondary side with  
Different Resistive Load (600/1200/2400 $\Omega$ )

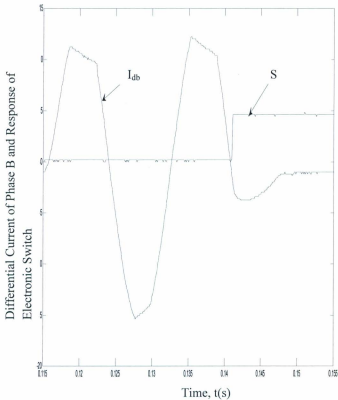


Figure D.65: Phase to Phase fault current (secondary side) in Phase B when secondary side of power transformer at different resistive load (600/1200/2400  $\Omega$ ) and response of electronic switch S.

$I_{db}$  = Differential Current of Phase B, S = Response of Electronic Switch

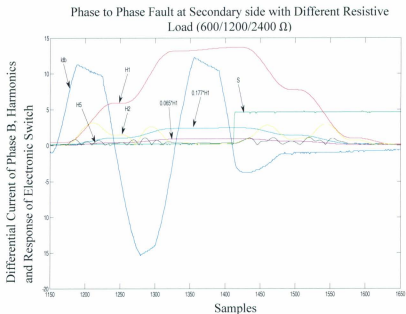


Figure D.66: Phase to Phase fault current (secondary side) in Phase B when secondary side of power transformer at different resistive load (600/1200/2400  $\Omega$ ) and response of electronic switch S.

$I_{db}$  = Differential current of phase B,  $H_1$ = Fundamental Harmonic,  $H_2$ = 2<sup>nd</sup> Harmonic,

$H_5$  = 5<sup>th</sup> harmonic and S= Response of Electronic Switch.

Results:

$$H_2 < 0.177 * H_1 \quad (D.26)$$

$$H_5 > 0.065 * H_1$$

Phase to Phase Fault at Secondary side with Different Resistive Load (600/1200/2400 $\Omega$ )

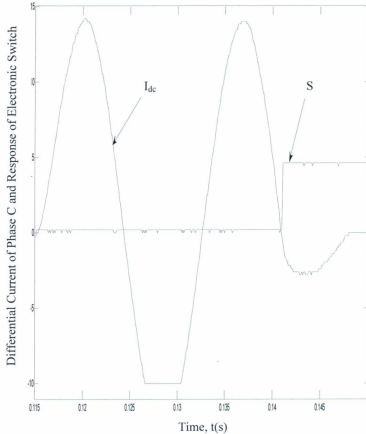


Figure D.67: Phase to Phase fault current (secondary side) in Phase C when secondary side of power transformer at different resistive load (600/1200/2400  $\Omega$ ) and response of electronic switch S.

$I_{dc}$  = Differential Current of Phase C, S = Response of Electronic Switch

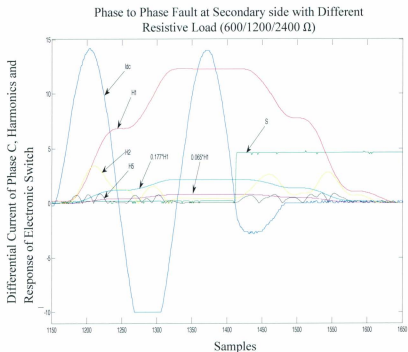


Figure D.68: Phase to Phase fault current (secondary side) in Phase C when secondary side of power transformer at different resistive load (600/1200/2400 $\Omega$ ) and response of electronic switch S.

$I_{dc}$  = Differential current of phase C,  $H_1$ = Fundamental Harmonic,  $H_2$ = 2<sup>nd</sup> Harmonic,

$H_5$  = 5<sup>th</sup> harmonic and S= Response of Electronic Switch.

Results:

$$H_2 < 0.177 * H_1 \quad (D.27)$$

$$H_5 > 0.065 * H_1$$

## Appendix E

### Program for Microcontroller

The code for extracting harmonics and instructions to the electronic control relay are given for execution of the electronic switch.

```
// Program for the Digital Protection of the Power Transformer

#if defined (__PCB__)

#fuses HS, NOWDT, NOPROTECT

#use delay(clock=20000000)

#use rs232(baud=9600, xmit=PIN_A3, rcv=PIN_A2)

#elif defined (__PCM__)

#include <16F877.h>

#fuses HS, NOWDT, NOPROTECT, NOLVP

#use delay(clock=20000000)

#use rs232(baud=9600, xmit=PIN_C6, rcv=PIN_C7)

#endif

#include <Ic1298.c>

#include <math.h>

float current1, current2, current3;

float sa[3], sb[3], sc[3], ca[3], cb[3], cc[3];

float h1, h2, h5;
```

```

int INST_TRIP=0;
int OVER_EXCITE=0;
int N=16;
int wait=0;
void measure_current()
{ set_adc_channel( 0 );
  current1 = Read_ADC();
  if(current1>130)
  { printf("phase a");
    INST_TRIP=1; }
  set_adc_channel( 1 );
  current2 = Read_ADC();
  if(current2 > 130)
  { printf("phase b");
    INST_TRIP=1;}
  set_adc_channel( 2 );
  current3 = Read_ADC();
  if(current3 > 130)
  { printf("phase c");
    INST_TRIP=1; }}
void measure_coeff(int sample,int c,int j)
{ sa[c]=sa[c]+(2/16)*current1*sin(2*j*3.1416*(sample/N));
  sb[c]=sb[c]+(2/16)*current2*sin(2*j*3.1416*(sample/N));

```

```

sc[c]=sc[c]+(2/16)*current3*sin(2*j*3.1416*(sample/N));
ca[c]=ca[c]+(2/16)*current1*cos(2*j*3.1416*(sample/N));
cb[c]=cb[c]+(2/16)*current2*cos(2*j*3.1416*(sample/N));
cc[c]=cc[c]+(2/16)*current3*cos(2*j*3.1416*(sample/N));
}

void input_samples()
{
    int i;
    for(i=0;i<N;i++)
    {
        measure_current();

        if(INST_TRIP==1)
        {
            break;
        }
        else
        {
            measure_coeff(i+1,0,1);
            measure_coeff(i+1,1,2);
            measure_coeff(i+1,2,5);

            // delay_ms(1);
        }
    }
}

void measure_harmonics()
{
    h1=sa[0]*sa[0]+sb[0]*sb[0]+sc[0]*sc[0];
    h1=h1+ca[0]*ca[0]+cb[0]*cb[0]+cc[0]*cc[0];
    h2=sa[1]*sa[1]+sb[1]*sb[1]+sc[1]*sc[1];
    h2=h2+ca[1]*ca[1]+cb[1]*cb[1]+cc[1]*cc[1];
    h5=sa[2]*sa[2]+sb[2]*sb[2]+sc[2]*sc[2];
    h5=h5+ca[2]*ca[2]+cb[2]*cb[2]+cc[2]*cc[2];
}

void main()
{
    wait=0;
}

```

```

INST_TRIP=0;

setup_port_a( ALL_ANALOG );

setup_adc( ADC_CLOCK_INTERNAL );

output_low(PIN_B3);

output_low(PIN_B4);

output_low(PIN_B5);

do { sa[0]=sa[1]=sb[0]=sb[1]=sc[0]=sc[1]=ca[0]=ca[1]=cb[0]=cb[1]=cc[0]=cc[1]=0;

    sa[2]=sb[2]=sc[2]=ca[2]=cb[2]=cc[2]=0;

    h1=h2=h5=0;

    input_samples();

    if(INST_TRIP==1)

        { output_high(PIN_B3);

          break;}

    measure_harmonics();

    printf("h1=");

    printf("%f",h1);

    printf("\n");

    printf("h2=");

    printf("%f",h2);

    printf("\n");

    printf("h5=");

    printf("%f",h5);

    printf("\n");

```

```
if(h5≤(0.065*h1))
{OVER_EXCITE=1;
  output_high(PIN_B4);
  break;}
if(h2≤(0.177*h1))
{ // if(wait==1)
  // {output_high(PIN_B5);
  OVER_EXCITE=0;
  // wait=0;
  break; // }
// else
// { // delay_ms(15);
// wait=1; // } }
while(TRUE);}
```

## Appendix F

### Diagrams for Microcontroller

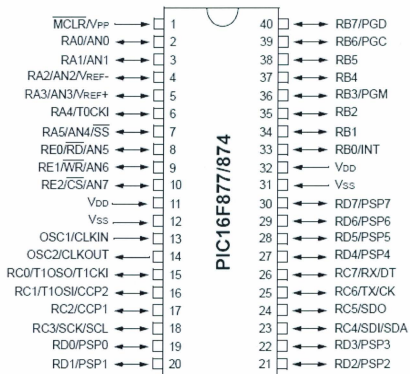


Figure F.1.1: Pin Diagram for Microcontroller-16F877

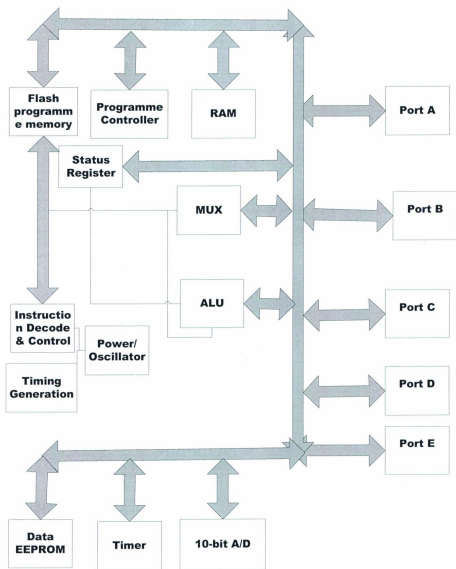


Figure F.1.2: Block Diagram of Programmable Controller (PIC 16F877)







